Manufacturing and characterization of single cell intermediate-temperature solid oxide fuel cells for APU in transportation application

Visweshwar Sivasankaran

UNIVERSITE DE BOURGOGNE

UFR Sciences et Techniques

Ecole Doctorale **CARNOT-PASTEUR**

LABORATOIRE INTERDISCIPLINAIRE CARNOT DE BOURGOGNE

ICB-UMR 6303 CNRS UB

INSTITUT FEMTO-ST UMR CNRS 6174

FCLAB FR CNRS 3539

THESE DE DOCTORAT

Discipline : Sciences

Spécialité : Chimie-Physique

Manufacturing and characterization of single cell Intermediate - Temperature Solid Oxide Fuel Cells for APU in transportation application.

Visweshwar SIVASANKARAN

Defended on 9th July2014 before Jury:

Prof. M.Cassir	*Ecole Nationale Superieure de Chimie de Paris, France,*	**President**
Dr. J. P.Viricelle	*Ecole des Mines de Saint.Etienne, France,*	**Reviewer**
Prof. A.Barbucci	*Université de Genova, Italie,*	**Reviewer**
Dr. P.Briois	*Université de Belfort-Montbeliard, France,*	**Invited**
Dr. L.Combemale	*Université de Bourgogne, France,*	**Co-Director of Thesis**
Prof. M.C.Pera	*Universite de Franche-Comte, France,*	**Co-Director of Thesis**
Prof.G.Caboche	*Université de Bourgogne, France.*	**Director of Thesis**

Acknowledgement

First of all, I would like to thank my beloved project advisors, *Prof. G.Caboche (UB), Prof. Marie–Cecile Pera (UFC), Dr. Lionel Combemale (UB)* for their constant support and guidance through the entire tenure of my thesis work.

I extend my hearty thanks to *Mr. Serge Vives, Mr. Laurent Girardot,* for their guidance in developing test bench in FC-LAB. I deeply acknowledge *Dr. Samir Jamei, Fabien Harel* for helping us in fruitful discussions in developing test bench. I also express my gratitude to *Mr. Patric Szabo* from DLR Stuttgart Germany, for his technical support in building of stack and development of test bench in FC-LAB. I am grateful to *Mr. Jean Marc Dachicourt, Ms.Marie Laure Leonard, Mr.* Nicolas Geoffroy, *Ms. Claudie Josse* for their support in performing Scanning Electron Microscopy and XRD measurements. I also acknowledge *Ms. Nathalie Roudergues* for her assistance in the ICB lab.

I would like to thank my lab directors, *Prof. Alain Dereux (Dijon), Raphael Ihringer* (Switzerland) EPFL scientific park A who have given a place for me to work in their esteemed laboratories. And I thank all my ICB, FC-LAB mates who made my stay, pleasant and peaceful in Dijon and Belfort.

I thank my financial supporters namely *Region de Bourgogne and Region de Franche Comte*. Finally it was all possible only with constant support and encouragement from my parents (*Mr and Mrs M.Sivasankaran*).

Visweshwar Sivasankaran

Table of Contents

Table of contents

General Introduction

I. General aspects of IT-SOFC

Solid Oxide Fuel Cells (SOFC) systems operating with humidified hydrogen as fuel emit no harmful effluents to atmosphere. This gives major interest on SOFC systems. The conventional systems use Yttria Stabilized Zirconia (YSZ) as an electrolyte material which operates best above 800°C imposes serious problems related to cost and commercialization. The only viable option for effective commercialization seems to be reduction of working temperature down 700°C or below called as Intermediate Temperature-SOFC (IT-SOFC). This system allows wide path for selection of new electrode, electrolyte materials, their synthesis process involved and fabrication process used.

The main goal of this work is to obtain a new inexpensive fabrication process, with large active area planar IT-SOFC for APU application. This work also covers the development of a new test bench and stacking of cells. This requires deep understanding, of conventional electrode, electrolyte materials used, the fabrication process involved, their advantages and disadvantages in particular.

II. Previous works done at ICB Laboratory

The previous PhD work performed in ICB lab Dijon was given as gist.

II.1. Study of surface and volume properties of oxides type of $La_{1-x}Sr_xMnO_{3\pm\delta}$

The objective of the thesis of P. Decorse [1] was to determine and compare the chemical composition and the oxidation state of Mn, a share in the volume of solid type $La_{1-x}Sr_xMnO_{3\pm\delta}$

and, secondly, in their diapers superficial. The surface layers played an important role in the overall properties (reactivity at the interface and transport to the electrolyte).

The study showed, in the case of a fine powder of $La_{0.8}Sr_{0.2}MnO_3$, the chemical composition in the surface layers is very dependent on the conditions of heat treatment under oxygen. The same was true for the average oxidation state of the Mn ion which is very close to the Mn^{4+} state.

In the case of sintered $La_{1-x}Sr_xMnO_{3\pm\delta}$ with varying compositions of (x = 0, 0.2, 0.5 and 1) in oxygen at high temperature, the surface was enriched in Sr with larger values of x. Moreover, whatever the composition, oxygen deficiency was always highlighted in the surface layers. A correlation between the surface concentration of Sr and the level of oxidation of the Mn was established.

II.2. Analysis of interfacial properties of system $LaMnO_3$/YSZ

The thesis of G. Bertrand [2] aimed at the realization of an experimental model of $LaMnO_3$ half-cell SOFC. This cell was adapted to the study of the degradation reaction at interface between the cathode and the electrolyte. This work was also designed to detect the formation of lanthanum zirconate, $La_2Zr_2O_7$ at the cathode-electrolyte interface, depending on the ratio La/Mn and analyze the mechanisms involved.

This study was distinguished by the choice of the synthesis method to prepare thin layer of the cathode at low temperature: by low pressure-MOCVD. This direct synthesis at low

temperature (600°C) and using as a substrate for single crystal YSZ has developed an ideal model system for the study of the degradation of the LM/YSZ interface.

The reactivity of these assemblies at higher operating temperature (1100°C) was discussed. The scanning Auger microscopy combined with electron diffraction and X-ray diffraction at grazing incidence had specified both the chemistry and crystallography of the interface in binding experimental conditions related to the insulating nature of the substrate. Data on the reaction products and their location depends on the composition of the films; the temperature and duration of treatment has been presented. A reaction mechanism was proposed for each chemical composition studied to optimize the aging of the half-cells.

II.3 Properties and reactivity of interfacial compounds of $La_{0.8}Sr_{0.2}Mn_{1-y}Fe_yO_{3\pm\delta}$ compounds as Fuel cell cathodes

The PhD work, done by M. Petitjean [3], presents new data on ferromanganites lanthanum-strontium $La_{0.8}Sr_{0.2}Mn_{1-y}Fe_yO_{3\pm\delta}$ (noted: LSMF) that can be used as cathode materials for IT-SOFC (700°C).

XPS analysis, conducted as part of this study showed the positive influence of iron on the electrocatalytic ability, of LSMF materials. The measurement of S.I.M.S. diffusivity of oxygen, coupled to a Mössbauer analysis showed that the Fe, little oxidizable in the crystalline network with respect to Mn, encourages the creation of anion vacancies and hence the diffusion of oxygen.

The chemical reactivity at 800°C of the electrolyte (YSZ) with the cathode LSMF, developed by thin layer magnetron sputtering, has also been studied by S.I.M.S., iron also played

an important role in the degradation of the interface, but greatly improved the mobility of oxygen vacancies. The optimization of the chemical composition and morphology of the cathode LSMF proposed was a strong point of this study.

II.4. Preparation and reactivity of interfacial oxide perovskites based on Lanthanum Strontium chrominum and Ruthenium (LSCrRu) as the anode materials for intermediate (IT-SOFC).

In the PhD work of L. Combemale [4], new data on the interest of ruthenium doped lanthanum strontium chromite $La_{1-x}Sr_xCr_{1-y}Ru_yO_{3\pm\delta}$ (LSCrRu) as an anode in IT-SOFC are presented. This also gives insights of micro wave synthesis of mixed oxides allowing shaping of half-cells and complete cells using sputtering and screen printing methods.

This work also deals with study and analysis of obtained powders as anode materials for IT-SOFC's with methane as fuel and its reforming property has been studied in mono-chamber system coupled with mass spectrometer.

A part of the work has been dedicated to study anode/electrolyte interfacial reactivity using SIMS and XRD on half cell model after ageing under H_2 at 800°C to obtain chemical composition of a film after heat treatment. The complete cells tested under working conditions, presents the selective dissolution of LSCrRu film, and also shows microstructure modification of anode/electrolyte interface which was not seen in XPS, SEM-EDX techniques.

II.5. Elaboration and characterization of $BaCe_{(0.9-x)}Zr_xY_{0.1}O_{3-\delta}$ as electrolyte material for Proton conducting fuel cells

The work of S. Ricote [5] dealt with the study of $BaCe_{(0.9-x)}Zr_xY_{0.1}O_{3-\delta}$ (x=0.3, 0.7 and 0.9) as electrolyte for Proton Conducting Fuel Cells (PCFC). The powders were synthesized by

solid state reaction, and sintered to form dense pellets at 1700°C. Its chemical, morphological, structural, and mechanical characterizations were done on samples using, ICP AES, SEM, XRD, Raman and dilatometery techniques respectively.

SIMS, XPS and XRD studies showed the insertion of protonic species in the samples, when treated in a moisturized atmosphere. Water uptake experiments provided quantification of the proton content between 400°C and 600°C: the protonic concentration increases with increasing Ce content and with decreasing temperature. The DC conductivity measured in wet atmosphere was expressed as the sum of a p-type component, prominent at high oxygen partial pressure, and an ionic contribution. A study of conductivity isotope effect revealed a significant protonic conductivity at 500°C and 600°C. When the cerium content increases, the activation energy, determined from Arrhenius plots of conductivity, increases and the resistivity of the grain boundaries decreased compared to that of bulk.

III. Contribution of this PhD thesis

The work presented here is the knowledge of the phenomena, obtained during the development of new simplified fabrication process of planar IT-SOFC with large active area. The development, optimization of the new simplified process [6] to achieve a large area planar cell, their limiting factors and difficulties in obtaining the cells will be discussed. The ultimate goal is to i) prepare large planar cells of active area 25 cm^2 in first instance. ii) Build a new test bench for adapting this geometry, iii) testing their electrochemical performance.

The new fabrication process, its optimization partly with respect to factors such as i) pore formers, ii) thickness of layers, iii) Optimization of sintering temperature are discussed.

The long term ageing performances in real time working conditions were studied and its results are presented. The products required and process involved in developing the new test bench and stack are described.

III.1. Fundamental Objectives

The fundamental objectives are:

- Fabrication of large active area planar cells by simple and cost effective process for stacking ;
- Obtaining 400 $mW.cm^{-2}$ for large area cells ;
- Studying long term ageing performance of single cell under real working conditions
- Building a new test bench to fit the stack geometry;

III.2. Synopsis of Manuscript

The manuscript is divided in three main chapters. The first chapter deals with a general introduction which briefly presents the history of energy consumption and the necessity to use fuel cells. It gives insights of different types of fuel cells, and their working principles. It also explains the materials used, its selection criteria as an anode, cathode, an electrolyte, an anode functional material, for IT-SOFC application; the different fabrication process used in the preparation of fuel cell.

The second chapter describes the synthesis of nano, bulk materials of cathode and electrolyte required for the work. It gives detailed study of the new fabrication process for obtaining planar cells with large active area. The brief insights about the progress, difficulties

faced, the optimization of single cell to achieve higher performance, and its supporting electrochemical results are discussed.

The third chapter deals with regards to the preparation of test bench. It gives information's of stack preparation and test bench preparation, like materials needed and used. It also throws light on long term ageing test results obtained.

The last part will deal with conclusions and perspectives of this work.

Chapter 1: Presentation of fuel cells as an energy transformer

Part I. General Introduction

I. The challenge of climate changes

Since the beginning of an epipaleolithic age, the development of industries from the nomadic people has led to committal of energy for different purposes. This need for energy has boosted with the different groups of people, and started increasing exorbitantly with the ages. Due to the increase in population and the development of modern civilization, this change has been accompanied with exponential increase in demand for energy and power needs from the people. From then, people have started using variant sources of available energy within easy reach. Vast supply of energy needs was fulfilled by combustion of fossil fuels and woods since industrial revolution [7]. People started to exploit coal and crude oil at a rapid rate which is cheap compared to renewable energy sources. With the development of science and technology and industrial modernization and globalization in the modern era, the energy consumption boomed very high and leads to new inventions. The Figure I.1 shows the electricity consumption in different regions of world from the time scale ranging from 1980 to 2030 [8]. This figure depicts the electricity consumption in Asia region which is expected to be doubled in the coming decades. The increase of electricity needs from other parts of world is also shown in the Figure I.1.

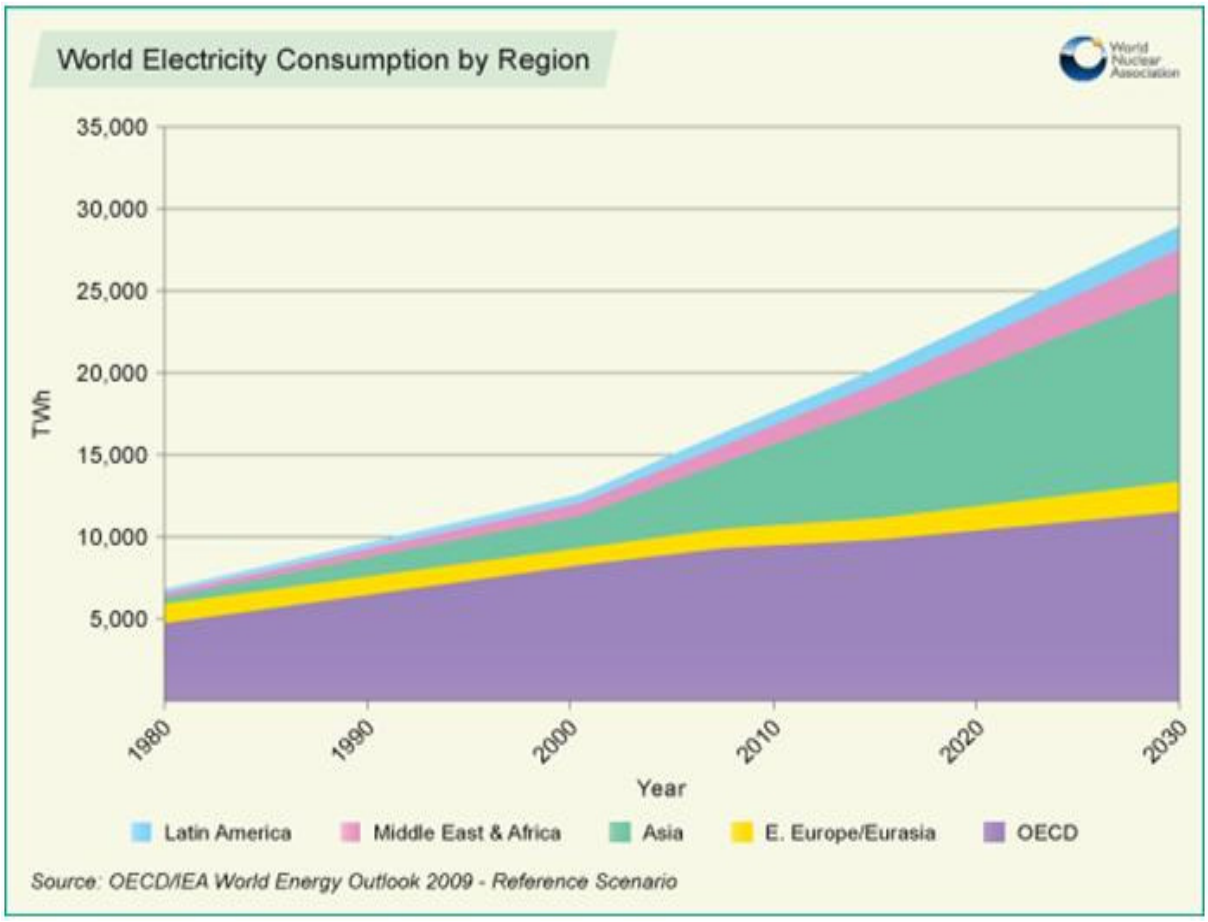

Figure I. 1 Graph showing electricity consumption in Terrawatthour Vs different parts and decades around the world [8]

Heat engines, power plants which produce necessary energy and electricity have started using fossil fuels to larger extent which in turn leads to rapid consumption and utilization rate of non renewable energy sources such as fossils fuels. Figure I. 2 shows the electricity generation in Twh (Terrawatthour) by different types of fuels. From the Figure I.2 it is clear that until, now the majority of electricity is produced by burning fossil fuels in power plants. The major atmospheric pollution arises due to the burning of fossil fuels to produce electricity.

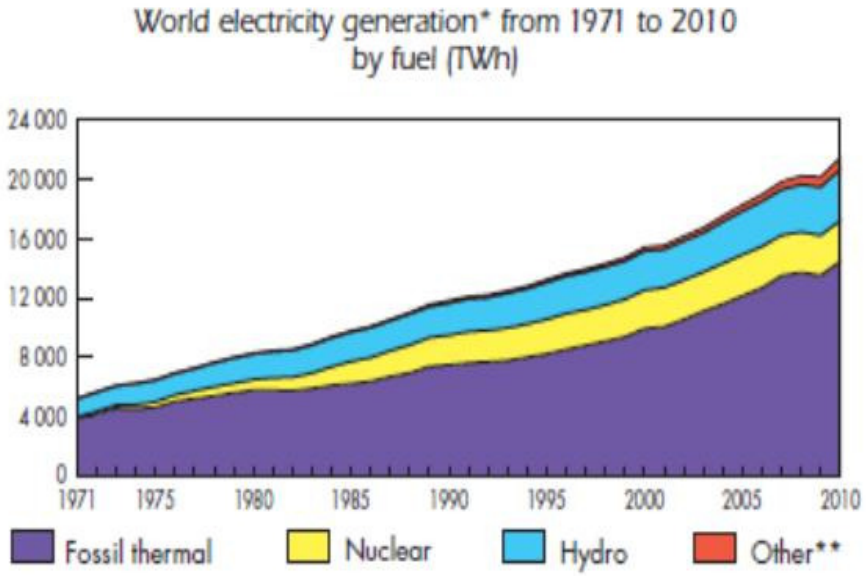

Figure I. 2 World electricity generation by different fuels [9]

So from the above graph it is also evident that fossil fuel demand increase greatly for the electricity generation. Due to this reason, there is an ecological imbalance like depletion of fossil fuels. This adds to significant increase in the contribution and concentration of carbon di-oxide with other green house gases (GHG) in atmosphere. This increase of GHG ratio in atmosphere causes series of problems including atmospheric pollution, large impact on global warming, climate change and health hazards of human kind, which has a moderate effect in the present generation but is expected to have a drastic effect on the future generations to come. Figure I.3 pie chart shows the energy supply from different sources. It is evident that during the development of technology, the dependence of fossil fuels was slowed down from 86.7% in 1973 to 81.1% in 2010 [9].

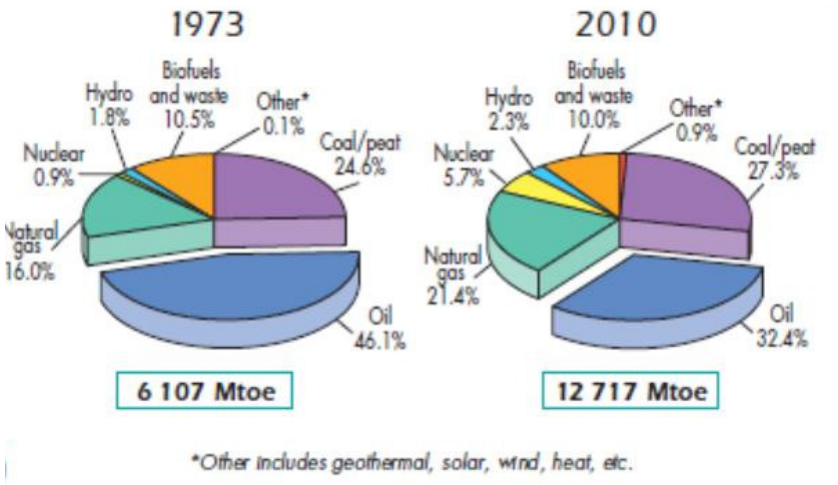

Figure I. 3 World energy supply from different fuels [9]

The Figure I. 4 shows CO_2 emissions in metric tons with respect to decades of the 20th century. It shows that whatever the type of fossil fuels being used, there is always emission of carbon di-oxide, and it's always been increasing exponentially. From the statistics one can observe about 88% increases of CO_2 emissions from 15 to 29 Gtons to atmosphere by combustion of fossil fuels between 1971 and 2010. The duty to preserve ecological balance and improve the quality of living for present and future generation is left to people and especially to researchers. Due to increase of green house gases in atmosphere, there is gradual increase of world temperature.

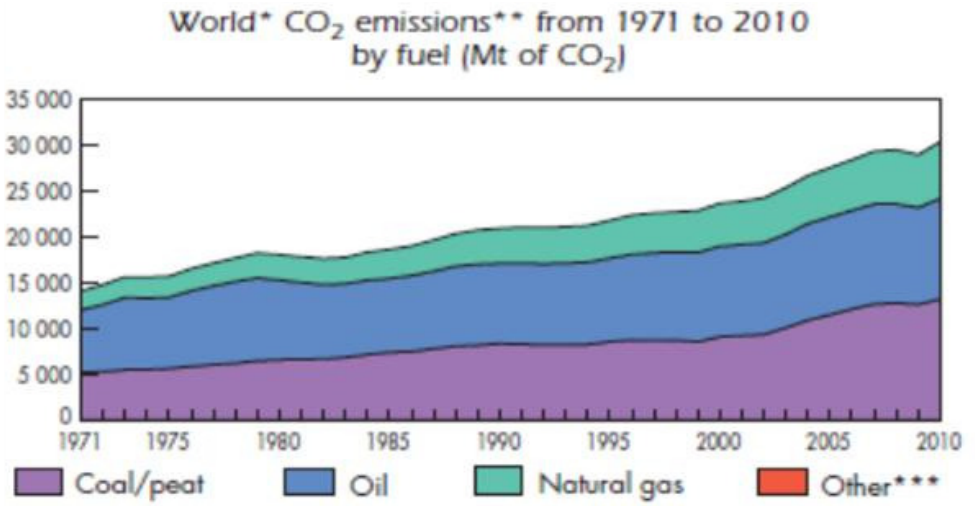

Figure I. 4 Emissions of CO_2 in metric tons by different types of fossil fuels with respect to time [9]

From Figure I. 5, it can be seen that during spring season from 1990-2010, there is a continuous increase of temperature from 1°C to 2°C in major parts of world. Worst is the difference of 5°C which is also seen in some parts, leading to the melting of glaciers and the increase of the sea level which in turn leads to submerging of lands close by the sea.

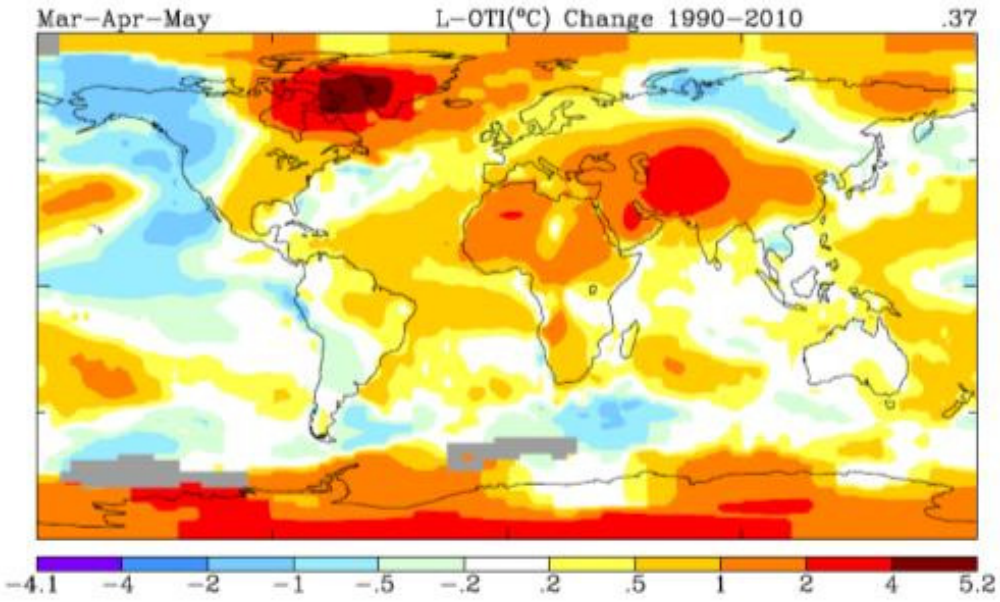

Figure I. 5 Temperature difference during spring from 1910-2010 across world [10]

II. Need for alternative energy.

Using fossil fuels leads to depletion of these resources, and create ecological imbalance in reserves and the increase of green house gases in atmosphere. This in turn affects the increase of atmospheric temperature gradually, thus leading to the melting of glaciers which automatically increase the sea level causing coastal areas to submerge. GHG also affect mankind badly with respect to health hazards. So all this detrimental effects to atmosphere and mankind suggests that there is a urgent need for researchers to save fossils fuels for the future generations, also to save present and future generations from all possible adverse effects.

The hard work of researchers and scientists have left us in the present stage of extensive and deep research on alternative energy fuels, renewable energy conversion, its storage, and usage of highly efficient systems.

The alternative energy research has been carried out for many decades on different fields like wind energy, nuclear energy, hydrothermal energy, solar energy, geothermal energy, biomass energy, marine energy and electrochemical energy. Among them, electrochemical energy has been widely spread due to the availability of raw materials in lab scale that can be commercialized into variety of household, portable and industrial applications. Interest in fuel cells started growing steadily with the realization of questions of how to provide electrical energy for supporting world growing energy economy without pollution. Today's fuel cells have an answer to all the questions and have an immiscible power to supply part of world energy needs for the future in case of oil crisis. This also has a great advantage concerning energy

efficiency, and environmental factors. Since fuel cell system has high efficiency, they are highly promoted for research among their peer systems as explained below. In Figure I. 6, it can be seen that the efficiency of fuel cells systems are quite high compared with present generation of power plants systems and also leaves fewer carbon print to environment.

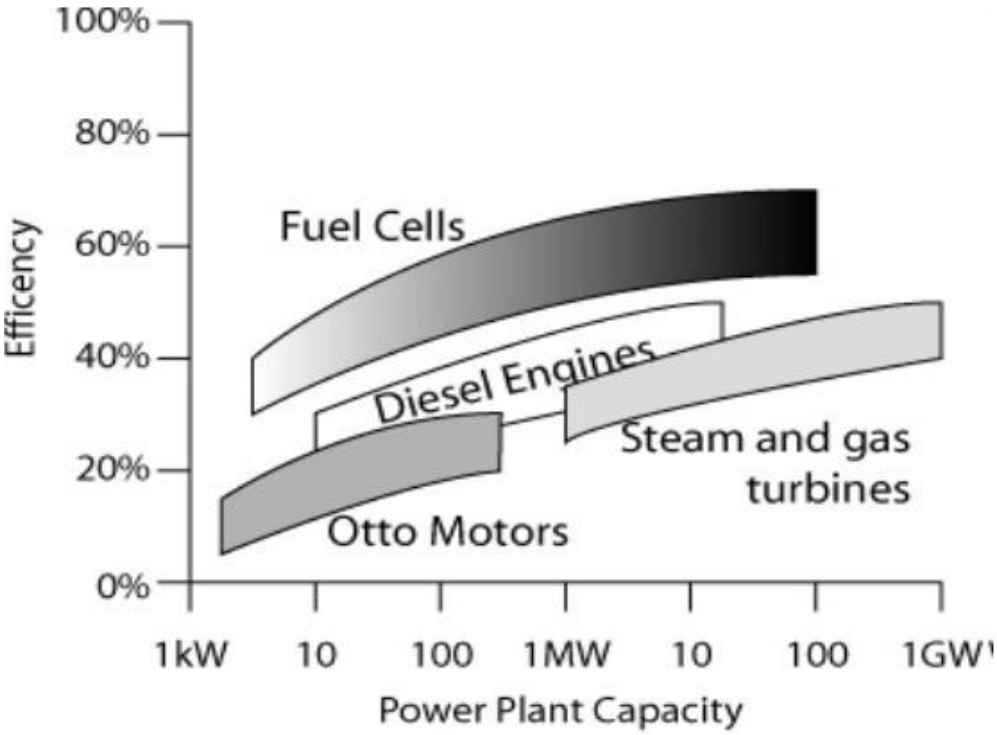

Figure I. 6 Efficiency comparison of fuel cells with other power plants [11]

The challenges for fuel cells are decreasing its high initial cost, increasing their reliability and durability. Prospects for commercial applications of fuel cells are gaining slow momentum, largely driven by significant technological advances and expectations. This enables different governments including European Union and around the world to consider turning to fuel cells for practical foundations and implementing public policies responding to provide safe environmental conditions and clean energy for its people.

III. History of fuel cell, its types and working principles

III.1. History of fuel cells

In early 1839, Sir William Robert Groove, a welsh judge and physicist was the first to discover the operating principles of fuel cell by reversing the electrolysis of water to produce electricity by introducing hydrogen and oxygen. Few decades later, the name was coined as fuel cells in 1889 by Ludwig Mond and Charles Langer who build big working fuel cells which gave enough electricity by using air as oxidant and industrial coal gas as fuel. Some are also claiming that William White Jacques was the one to define the term fuel cells. The serious research in the field of fuel cells took place nearly after 100 years of initial proposal of fuel cell operating principles.

"Fuel cell is an electrochemical device that continuously converts chemical energy to electrical energy as long as fuel and oxidant are supplied" [12].

In 1920, fuel cell research in Germany has opened the gateway of carbonate cycle and Solid Oxide Fuel Cells (SOFC) of today. In 1932, Francis T. Bacon started an extensive research in the field of fuel cells. After almost three decades, he demonstrated 5 kilowatt (kW) fuel cell and named it as "Bacon cells". During early 1960, General Electric power has designed fuel cell system that powered NASA's Gemini and Apollo space shuttles. These also had an additional advantage by supply water to the crew members.

During the same decade Baur and Pries, in 1937 [12], developed SOFC. They investigated ceramic materials as electrolyte from 1050°C to 1100°C, which showed high resistance due to its large volume in the system. Series of compositions was tested and the term "Nernst mass" was coined. It is a mixture of 85% of ZrO_2 and 15% of Y_2O_3, which exhibited the least resistance among the different compositions studied. In 1962, Ruka and Weissbart from Westinghouse Electric Corporation developed tubular SOFC with 85% ZrO_2 and 15% CaO as an electrolyte, porous platinum as electrodes. From then there is continuous research and developments taking place with SOFC technology to make it commercially viable and reliant systems for power generation.

III.2. Fuel cell Types

Scientists and researchers have designed many different types and sizes of fuel cells in search of higher efficiency. The technical insights of each kind vary. Mainly fuel cell developers are constrained by the choice of electrolyte. The selection of materials for electrodes depends on electrolyte. Today, the main electrolyte types used in fuel cells are alkali, molten carbonate, phosphoric acid, proton exchange membrane, direct methanol, and solid oxide. The first three types use liquid as an electrolyte; last three use solid electrolytes: proton exchange and direct methanol using polymer as an electrolyte and solid oxide using ceramic material as an electrolyte respectively. The type of fuel to be fed depends on electrolyte, and also on working temperature. Some types need pure hydrogen for example, polymer electrolyte is very sensitive to impurities, hence it requires pure hydrogen. Solid oxide (ceramic electrolyte) can handle minor quantities of impurities since its operating temperature is very high around 1000°C. Liquid electrolytes circulate in alkali fuel cells, which require pumps. The type of electrolyte also dictates the

operating temperature of cells, for instance “Molten” carbonate run hot, just as the name implies. The operating temperature of this type is around 600°C.

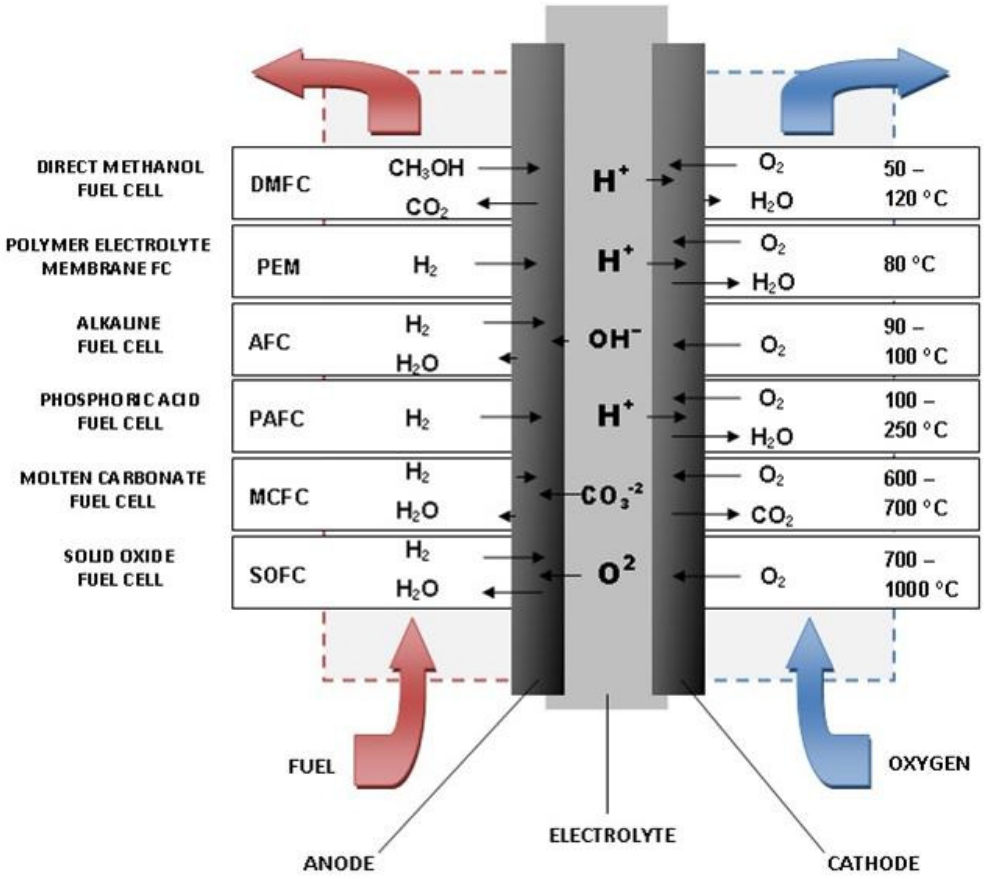

Figure I.7 Different fuel cells with its corresponding operating temperature and its reactions [13].

The Figure I.7 explains different types of fuel cells, their operating temperature and conducting ions involved in each type of cells.

In this study, SOFC is of main interest.

Solid Oxide Fuel Cells: This type of fuel cells uses hard ceramic compounds like calcium or zirconium oxides as electrolytes. Efficiency of this type of systems is about 60% and 85% in cogeneration and its operating temperature varies from 500°C to 1000°C. Stack output are up to

100 kW. At such high temperature a reformer is not mandatory to extract hydrogen from the fuel in case of usage of hydrocarbons. The waste heat can be recycled to make additional electricity and improve efficiency of systems. However, the high temperature limits the applications of SOFC units, and also it will be large in size to accommodate in transportation systems. The cells operated in range of temperatures from 500°C to 700°C are called as an IT-SOFC which uses doped cerium oxide as their electrolytes.

III.3. Motivation to choose SOFC and IT-SOFC

SOFC's are unique systems among its peers, which have an ability to use wide range of fuels like biogas, gasoline, hydrogen, jet fuel, natural gas, or any other oxidizable fuel for its operation. These systems have been very prolific in doing this with high electrical efficiency of about 50-65% in lower heating value of fuel (LHV), and for cogeneration systems with combined heat and power efficiency is expected to reach 80-90% [14]. Further combined heat and power generation systems demonstrated in 2009 by Japan new energy foundation achieved 70% efficiency under working conditions, which is generally twice of fossil fuel power plants that can be confirmed from Figure I. 6 [15]. This is possible because of low exergetic losses with SOFC's [16].

Furthermore SOFC have the highest gravimetric and volumetric energy density of any energy technology. This can be seen from Figure I.8 [17].

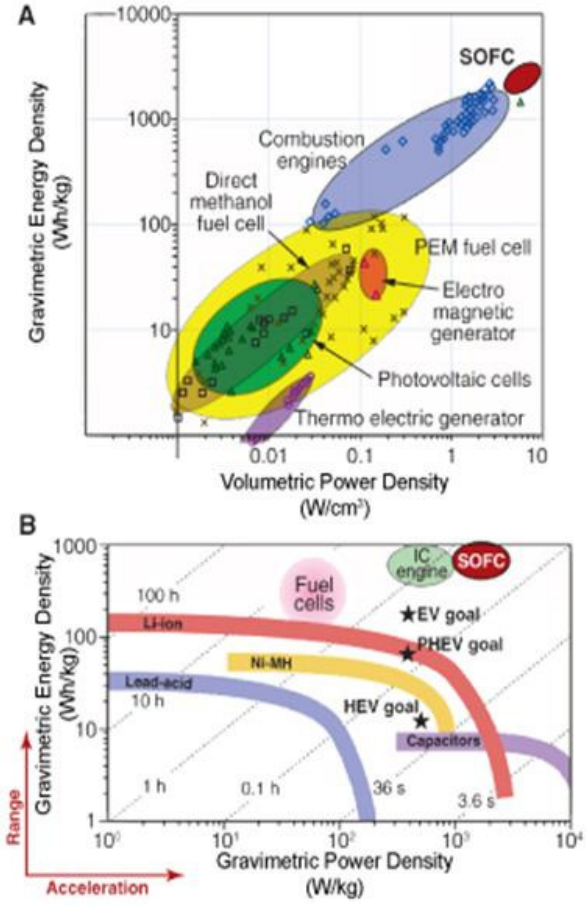

Figure I. 8 Graphs showing highest volumteric and gravimeteric enerygy density among its peers [17]

The other major reason for choosing SOFC is that, it is reliable for long term, this was recently demonstrated in FZ Julich for 40,000 hours (5years) with lowest possible degradation[18]. High efficiency is directly related to reduced costs for heat, power and possible extension of fossil fuel reserves for future generation. SOFC's don't produce sulphur and nitrogen oxide by burning fossil fuels, so SOFC are highly attractive as, clean, almost non polluting source of energy and it also reduce health related expenditure of common people. The

effluents of SOFC's operating with hydrocarbon contain humidified CO_2, and thus it can be used in CO_2 capturing technology, reducing the green houses gases emitted in to the atmosphere.

SOFC's can easily adopt any fuel supply. They also serve as secure and reliable stationary application in remote places, that can be used as clean and continuous power sources with lower emissions compared with other energy sources. Since SOFC's can be easily adapted as stationary application source, as they tend to reduce the transmission losses caused in long distance transmission of electricity [19].

SOFC's does not need noble metals for operation, high quality of exhaust heat is useful for cogeneration in large scale. They do not have problems with electrolyte management and electrolyte losses are eliminated. In case of liquid electrolyte, they can cause corrosion which is not seen in SOFC.

All the other power plants be it, a thermal power plant, solar power plant, hydro powerplant, wind power plant, requires huge volume of land areas for large group of population. SOFC's use much smaller land areas compared to the others and thus helps in cost savings with related to land. Other thermal power plants needs huge quantity of water for cooling purposes where as the amount of water used for SOFC's are quite low, thus helping in water conservation and cost related to it [20].

SOFC's are fuel flexible, they can reform methane internally when using carbon monoxide as a fuel. This internal reforming is heat absorbing reaction where it tends to cool the

stack and module, which can pave the way to reduce power supply needed for reforming. SOFC's are partly tolerant to sulphur impurites in fuels supply, thus helping it to adapt to present commercial desulphurization process.

SOFC's have the modularity characteristics, means these can be easily increased or decreased in size. Thus SOFC modular cells can be tailored to any size, according to the requirements. Since the efficiency of fuel cell is relatively independent of size, it can be easily designed to follow loads quickly without much efficiency loss at part load operations.

With the ability to produce in modular sizes, they can be easily placed in different locations with minimum sitting requirements. They don't have moving parts, so the operation of SOFC is quiet, the acceptable sound arises only from auxillary equipments. Consequenly this makes it suitable to adapt them in its work places directly such as residential areas, malls, offices.

Even with various advantages of SOFC, the elevated operating temperature of conventional SOFC (800°C-1000°C) imposes its own limitations in selection of choice of materials, its compatibility to use in large scale and implementation of expensive materials for short life time. This results in new research interest in the same field with respect to reduction of operating temperature, while maintaining all its advantages like high power density, high efficiency and usage of different fuels. Generally from conventional operating temperatures (800°C-1000°C) it is reduced to intermediate range of (500°C-700°C) and called as Intermediate-Temperature Solid Oxide Fuel Cells (IT-SOFC). This reduction of temperature

adds more advantages like reduction cost of selection of materials. By this way it enhances the possibility of commercialization, like the reduction of the cost of the whole system. It also increases its durability by reducing the possible degradation of materials caused in reaction at high temperature and interdiffusion. This IT-SOFC solves the problem of thermal cycling and increases the overall performance of the system. On contrary reducing the operating temperature reduces the ionic conductivity of electrolytes resulting in fewer cell voltage and power. Thus for facing effective commercialization of IT-SOFC, the main challenges like the selection of right materials, and a cost effective fabrication process should be addressed.

Part II: Fuel cells working principles, Materials and Techniques used

I. Solid Oxide Fuel cells working principles

Fuel cells are devices which generate electricity, provided the fuel gases are supplied continuously. All SOFC's has three parts namely, porous positive electrode called cathode, porous negative electrode called anode and dense electrolyte. The fuel, oxidants are passed through anode and cathode respectively. In case of IT-SOFC the fuels can be hydrogen, or hydrocarbons and oxidant can be air or oxygen. In this case, hydrogen was taken as fuel and air as an oxidant. These two gases are separated by dense electrolyte in the cell. In cathode side where air is supplied the catalytic activity of the cathode itself dissociates and reduce the adsorbed oxygen to form oxygen ions. These oxygen ions pass through ionic conducting electrolyte to the anode side where oxidation takes place, thus reducing the incoming hydrogen to form water and releases electrons. The presence of electrons in anode side creates higher electronic potential at one end and creates a potential difference between two electrodes causing passage of electrons through the external circuit producing electricity. This way of producing electricity from chemical reaction is called an electrochemical reaction. The schematic and working principle of SOFC is shown in Figure I. 9.

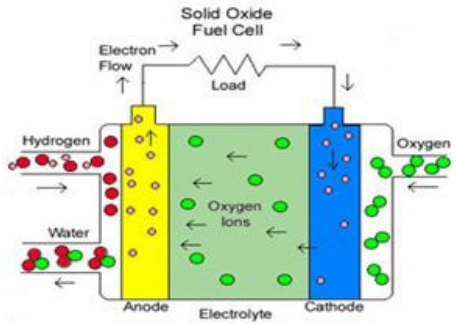

Figure I. 9 Schematic and working principle of SOFC

The cell reaction taking place at the cathode, reduction of oxygen gas, is given by equation 2.1

$$(1/2)O_{2(g)} + V_O^{\bullet\bullet} + 2e^{'} \Rightarrow O_O^X \quad (2.1)$$

The cell reaction taking place at the anode, reduction of hydrogen, is given by equation 2.2

$$H_{2(g)} + O_O^X \Rightarrow H_2O_{(g)} + V_O^{\bullet\bullet} + 2e^{'} \quad (2.2)$$

The overall cell reaction is given by equation 2.3

$$H_{2(g)} + 1/2\, O_{2(g)} \Leftrightarrow H_2O_{(g)} \quad (2.3)$$

The maximum electrical work which can be produced from an electrochemical cell at standard temperature and pressure is given by change in the Gibbs free energy ΔG°

$$\Delta G^\circ = - nF.E^\circ \quad (2.4)$$

n is number of free electrons, F is Faraday's constant 96485 $C.mol^{-1}$. E° is the reversible potential of the cell considering standard state for reactants and products at (25°C, 1 atm).

Considering a cell reaction

$$aA + bB \Rightarrow cC + dD \quad (2.5)$$

The Gibbs free energy of a reaction at standard condition can be given by

$$\Delta G = \Delta G^\circ - RT \ln \frac{[c]^c[D]^d}{[A]^a a[B]^b} \quad (2.6)$$

Substituting equation 2.4 in equation 2.6 gives

$$E = E^\circ - \frac{RT}{nF} \ln \frac{[C]^c\ [D]^d}{[A]^a[B]^b} \quad (2.7)$$

This shows that potential of a fuel cell can be directly related to concentration of products and reactants.

The concentration which contributes to chemical activity is also related to partial pressures of gases. In case of hydrogen and oxygen fuel cells, 2 electrons are involved and the equation can be written as

$$O_2 + 4H^+ + 4\,e^- \rightleftarrows 2\,H_2O \qquad (2.8)$$

equation 2.8 another represention of linear combination of equation 2.1 and 2.2 where E° =1.23V

$$E = E° + \frac{RT}{2F} \ln \frac{PH_2 . P(O_2)^{\frac{1}{2}}/}{P(H_2 o)} \qquad (2.9)$$

The equilibrium voltage or open circuit voltage (OCV) is the one at which there is no net current flowing through the cell.

R is the universal gas constant 8.3144 $J.mol^{-1}.k^{-1}$. T is temperature, P_{O2} is the partial pressure of oxygen at cathode and P_{H2} is the partial pressure of hydrogen. The OCV at ideal conditions for pure hydrogen and oxygen is 1.23 V. The obtained equilibrium voltage will be less compared to theoretical OCV due to losses. The equilibrium voltage obtained generally decreases with increasing temperature, and the cell is more efficient at higher temperature due to lower electrical losses.

II. Deviation from theoretical to actual performances

Fuel cells are not subjected to Carnot limitations, they have three times higher efficiency compared to internal combustion engine. At higher temperature of about 900°C their efficiency reaches to 70%, when it is connected to external devices, the internal resistance increases and potential decreases due to various phenomena occurring at the cell.

They can be explained by the following picture (see Figure I. 10).

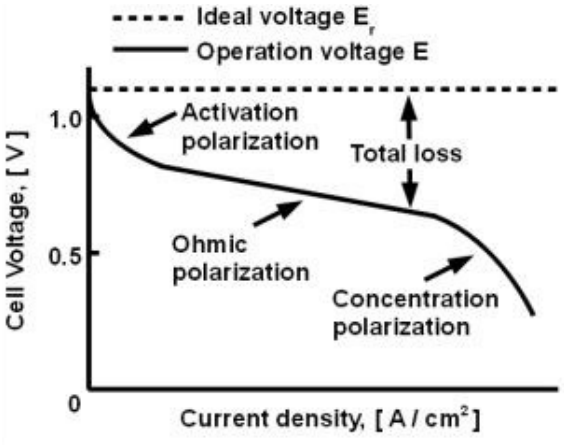

Figure I. 10 Graph showing different losses in actual performance of cell

II.1. Activation polarization or charge transfer polarization

For chemical and electrochemical reaction to occur, the energy barrier has to be overcome by the reacting species. This activation energy or energy barrier results in activation polarization or charge transfer polarization. Generally, this is irreversible loss; a part of energy is spent on stepping up the required rate of electrochemical reaction from slow rate of reaction as per required current. This is related to current densities and it is denoted by η_{act}. For electrochemical reaction η_{act} is approximately 50-100mV, a is the charge transfer coefficient, i is the current density and i_0 is exchange current density.

$$\eta_{act} = \frac{RT}{anF} ln \frac{i}{i_0} \qquad (2.10)$$

II.2. Ohmic or Resistance polarization

The resistance of ions through electrolyte, the resistance of electrons through electrodes, current collectors and the contact resistance between different cell components create ohmic resistance. This can be reduced by decreasing the thickness of an electrolyte and also by

improving the conductivity of electrolyte materials. All the electrolyte and electrode materials undergo ohmic losses quoted η_{ohm}. The ratio of ohmic loss to current is given by

$$\eta_{ohm} = I.R \tag{2.11}$$

Where I is current and R is total ohmic resistance of the cell (ionic+contact+electronic).

II.3. Diffusion or concentration polarization

The mass transport becomes a limiting factor when the flow of concentration of reactants or removal of products from the electrochemical sites is slower than the corresponding charging or discharging current. This occurs mainly due to concentration gradient and at higher current density; it can be reduced by using optimized electrode microstructures. It is denoted by η_{con}.

$$\eta_{con} = \frac{RT}{nF}\ln(1-\frac{i}{il}) \tag{2.12}$$

i_l is limiting current.

The actual voltage of the cell is given by

$$v = E - \eta_{act} - \eta_{ohm} - \eta_{con} \tag{2.13}$$

Even after the different losses it is still possible to have an efficiency ε of cell. The total efficiency of cell is given as the product of different efficiency related to different losses.

$$\varepsilon = \varepsilon_v.\varepsilon_f.\varepsilon_h \tag{2.14}$$

Where ε_v is voltage efficiency ε_f is fuel efficiency and ε_h is heating efficiency

ε_v is the ratio of actual voltage obtained to the OCV

$$\varepsilon_v = \frac{V}{E_{ocv}} \tag{2.15}$$

ε_h is the heating efficiency. It is the ratio of the amount of enthalpy of fuel species present in fuel to generate electricity ΔH^0 to total enthalpy of all combustible species in the fuel ΔH_m.

$$\varepsilon_h = \frac{\Delta H_0}{\Delta H_m} \tag{2.16}$$

ε_f is the fuel efficiency and also called as fuel utilization. This the ratio of fuel used in the process to fuel fed to the system.

$$\varepsilon_f = \frac{\text{Fuel used}}{\text{Fuel fed to the system}} \tag{2.17}$$

The total efficiency of SOFC system can give more than 60% electrical efficiency. The overall efficiency can reach to 85% in combined heat and power systems CHP.

III. Different designs of SOFCs

One of the main concerns related to effective commercialization of SOFC lies with its design. Recently, there are different designs of fuel cells which can be sub-categorized under two main designs namely planar and tubular. The tubular design was investigated and first put forward by Siemens Westinghouse Power Corporation in 1960's [21]. These cells are predominantly with diameter greater than 20 mm and length 1.5m. It was cathode supported cell fabricated by electrochemical vapor deposition. The air flowed through the cathode in the center of tube and fuel hydrogen in same direction but outside the tube. Dense electrolyte serves as a barrier between them. The main snags for this type of cells are high manufacturing costs, low power density and high polarization resistance compared to its planar peer. The Figure I.11 shows the tubular SOFC. Micro tubular SOFC are used for miniature electrical appliances. The only advantage of this type is using cheap sealing materials; it can also be used as seal less stack sometimes. They performed for 70,000 hours with 0.1% degradation per 1000 hours [22].

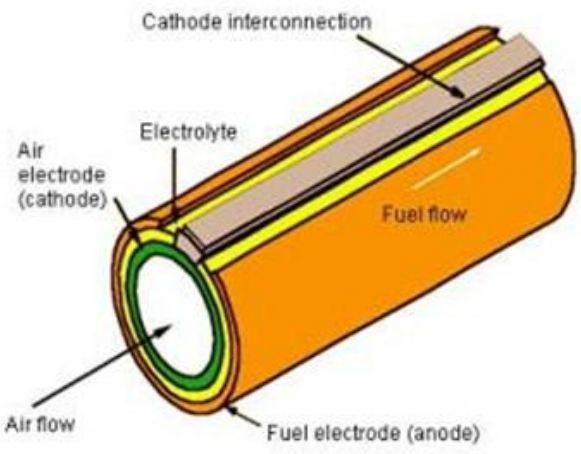

Figure I. 11 Tubular SOFC design [21]

In planar SOFC's the anode, cathode and electrolyte were sandwiched as flat plate which are connected in series. This type enjoys various advantages with its peer, like low polarization losses, high power density, ease of fabrication by conventional technique at low cost, provides negligible leakage through electrolyte and avoids short circuit.

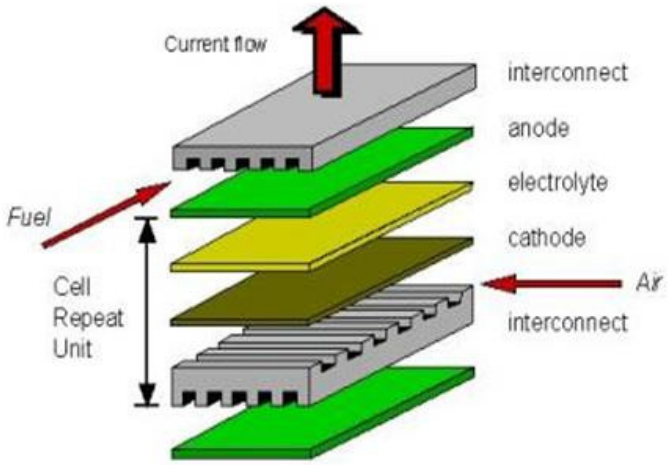

Figure I. 12 Planar SOFC design [21]

The Figure I.12 shows different parts of planar SOFC necssary to form a stack. The three major sub type of planar cell are rigorously studied.

i) Self supported or electrolyte supported cells (ESC): The electrolyte in these cells serves as mechanical support and on which electrodes are fabricated. The main disadvantages of these cells are higher resistance due to low conductivity of the electrolyte and higher operating temperatures are required to reduce its ohmic losses. Figure I.13 explains different types of planar cells.

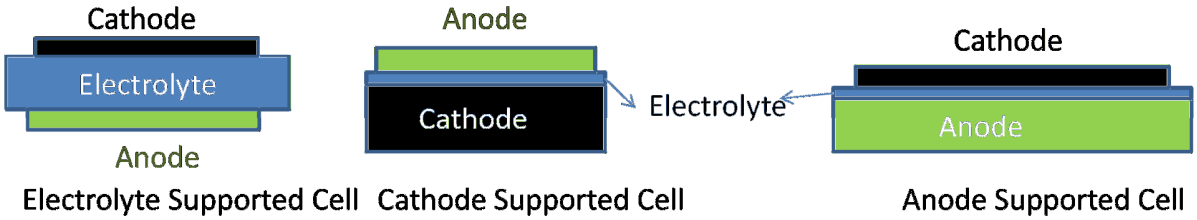

Figure I. 13 Different types of planar cells

ii) Cathode supported cells (CSC): In this type, cathode serves as mechanical support on which electrolyte and anode are fabricated. It enjoys low operating temperature by use of thin electrolyte and it suffers from low conductivity, high concentration losses due to thick cathode layer.

iii) Anode supported cells (ASC): This type of cells have high power density, low polarization losses, highly conductive anode, and low operating temperature by use of thin electrolyte. In this type, anode serves as mechanical support and also reduce the polarization losses occurring in the cells. Due to its advantages this type of cells is studied in detail and its fabrication process will be explained in later part of this thesis. From now on, the focus in this work will be towards only anode supported planar cells. All materials requirements and fabrication types will be choosen for ASC.

IV. Materials for IT-SOFC's

In the last four decades, SOFC is extensively studied for its greatest advantages like higher efficiency, low pollution, no noise, ability to use variety of fuels. The main challenge is to make it a strong competitor among the present energy technologies and as a reliable alternative energy source of the future to lead it to commercialization.

The main problems focused in research are to develop i) high quality conducting materials for electrolyte and electrodes, ii) reduce the cost of fabrication of cells, iii) increase performance at low temperature for thus making it available for transportation applications, iv) use of less expensive catalysts or no catalyst, v) reducing the degradation of cells and increasing their reliability, vi) modularity in design to adapt to consumer specification, vii) usage of low cost, toxic free sealants, coatings and interconnectors for stacks to reduce cost of systems.

There are different views in literature with respect to electrodes and electrolyte. The main requirements to choose different electrode and electrolyte materials are discussed below.

IV.1. Electrolytes

SOFC electrolyte is a solid non-porous ceramic oxide material possessing ionic conductivity and should conduct oxide ions through them. There are some specific characteristics that electrolyte should possess for its usage in SOFC. The general requirements are as follows:

1) It should be ionically conductive [23]

2) Electronically insulating,

3) Chemically stable at high temperature (500°C-700°C for IT-SOFC,800°C- 1000°C for SOFC) ,

4) Chemically stable in reducing and oxidising environments,

5) Should be as in expensive as possible,

6) Should be gas tight/free of porosity,

7) Their Thermal Expansion Coefficient (TEC) should match electrodes and corresponding contacting elements.

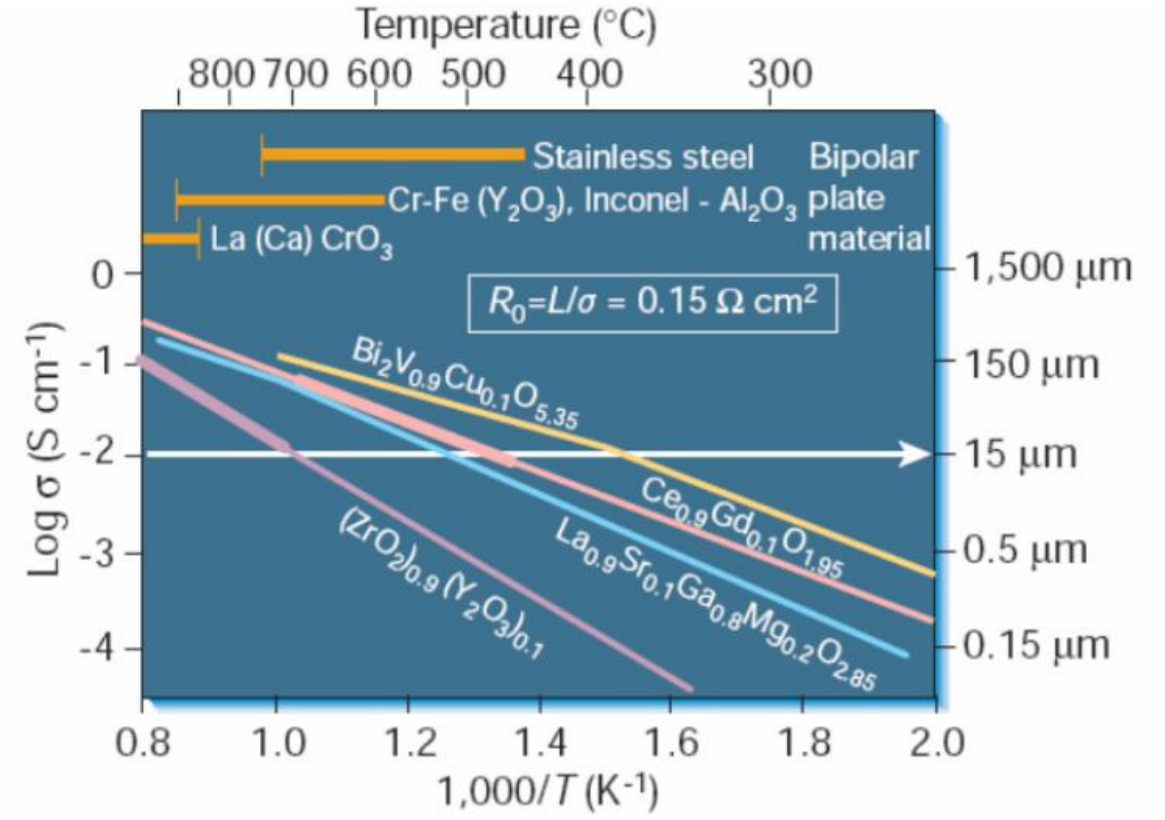

Figure I. 14 Evolution of ionic conductivity as a function of temperature for different electrolyte materials [13]

Figure I.14, shows the different possible electrolyte and its ionic conductivity at different temperatures. In SOFC, the operating temperature plays a major role in selecting electrolyte materials. Generally electrolytes for SOFC are classified under four categories namely i) fluorite

based materials (doped Zirconia oxide, Ceria oxide, Bismuth oxide and Pyrochlore materials), ii) perovskite based materials, and related growth structures (Lanthanum gallate, brown millerites, BiMeVOx), iii) Lanthanum based materials (LAMOX) and iv) apatites with general formula $[M_{10}(XO_4)_6O_2]$. For intermediate temperature (500°C-700°C) the electrolyte should be very thin of about 10-20µm to reduce polarization losses and it is generally fabricated on either anode or cathode substrate. The Figure 1.15 represents the specific ionic conductivity of electrolytes for intermediate temperature range.

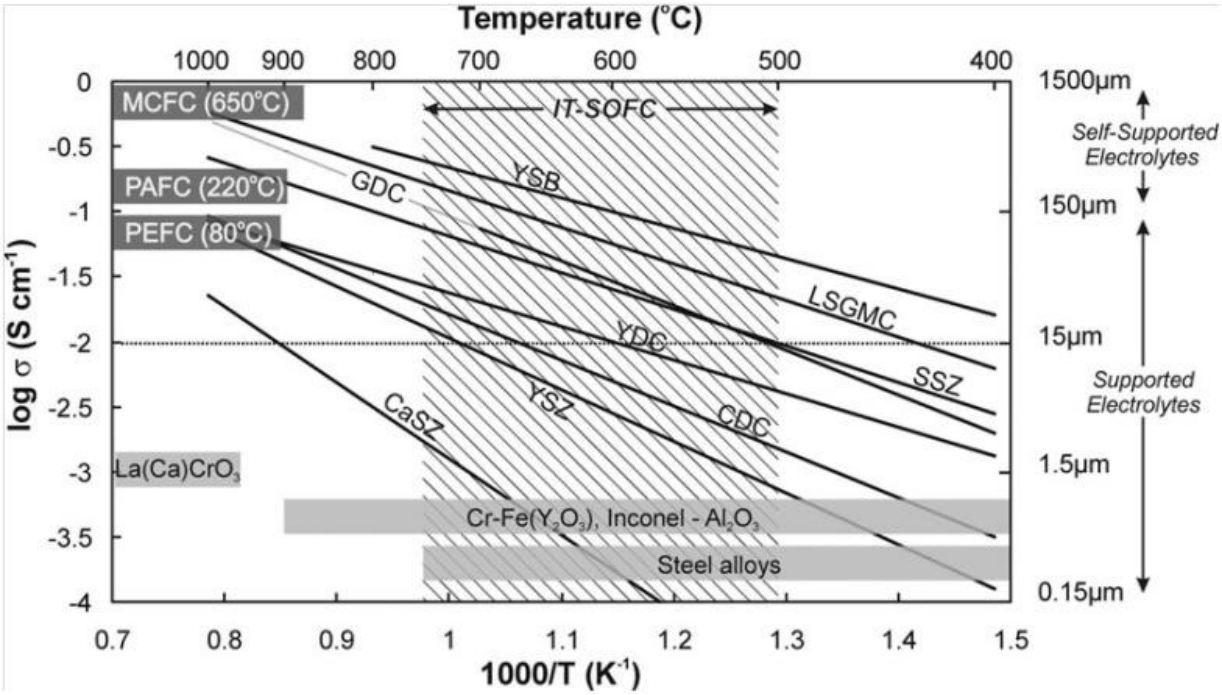

Figure I. 15 Specific ionic conductivity of electrolyte for IT-SOFC [24]

The values shown above are tending to change according to fabrication technique, sintering process, sintering temperature and the microstructure of the material. Generally fluorite materials are doped like Zirconia with Scandia but it's costly. Yttria Stabilized Zirconia (YSZ)

exhibits best performance in operating temperature range of 800-1000°C and present compromise between price and performance. Normally, 8% doped YSZ possess ionic conductivity ranges between 5.0 x 10^{-2} S.cm^{-1} and 6.2 x 10^{-2} S.cm^{-1} at 800°C and 600°C [25]. Replacing yttria by scandia gives higher ionic conductivity than YSZ but yttria is more commonly available and low cost material compared to expensive Scandium. This zirconia doped materials tends to react with lanthanum based cathode and hence while using them in a cell, a barrier layer between electrolyte and cathode is necessary. It results in low ionic conductivity at intermediate working temperature range.

Doped ceria discovery was exciting and it helped to reduce the operating temperature, and it was sufficient to replace YSZ for the intermediate temperature range. Gadolinium Doped Ceria (GDC) has the highest ionic conductivity at temperature range of 500-650°C, thus making it the best suitable candidate for IT-SOFC. The conductivity of $Ce_{0.8}Gd_{0.2}O_{1.9}$ is 6.5 x 10^{-2} S.cm^{-1}, 1.3 x 10^{-2} S.cm^{-1} at 800°C and 600°C, respectively [26-32]. The other available doped ceria's are Yttria Doped Ceria (YDC) [33], Samarium Doped Ceria (SDC) [34], but their conductivities are lower than GDC. The ceria based electrolytes have some instability and suffers from partial reduction of Ce^{4+} to Ce^{3+} at low partial pressure of P_{O2} at temperature above 650°C. The anode degradation also affects this type of electrolyte material and cause lattice expansion, creating micro cracks in the electrolyte, thus in turn reduces the OCV. Sometimes these cracks also cause short-circuit of cell by electronic conduction through them, and make the cell dead completely.

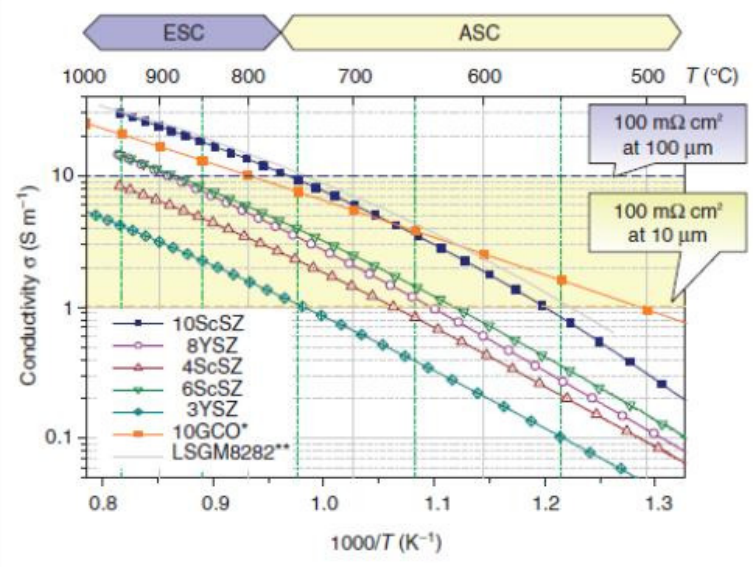

Figure I. 16 Ionic conductivities for anode support and electrolyte supported cells

The Figure I.16 shows ionic conductivities of different electrolytes suitable for electrolyte supported cells and anode supported cells.

To address the problem of choosing the best ceria electrolyte for intermediate range, investigations were carried on doping levels, maintaining high ionic conductivity at low temperatures. $Ce_{0.9}Gd_{0.1}O_{1.95}$ (GDC10) was chosen as an ideal candidate for IT-SOFC operation. The other perovskite materials such as lanthanum gallates doped with strontium and manganese [$La_xSr_{1-x}Ga_yMg_{1-y}O_3$ (LSGM)] were also studied as an alternative to YSZ. These materials exhibited higher ionic conductivity than YSZ and GDC, the ionic conductivity of $La_{0.8}Sr_{0.2}Ga_{0.8}Mg_{0.2}O_3$, (LSGM) at 800°C was found be to $0.1 S.cm^{-1}$ [35], it has the lowest possible electronic conductivity at low partial pressures of oxygen and good chemical stability. However, they are very expensive compared to YSZ and GDC. They can give best possible results only when operated below 400°C, they are not stable in reducing atmospheres of

hydrogen, and they have parasitic reactions with NiO forming $LaNiO_3$[36]. Lanthanum based materials of LaMOx ($La_2MO_2O_9$) materials were investigated. Various substitutions have been studied in this family to have stabilized material at room temperature with good conductivity; they proved to have low stability at low partial pressures of oxygen, they are reduced partially creating electronic conductivity [37, 38].

The apatites which have good ionic conductivity at moderate temperatures were also one among the candidates for electrolyte. Their general formula is $M_{10}(XO_4)_6O_2$, where M is rare earth metal or alkaline earth metal and X corresponds to P, Si, Ge. Lanthanum silicates has highest and purest ionic conductivity in wide range of oxygen partial pressures, their main problem relates to requirement of sintering temperature above 1600°C to achieve dense electrolyte. Their conductivity is based on interstitial oxygen ions compared to oxygen ion vacancies in fluorite and perovskite based materials [39-41]. They are best suited for operating temperature below 600°C [36].

The planar type design of anode supported cells exhibit the best performances. The thickness of electrolyte on this type should be in the range of 10-20µm, to have the lowest possible ohmic resistance. The table I.1 throws light on TEC values of different solid electrolytes in air condition which can be used to obtain good thermo mechanical stability of cells.

So, for obtaining the best results for working at intermediate temperature GDC10 ($Ce_{0.9}Gd_{0.1}O_{2-\delta}$) was chosen as an electrolyte in this study to match with TEC of its adjacent materials. From now on the focus will concentrate majorly on GDC10. The density studies of

GDC10 have been conducted in this work, by varying their sintering temperature to obtain best possible density in cell to give higher performance of cell.

Electrolyte composition	TEC $*10^{-6}K^{-1}$	T(K)
$Ce_{0.9}Gd_{0.1}O_{2-\delta}$ [42]	13.4± 0.1	300-1100
$Ce_{0.85}Gd_{0.15}O_{1.925}$ [43]	11.6	
$Ce_{0.80}Gd_{0.20}O_{2-\delta}$ [42]	11.8±0.1	300-1100
$Ce_{0.80}Gd_{0.18}Pr_{0.02}O_{2-\delta}$ [44]	11.5+0.1	300-1050
$Ce_{0,8}Sm_{0,2}O_{1,95}$ [28, 45-47]	8-10	300-1273
$Ce_{0.83}Sm_{0.17}O_{1.915}$ [48]	8.6	
$Ce_{0.8}Sm_{0.12}O_{1.9}$ [49]	11.4	300-1173
$Ce_{0.8}Sm_{0.1}Mg_{0.1}O_{2-\delta}$ [50]	12.34	473-1073
$Zr_{0.9}Y_{0.1}O_{2-\delta}$ [51]	11	300-1273
$Zr_{0.92}Y_{0.08}O_{2-\delta}$ [52]	10	300-1273
$Zr_{0.85}Y_{0.15}O_{2-\delta}$ [51]	10.9	300-1273
$La_{0.9}Sr_{0.1}Ga_{0.8}Mg_{0.2}O_{2.85}$ [53]	11.6	300-1273
$La_{0.8}Sr_{0.2}Ga_{0.8}Mg_{0.2}O_{3-\delta}$ [53]	11.4	300-1273
$La_{0.8}Sr_{0.2}Ga_{0.76}Mg_{0.19}Co_{0.05}O_{3-\delta}$ [54]	12.7	300-1473
$La_{0.9}Sr_{0.1}(Ga_{0.9}Co_{0.1})_{0.8}Mg_{0.2}O_{3-x}$ [53]	13	300-1273

Table I. 1 Different electrolytes and their TEC values

IV.2. Anodes

One of the main advantages of SOFC over PEMFC is their fuel flexibility. SOFC's can be operated with different fuels such as hydrogen, carbon monoxide, hydrocarbon fuel like natural gas and gasified coal. Anode is the place in SOFC where electrochemical oxidation of fuel takes place. Then it transfers electrons to external circuit through a conducting wire in a single cell and for terminal cell in stack. The general characteristics that anodes for SOFCs should possess are listed as

1) Good electronic conductivity [23],

2) Chemical compatibility and stability in reducing environment,

3) TEC must match other components of cell, like electrolyte and interconnectors,

4) Should be inexpensive materials,

5) Should be a good catalyst for fuel oxidation.

At initial stages of SOFC research, platinum and gold were used as an anode material. Since they are expensive, some transitions metals like iron and nickel were also used. These metals meet most of the requirements being less expensive. Nickel is a good catalyst, still it has high a TEC of $13.4*10^{-6}{}^{\circ}C^{-1}$ [55]. Nickel performance with respect to hydrogen is the highest among its peers of transition metals [56-58]. So nickel was chosen as anode. However during the course of the reaction, there is grain growth and it tends to coarsen the microstructure. So in order to reduce the TEC and avoid coarsening of microstructure, nickel oxide is used with ceramic materials like Yttria Stabilised Zirconia (YSZ) or Gadolinium Doped Cerium (GDC). This composite is called cermet (ceramic+metal). This cermet helps to maintain the necessary porosity which induces transfer of gases and helps in formation of the necessary Triple Phase

Boundary (TPB) where the electrochemical reaction occurs. NiO present in cermet is reduced to nickel during the reaction and thus caters oxidation of fuel. To improve the performances of cell, different compounds like Ni/Al_2O_3 and Ni/TiO_2 were used as subtrate in combination of Ni/YSZ [59, 60]. In contrary to expectation, observed electrochemical performances are reduced.

Ni/YSZ is sensitive to sulfur present in the natural gas fuel that it can poison the electrode. When the water in the fuel is less than the required amount, it forms coking of anode and reduces the overall performances of the cells. To overcome this, anode containing copper were tried as an alternative. Copper does not favor oxidation but it inhibits carbon formation, still serves as a good conductor of electricity. Copper has low melting point and is normally used at low temperature compared to Nickel anode. [61, 62]. Alloys of copper cobalt, copper nickel were tried to overcome carbon forming. This Cu-Co, Cu-Ni alloys shows better performance with hydrogen and improved resistance to carbon forming [63]. The fabrication of thin film of Yttria doped ceria (YDC) between YSZ and Ni-YSZ improves oxidation for methane at low temperatures. The composite of $Cu\text{-}CeO_2$-YSZ/SDC gives higher performance for all hydrocarbon fuels [64-68].

Ru-YSZ were developed and investigation on it exhibits lower polarization compared to Ni-YSZ and as Ru has higher sintering resistance, $Ru\text{-}Al_2O_3$ shows carbon forming resistance and performs high reforming reacting activities [69,70]. However Ru is an expensive metal and it's ruled out for commercialization. Some other bimetallic and trimetallic alloys were also tested as anode for SOFC. The cell consisting of trimetallic anode of $[Fe_xCo_{0.5-x}Ni_{0.5}/ Sm_{0.2} Ce_{0.8}O_{1.9}]$ with GDC electrolyte layer, and composite cathode of samarium strontium doped

cobalt/strontium doped ceria alloys exhibits low interfacial resistance, providing high power density for X=0.25 [71].

Other materials studied in the literature were $(Sr,La)TiO_3$, $(Sr,Y)TiO_3$, $(La,Sr)(Cr,Mn)O_3$, $(La,Sr)CrO_3$, $(La,Sr)(Al,Mn)O_3$, $(La,Sr)(Ti,Mn)O_3$, but they exhibited lower performances than Ni-YSZ due to mismatch of some of the basic requirements as an anode. So to improve their performances, doping of these compounds was suggested (Sr, Y) TiO_3/YSZ/Ru, (Sr, Y) TiO_3/YSZ/Ni, (Sr, La) TiO_3/YSZ/Pd–CeO_2, (Sr, La) TiO_3/Ni/YSZ [72-75]. The other pyrochlore materials, perovskite materials and fluorite materials were also tried as an anode material. Among all of them, only Ni possesses the most preferable qualities to serve as an anode for SOFC. The composite of Nickel cermet is widely selected as anode material for SOFC. Ni/GDC has the best anode properties to operate in intermediate temperature range, and it is chosen as anode in this work.

IV.3.Cathodes

Design requirements for cathode materials are as follows:

1) High electronic conductivity [23] ,

2) Chemically compatible with electrolyte,

3) Stable in oxidising atmosphere,

4) Large triple phase boundary,

5) High ionic conductivity,

6) Inexpensive materials and simple for fabrication.

In material selection of cathode for SOFC, high priority is given to the operating characteristics of cell, mainly the operating temperature.

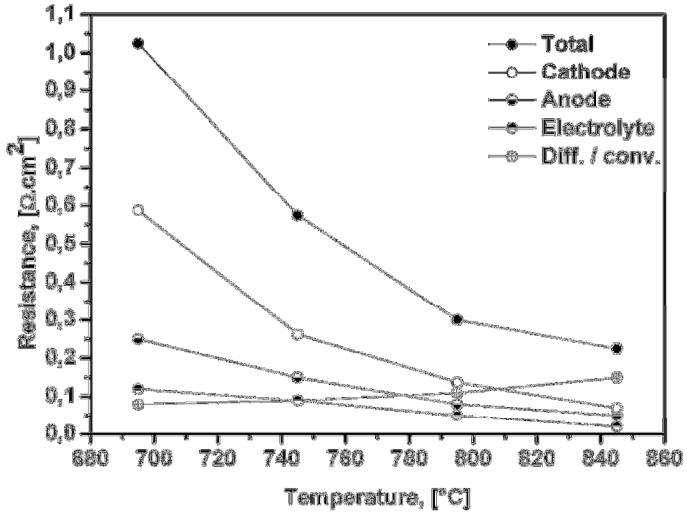

Figure I. 17 Polarization resistance as a function of temperature for major components of a cell

From Figure I.17, it is clear that the cathode exhibits the most important contribution in overall polarization resistance of the cell, mostly when the SOFC working temperature decreases. In lower working temperature cathode forms the major limiting resistance of the cell, because of its larger overpotential. This large overpotential arises due to the large activation and concentration polarizations at low temperature. Researchers and scientists always focussed on maintaning the major requirements also balancing the complex system of SOFC while attempting a new cathode material.

Platinum was used as cathode in earlier stages of development of SOFC, when other materials were not yet investigated. With regard to platinum cost, it makes the cell expensive. Reducing the amount of platinum results in reduced performance of the system. Due to the cost

of platinum, researchers investigated for other possible alternative cathode materials. The discovery of perovskites crystal structure of ABO_3 was attractive, in this hunt of alternative cathode. ABO_3 possessed all the major requirements and had the possiblity to use in optimized quantities to make cost effective system. The most commonly used cathode material is either pure perovskite or composite of perovskite and electrolyte. A number of different families of perovskite have been researched. Perovskites are oxides with the property of relatively good electronic conduction at high temperature in oxidising atmosphere.

In 1969, first cathode perovskite lanthanum cobaltite ($LaCoO_3$) was tested and it showed good initial performance in the cell. When long term ageing test were performed, it reacted with YSZ electrolyte and had serious degradation problem. The family of LSM [$(La_{1-x}Sr_x)\ MnO_3$] was tested by Siemens Westing House and ABB companies. These cathodes were characterized as good candidates with respect to good stability and long term experiments with YSZ at higher temperatures. LSM also exhibited good catalytic activity towards oxygen dissociation. LSM is an electronic conductor and oxygen reduction is restricted only to TPB sites. In order to extend TPB sites, composite electrode is used. This composite reduces the high TEC of cathode to make it viable for usage without any TEC mismatch problem, thus it helps in improving chemical compatibility of cell.

The other cobaltite tested was $Pr_{1-x}SrCoO_3$. This compound was observed to be reactive with YSZ and thus resulting in formation of an electro active layer at cathode/electrolyte interface [23]. This compound can be used as potential cathodes along with ceria based electrolyte. Another interesting cobaltite material is gadolinium strontium cobaltite, which also

reacts with YSZ electrolyte and thus forming secondary phase. But they do not react with ceria based electrolytes and can possibly be used in intermediate temperature application. To overcome all the degradation, there was necessity for improved performance and stable materials that can worked in intermediate and as well as at low temperature. The mixed ionic and electronic conductor (MIEC) was a fruitful discovery in cathode field. These compounds belonging to the other common perovskite of lanthanum strontium cobaltite (LSC) was tested for SOFC. It exhibited good conductivity and was stable in oxidizing environments. However the issues related to LSC are its reactivity with YSZ materials and it's reducing property at lower oxygen partial pressure. This is non reactive with ceria based electrolyes and it has high TEC causing TEC mismatch with electrolyte used. Their reactivity with YSZ can be suppressed by applying a Ceria layer between cathode and electrolyte. The most common ferrite cathode material is $La_{1-x}Sr_xCo_yFe_{1-y}O_3$ (LSCF) [26]. These are characterized by good chemical compatiblity with ceria based electrolyte and shows low resistance losses while being mixed ionic and electronic conductor. The addition of pure lanthanum iron oxide ($LaFeO_3$) has shown poor ionic and electronic conductivity at low concentrations of vacancies and Fe^{2+} ions, but processing of doping strontium ions into A site (ie) lanthanum site gradually increases the electrical conductivity of the compound [76].

Since LSC compounds have high TEC, using a composite with electrolyte material helps to overcome this problem. Cathode material performance is dependent on temperature, size, micro structure, and the formation or deposition process. The most popular ferrite perovskites for intermediate temperature range is $La_{0.6}Sr_{0.4}Co_{0.2}Fe_{0.8}O_{3-\delta}$ (LSCF 48). It has significant electronic conductivity at 600°C [76] and also gives better performance with GDC electrolyte because of its

stability [35] and thermal expansion compatibility [42]. The TEC of pure LSC was 20.5*10^{-6} K^{-1} and 17.5*10^{-6} K^{-1}[77]. Replacing Co with Fe reduces TEC to 13.8*10^{-6} K^{-1}. Conductivity of LSCF decreases with increasing Fe Content [53]. It also has the advantage of exhibiting low power loss at lower temperature and less susceptibility to poisoning by chromium [78].

The table I.2 shows cathode materials and their respective TEC values at corresponding temperature.

Composition	TEC *$10^{-6}K^{-1}$	T(K)
$La_{0.6}Sr_{0.4}Co_{0.2}Fe_{0.8}O_{3-\delta}$ [53, 77]	17.5	300-1000
$La_{0.58}Sr_{0.4}Co_{0.2}Fe_{0.8}O_{3-\delta}$ [87]	17.4	300-1000
$La_{0.6}Sr_{0.4}Co_{0.2}Fe_{0.8}O_{3-\delta}$ [88]	13.7	100-500
$La_{0.9}Sr_{0.9}Mn_{0.3}$ [89]	11.2	300-1000
$Nd_2NiO_{4+\delta}$ [84, 90]	11.6	300-1000
$La_2NiO_{4+\delta}$. [84, 91]	13.6	300-1000
$Dy_{0,2}Sr_{0,8}CoO_3$ [92]	19	300-1000
$La_{0.3}Sr_{0.,7}CoO_3$ [53]	25	300-1000
$La_{0.6}Sr_{0.4}CoO_3$ [53, 93]	20.5	300-1000

Table I. 2 Different cathodes and their TEC values

The other family of materials was tested by changing A (lanthanum site) and B (cobalt site) of the perovskites by changing the concentrations of these elements. The compound $Ba_{0.5}Sr_{0.5}Co_{0.8}Fe_{0.2}O_3$ has large TEC and also possesses high oxygen ion mobility. Because of this property, its use is minimal, and also shows high degration for CO_2 containg atmospheres [79,

[80]. During recent years, to obtain the best optimal performance, research in cathode is of great interest, which leads to discovery of double perovskites. The oxides with K_2NiF_{4+x} structures are referred as Ruddlesden-popper phases. These have high oxygen exhange kinetics and posses high ionic conductivity. However even possessing high ionic conductivity, it shows low electronic conductivity, which proves to give good performance results in intermediate working temperature range [81-85]. The other recent researched structures are called ordered double layered perovskites. Their general formula is $LnBaCo_2O_{5+\delta}$ where (Ln= Pr, Nd, Sm, Eu, Gd, Tb, Dy, and Ho). These are known showing encouraging performance at intermediate working temperature [86]. So with respect to meeting all requirements for best cathode material, LSCF48 was chosen in this study for IT-SOFC. From now on the discussion of cathode will be based on only LSCF48.

IV.4. Interconnectors

The interconnectors are also called bipolar plates. Since SOFC single cell gives maximum of one volt, in order to obtain desired voltage, interconnectors are much essential part to form SOFC stack which can be tailored to meet essential voltage and power requirements. They also provide mechanical strength to cell in the stack. They play another major role of electrical connection between cells. Interconnectors are covering the electrodes; they ensure the even gas distribution throughout the surface of electrodes, and help in gas separation between cells. The desired qualities of a material to be choosen for interconnectors are listed below.

1) Good chemical and thermal stability with fuel and oxidant gases,

2) Low contact resistance,

3) Low cost,

4) Good mechanical strength,

5) Good thermal and electrical conductivity and corrosion resistance,

6) Their TEC should be compatible with adjust components, so that mismatch is avoided between electrodes and interconnectors. The selection of this material is very critical to its working temperature. The main interconnector materials are choosen from two wide classes of ceramic materials, or metallic alloys.

For high temperature SOFC whose working temperature is higher than 800°C, ceramic materials were used as interconnectors in initial stages. The available ceramic material which best fits into requirements is $LaCrO_3$.There are certain disadvantages of this material, since it belongs to rare earth group, it is expensive, and the second being since it is a ceramic material, its fabrication process restricted to geometry is tedious. This ceramic material needs specific sintering methods to obtain the maximum density, which adds to fabrication cost of the cell. So alternative materials research leads to discovery of metallic alloys.

Metallic alloys are best suited for high temperature SOFC and IT-SOFC. These alloys are classified into three major types as chromium based alloys, Fe-Cr based alloys, and Ni-Cr based alloys. Chromium containing alloys has problem of Cr evaporation at high temperature and it can be avoided by usage of coating in the alloys. For IT-SOFC operation low cost ferritic alloys are best suited and are selected for study in this work.

IV.5. Sealants

The sealants are one of the major components of planar SOFC stack system. This helps in avoiding mixing of fuel gas and oxidant gas, and also prevents leakage of gases. By ensuring gas

tight system, these sealants can gradually improve the stack efficiency. The main requirement for sealants is that it should be an electrical insulator to avoid short circuit in the stack. They should have compatible TEC that should match adjusting components. There are two types of sealants; i) bond sealants and ii) compressive seals.

Bonded seals are glass seals or glass ceramics; these are sealants which does not need any load during operation to ensure gas tight system. This seal are best operated above 625°C the Tg glass transition temperature of glasses. They can break when mismatch of TEC occurs. Compressive seals are sealants which require certain load during operation. These seals will soften at high temperature and hence it requires load in the form of spring load system with bolts or direct load applied during operation. In some system like probostat gold rings are also used as sealants. Since gold rings are very expensive, compressive seals are selected for study in this work.

So to summarize the materials selected for this work, GDC10 is selected as an electrolyte, NiO is selected as anode which is used as a composite with GDC10, and LSCF48 will be used as cathode in composite with GDC10. Ferritic alloys were chosen as interconnectors, and compressive seal will be used in stack.

IV.6. Balance of Plant (BOP)

For the development of inbuilt test bench and stack system, there are many other major criteria that should be addressed. The interconnectors, sealants, current collectors, gas manifolds, heat exchangers, gas tubes for feed and exhaust, gas reforming unit, safety valves are collectively termed as balance of plant. Other then selection of anode, cathode and electrolyte, the selection

of BOP is very important to achieve good performance, high efficiency, and longer life time of the stack system. These BOP accounts to major part of the cost associated while building the system. So selection of BOP along with electrodes and electrolytes becomes very important for effective and inexpensive system performance.

V. Cell preparation techniques

Once all the electrode and electrolyte materials were chosen, the next step is the fabrication of cell. The cell preparation is an important factor which play significance role in the performance of the cells. Since planar SOFC is selected in this study, the conventional fabrication of a complete cell implies different techniques. It requires high initial cost for equipments and many different application of each layer of the cell. This also includes many steps of sintering which add to cost of the system.

Conventionally for an ASC planar SOFC cell preparation, the anode substrate is mostly fabricated by tape casting technique, the application of electrolyte and cathode layers and sintering them are tedious and require costly equipments. There are different and many stages of sintering and fabricating a full cell. Some of the common fabrication techniques used in preparation of planar cells is described below.

V.I. Screen printing

Screen-printing is one of the relatively expensive and common techniques used to deposit electrolyte and electrode materials on substrate. The electrode or electrolyte layers are deposited from a suspension which consists of an organic solvent. The corresponding electrolyte or

electrode suspensions are prepared by dispersing the powder in a 3 wt% solution of ethyl cellulose in terpineol, where the former acts as a binder and the latter as the solvent [94]. Fabrication of larger area geometry is possible by this technique, its disadvantage being that it requires high initial investment, many sintering steps and stages. Cheaper and cost effective fabrication technique is much preferred to reduce the cost of the whole system.

V.2. Physical vapour deposition

Half cell or anode substrate is generally prepared by tape casting. PVD equipment is used for making thin film electrolyte and cathode coatings. Radiation heater and electron beam were used to increase substrate temperature. The deposition was done at high vacuum of 10^{-2} Pa by turbo molecular pump and distance between substrate and evaporation target was 250 mm [95] This equipment installation requires high initial cost. This involves sequential high temperature sintering for electrolyte, followed by the deposition of the electrode layer. Finally by the sintering of cathode one can obtain a complete cell [95]. So expensive, complex nature of this system and fabrication steps involved allows users to opt for an alternative cheaper techniques.

V.3. Spin coating

This is one of the techniques used to fabricate thin film of electrolyte and electrode. The anode substrate is placed for deposition of different consecutive layers. Electrolyte layer was prepared by a so called wet route using polymer precursors. The precursors were prepared by dissolving cerium nitrate and gadolinium nitrate in ethyl glycol and water. These were slowly heated to 70-90°C for 24 h then water was fully evaporated and ethyl glycol also starts to evaporate. The viscosity was measured at 0.02-12 Pa at constant temperature and blade gap of 500 µm. The prepared solutions were deposited on half cells and spin coated at 2000 rpm. After

this, layer was dried in a conveyor belt furnace at 250°C at 30 min except where noted. [96] The electrolyte layer is sintered, and then cathode layer deposited is sintered again to obtain a complete cell. So all the conventional process involves multi step sintering and is expensive. Considering the complexity and different steps involved to make a cell, cheaper fabrication techniques will be preferred to reduce the system costs and effective commercialization of SOFC systems in large scale.

V.4. Tape casting.

Tape casting is a convenient and the cheapest shaping technique to fabricate two-dimensional thin ceramic plates from 10–1000 µm thickness. This can be done either manually or in an automatic way. Commonly automated machines are preferred for tapecasting to avoid uneven thickness of tape. A paste-like suspension, consisting of powder, organic solvent, dispersant, polymer (binder) and plasticizer is cast on a clean glass substrate by a moving doctor blade at a constant speed rate. The dried green tape obtained is flexible; care should be taken to remove the tape from glass plate without any deformation. A half cell is usually prepared by this method. [97]

By tape casting, one can obtain a large area tape, without any hurdles. This technique requires less maintenance and operating costs compared to other fabrication techniques.

This work is a new attempt in fabricating an anode supported cell consisting of thick anode substrate, an anode functional layer, a thin electrolyte layer, and a thin cathode layer. The multilayer tape is prepared only by tapecasting. So by using this process, expensive deposition techniques like screen printing, PVD, and spin coating can be avoided. This patented process

will explain the possiblity to obtain a complete working planar cell by one step sintering. By using this technique the cost of fabricating cell is gradually reduced and mass production at large scale is feasible.

VI. Scope of this Thesis

The objective of this present thesis is to obtain a cost effective technique to fabricate a single operating full cell of large area above 25 cm^2 only by tape casting and later improved tape casting along with single step sintering. The process of tapecasting involves selection of required electrode, electrolyte materials respective binders, solvents, and dispersant. The selections of composition of materials are explained previously. The influence of sintering temperature, pore formers, load required during sintering are also explained in detail. The electrochemical performances of the obtained cells are discussed in chapter 2. Chapter 3 throws light on long term ageing results, building of new test bench and stacking process of cell. Finally conclusions and perspectives of this work are given.

References

1. P. Decorse, "Etude comparative des propriétés de surface et de volume d'oxydes de type pérovskite $La_{1-x}Sr_xMnO_{3\pm\delta}$ ($0\leq x\leq 1$) utilisables dans les piles à combustible haute température", Thèse LRRS Dijon, France, 1997.
2. G. Bertrand, "Films minces de manganites de lanthane ($La_xMn_yO_{3+\delta}$) sur zircone yttriée ((100) YSZ) comme modèle de demi-pile à combustible à oxydes solides (SOFC) : élaboration par LP-MOCVD et propriétés interfaciales", Thèse LRRS Dijon, France, 2000.
3. M. Petitjean, "Propriétés et réactivité des ferromanganites de lanthane strontium cathodes de piles à combustible SOFC", Thèse LRRS Dijon, France, 2003.
4. L.Combemale, "Elaboration et réactivité interfaciale d'oxydes pérovskites à base de Lanthane Strontium Chrome Ruthénium (LSCrRu) comme composés d'anode de piles à combustible à température intermédiaire (ITSOFC) ", Thèse LRRS Dijon France, 2005.
5. S.Ricote "Elaboration et characterization du materiau D'electrolyte pour pile a combustible a conduction Protonique $BaCe_{0.9}$-x Zr x$Y_{0.1}$ O3-δ", LRRS Dijon, France, 2008.
6. V.Sivasankaran*, L.Combemale, Gilles Caboche, Method for Preparing a Fuel Cell, filed on 10.10.2012, *FR12/59643* French Patent.
7. T.S. Zhao, K-D.Kreuer, Trung Van Nguyen, *Advances in fuel cells* vol 1 2007.
8. http://world-nuclear.org/info/Current-and-Future-Generation/World-Energy-Needs-and-Nuclear-Power/#.UhqdvBuWTUM
9. http://www.iea.org/publications/freepublications/publication/kwes.pdf
10. Nasa goddrad institute for space studies.
11. Kordesh, K. and G. Simader, *Fuel cells and their applications*. Weinheim: VCH. 1996.

12. Gregor Hoogers, Fuel cell technology handbook *CRC* press 2003.

13. Steele, B.C.H. and A. Heinzel, *Materials for fuel-cell technologies.* Nature, 414, 345, 2001.

14. Maru, H. C. National Renewable Energy Laboratory 1-10 kW Stationary Combined Heat and Power Systems Status and Technical Potential: Independent Review. 2010.

15. Hosoi, K. & Nakabaru, M. Status of National Project for SOFC Development in Japan. *ECS Transactions* 25, 11, 2009.

16. P. Nehter. Thermodynamische und ökonomische Analyse von Kraftwerksprozessen mit Hochtemperatur-Brennstoffzelle SOFC. Shaker Verlag, Dissertation, 2005.

17. E.D wascmann *Science* 334, 935, DOI: 10.1126/science.1204090, 2011.

18. Blum, L., Packbier, U., Vinke, I. C. & de Haart, L. G. J. Long-Term Testing of SOFC Stacks at Forschungszentrum Juelich.*Fuel Cells*, Online Early View, 2012.

19. http://www.sofccanada.com/

20. http://www.bloomenergy.com/clean-energy/

21. Subash C.Singhal, Kevin Kendall *High temperature solid oxide fuel cells* 2003.

22. R. A. George. Status of tubular SOFC field unit demonstrations. *Journal of Power Sources*, 86,1-2:134, 2000.

23. K. C. Wincewicz and J. S. Cooper*, J. Power Sources,* 140, 280, 2005.

24. Daniel J. L. Brett, AAtkinson, Nigel P. Brandon and SJ. Skinner DOI: 10.1039/b612060c.

25. Menzler N.H., Tietz F., Uhlenbruck S., Buchkremer H.P., Stoever D.*, J. Mater. Sci*., 45 3109, 49, 2010.

26. S. Wang, T. Kato, S. Nagata, T. Kaneko, N. Iwashita, T. Honda , M. Dokiya, *Solid State Ionics*, 152–153, 477, 2002.

27. B. C. H. Steele, *Solid State Ionics*, 134, 3, 2000.

28. B. C. H. Steele, *Solid State Ionics*, 129, 95, 2000.

29. T. S. Zhang, J. Ma, L. B. Kong, P. Hing and J. A. Kilner, *Solid State Ionics*, 167, 191, 2004.

30. T. S. Zhang, J. Ma, L. H. Luo and S. H. Chan, *J. Alloys Compd*., DOI: 10.1016/j.jallcom.2005.11.049.

31. Y. J. Leng, S. H. Chan, S. P. Jiang and K. A. Khor*, Solid State Ionics*, 170, 1-2, 9, 2004.

32. C. Hatchwell, N. M. Sammes and I. W. M. Brown, *Solid State Ionics*, 126, 201, 1999.

33. Ye, F.; Mori, T.; Ou, D. R.; Takahashi, M.; Zou, J.; Drennan, J. *J. Electrochem. Soc*. 154, B180, 2007.

34. Balazs, G. B.; Glass, R. S. *Solid State Ionics,* 76, 155, 1999.

35. O. Yamamoto, *Electrochim. Acta,* 45, 2423, 2000.

36. Huang K., Tichy R.S., Goodenough J.B., *J. Am. Ceram. Soc.* 81, 2581, 2000.

37. D. Marrerolopez, J. Canalesvazquez, J. Ruizmorales, J. Irvine, and P. Nunez, *Electrochimica Acta*, 50, 4385, 2005.

38. S. Georges, F. Goutenoire, O. Bohnke, L.M. Stei, S. Skinner, H. Wiemhofer, and P.Lacorre, *Journal of New Materials for Electrochemical Systems*, 7, 51, 2004.

39. S. Nakayama, *Journal of the European Ceramic Society*, 19, 507 1999.

40. M. Higuchi, Y. Masubuchi, S. Nakayama, S. Kikkawa, and K. Kodaira, *Solid State Ionics*, 174, 73, 2004.

41. S. Nakayama and M. Sakamoto, *Journal of the European Ceramic Society*, 18, 1413, 1998.

42. Kharton, V. V.; Figueiredo, F. M.; Navarro, L.; Naumovich, E. N.; Kovalevsky, A. V.; Yaremchenko, A. A.; Viskup, A. P.; Carneiro, A.; Marques, F. M. B.; Frade, J. R. *Journal of Materials Science 36*, 1105, 2001.

43. Zajac, W.; Swierczek, K.; Molenda, J. *Journal of Power Sources 173*, 675, 2007.

44. Kharton, V. V.; Kovalevsky, A. V.; Viskup, A. P.; Shaula, A. L.; Figueiredo, F. M.; Naumovich, E. N.;Marques, F. M. B. *Solid State Ionics, 160*, 247, 2003.

45. H. Inaba and H. Tagawa, *Solid State Ionics*, 83, 1, 1996.

46. J. VanHerle, *Solid State Ionics*, 86-88, 1255, 1996.

47. W. Huang and P. Shuk, *Solid State Ionics*, 95, 337, 1997.

48. Huang, W.; Shuk, P.; Greenblatt, M. *Solid State Ionics. 113*, 305, 1998.

49. Sameshima, S.; Ichikawa, T.; Kawaminami, M.; Hirata, Y. *Materials Chemistry and Physics 61*, 31, 1999.

50. Zheng, Y.; Gu, H.; Chen, H.; Gao, L.; Zhu, X.; Guo, L. *Materials Research Bulletin*, *44*, 775, 2009.

51. Tietz, F. *Solid State Ionics 5*, 129, 1999.

52. Mori, M.; Abe, T.; Itoh, H.; Yamamoto, O.; Takeda, Y.; Kawahara, T. *Solid State Ionics. 74*, 157, 1994.

53. Ullmann, H.; Trofimenko, N.; Tietz, F.; Stöver, D.; Ahmad-Khanlou, A. *Solid State Ion*ics *138*, 79, 2000.

54. Stevenson, J. W.; Hasinska, K.; Canfield, N. L.; Armstrong, T. R. *J. Electrochem. Soc. 147*, 3213, 2000.

55. Encyclopedia of Electrochemical Power Sources ISBN: 978-0-444-52745-5.

56. Eguchi K, Setoguchi M, Sawano M, Tamura S, Arai H, *Proceedings of international symposium on SOFC* 603, 1991.

57. Digiuseppe, G.; Selman, J. R. *J. Mater. Res*., 16, 2983, 2001.

58. Sunagawa, Y.; Yamamoto, K.; Muramatsu, A. *J. Phys. Chem*. 2006, 110, 6224, 2006.

59. Tietz F., Dias F.J., Naoumidis A. In: Stevens P. *Proceedings of 3rd Eur. SOFC Forum,* vol 1, 171. 1998.

60. Meschke. F, Dias F.J, Tietz F, *J.Mater.Sci* 36, 5719, 2001.

61. . S.Park, R. Cracium, J.M. Vohs, R.J. Gorte R. *J. Nature* 404, 6775, 265, 2000.

62. Gorte, R. J.; Park, S.; Vohs, J. M.; Wang, C. *Adv. Mater.* 12,1465, 2000.

63. Lee, S.-I.; Ahn, K.; Vohs, J. M.; Gorte, R. J.Electrochem. *Solid-State Lett.,* 8, A48–A51, 2005.

64. E.P. Murray, T. Tsai, S.A. Barnett, *Nature* 400, 649, 1999.

65. S. Mcintosh, J.M. Vohs, R.J. Gorte, *Electrochima. Acta* 47, 3815, 2002.

66. S. Park, R. Cracium, J.M. Vohs, R.J. Gorte, *J. Electrochem. Soc.* 146 3603, 1999.

67. C. Lu, W.L. Worrell, R.J. Gorte, J.M. Vohs, *J. Electrochem. Soc*. 150 A354, 2003.

68. B.C.H. Steele, P.H. Middleton, R.A. Rudkin, *Solid State Ionics* 40-41,388, 1990.

69. Suzuki M, Sasaki H, Otoshi S, Ippomatsu M, *International symposium on SOFC* 585-591.

70. Zhan, Z.; Barnett, S. A. *Science* 308, 5723, 844, 2005.

71. Z. Xie, W. Zhu, B. Zhu and C. Xia, *Electrochima. Acta*, 51, 3052, 2006.

72. Kurokawa H., Yang L.M., Jacobsen C.P., De Jonghe L.C., Visco S.J., *J. Power Sources* 164, 510, 2007.

73. Fu Q.X., Tietz F., Sebold D., Tao S.W., Irvine J.T.S., *J. Power Sources* 171, 663, 2007.

74. Kim G.T., Gross M.D., Wang W.S., Vohs J.M., Gorte R.J., *J. Electrochem. Soc.* 155 B360. 2008.

75. Pillai M.R., Kim I.W., Bierschenk D.M., Barnett S.A., *J. Power Sources* 185,1086, 2008.

76. Y.Chen, Veronica Alexandra B.Almeida, Francois Gitzhofer, *J.Thermal spray Technology* 20, 1-2, 145,2011.

77. Anthony petric, Peng Huang Frank Tietz, *Solid State Ionics,* 135, 1-4, 719, 2000.

78. Ken Kuang, keith Easler, *Fuel cells electronics and packaging,* 2007.

79. Yan A., Cheng M., Dong Y.L., Yang W.S., Maragou V., Song S.Q., Tsiakaras P.*, Appl. Catal. B* 66,64, 2006.

80. Bucher E., Egger A., Caraman G.B., Sitte W.*, J. Electrochem. Soc*. 155, B1218, 2008.

81. Takeda Y., Nishijima M., Imanishi N., Kanno R., Yamamoto O., Takano M., *J. Solid State Chem.* 96,72, 1992.

82. Skinner S.J., Kilner J.A., *Solid State Ionics* 135,709, 2000.

83. Boehm E., Bassat J-M., Dordor P., Mauvy F., Grenier J-C., Stevens P., *Solid State Ionics*, 176, 2717,2005.

84. Munnings C.N., Skinner S.J., Amow G., Whitfield P.S., Davidson I.J., *Solid State Ionics* 176 1895,2005.

85. Sayers R., De Souza R.A., Kilner J.A., Skinner S.J., *Solid State Ionics,* 181, 386, 2010.

86. Maignan, A.; Martin, C.; Pelloquin, D.; Nguyen, N.; Raveau, B., *J. Solid State Chem.* 142, 247, 1999.

87. Mai.A, Haanappel, V.A, Uhlenbruck.S, Tietz.F, Stover *Solid State Ionics*, 176, 15-16, 1341, 2005.

88. Swierzcek.K, *Solid State Ionics*, 179, 1,126, 2008.

89. Jiang S.P *J.Mat.Sci* 43, 6799, 2008.

90. T. Nakamura, K. Yashiro, K. Sato, and J. Mizusaki, *Solid State Ionics*, 181, 402, 2010.

91. S. Skinner, *Solid State Ionics*, 135,709, 2000.

92. H. Tu, Y. Takeda, N. Imanishi, and O. Yamamoto, *Solid State Ionics*, 100, 283,1997.

93. W. Sitte, E. Bucher, and W. Preis, "Nonstoichiometry and transport properties of strontium-substituted lanthanum cobaltites," *Solid State Ionics*, 154-155, 517, 2002.

94. C.J.Fu, Q.L.Liu, S.H.Chan, X.M.Ge, G.Pasciak, *Int.J, Hydrogen energy* 35, 11200, 2000.

95. Bin Meng, Xiaodong He, Yue Sun, Mingwei Li. *Material Science and Engineering*, 150, 83, 2008.

96. Pawel Plonczak, Mario Joost, , Johan Hjelm, Martin Sogaard, Mats Lundberg, Peter Vang Hendriksen *J.Power sources*, 196, 1156, 2011.

97. Lorenz P.meier, Lukas Urech, LudwigJ.Gauckler, *J. European Ceramic Society* 24, 3753, 2004.

Chapter 2: Synthesis, development, formulation and optimization of suspensions for tape casting process

Chapter 2: Synthesis, development, formulation and optimisation of suspensions for tape casting process

Part I

I. Electrolyte and electrode properties

I.1. Electrolyte (GDC 10) nano particles synthesis and their characterization

As discussed earlier, the ionic conductivity of Gadolina Doped Ceria [$Ce_{0.9}Gd_{0.1}O_{1.95}$ (GDC10)] based solid solutions is highest among its class of electrolytes. For this reason GDC10 suits itself best for IT-SOFC (500°C-700°C) applications. There are several techniques available for preparation of GDC10, like powder mixing, glycine nitrate process [1,2], hydrothermal synthesis [3] and oxalate co-precipitation [4,5]. In this work citrate process was followed for synthesis of nano particles of GDC as described below. This was considered as the quickest and effective process for producing required nano particles.

I.2. Experimental procedure for synthesis of GDC nano powder

The different percentage of GDC were synthesized and finally concluded to proceed with GDC10 as discussed in chapter 1. For the preparation of this nano powder sol-gel, synthesis method by citrate process was chosen [6, 7]. The selected percursors were cerium nitrates hexahydrate Ce $(NO_3)_3$, $6H_2O$, and gadolinum nitrate hexahydrate Gd $(NO_3)_3$, $6H_2O$. These precursors were dissolved in deionised water individually and the solutions were mixed under constant stirring for one hour. Anhydrous citric acid was dissolved in deionised water and added to nitrate solutions. The molar ratio of oxides and citric acid used was 1:2 ratios. All these solutions were mixed together in one large beaker followed by constant stirring, to make it a homogenised solution. This homogeneous solution was heated in the water bath at a temperature

of about 80°C to remove excess water to transform it into a gel. The gel was transferred to alumina crucible and calcined in furnace at 500°C for 1 hour. The nitrates were evolved around 250°C and the final powders were collected and characterized by different techniques such as XRD, SEM. The results are discussed below.

I.2.1.GDC properties and characterization by X-Ray Diffraction

The Figure II.1 shows the crystal structure of GDC10. It possesses a fluorite type crystal structure. The Gd and Ce atoms are shown in purple color and oxygen atom is shown in red color. This falls in Fm3m space group. This structure was later characterized by XRD for purity and for surface area measurements by Brunauer–Emmett–Teller (BET) method.

Figure II. 1 GDC crystal structure drawn by Topaz software

The Figure II.2 shows the X-Ray Diffraction (XRD) pattern of synthesized GDC10 powders. The pattern was recorded in a Bruker D8 device, equipped with Kα radiation. This experiment was performed to study the crystal structure of the compound.It exhibits cubic structure a=b=c= 5.418(Å). This parameter was calculated by topaz software after XRD

measurement. This was also confirmed from literature [7]. The purity of powders was also verified with this XRD pattern. The peak in black shows the nano powers obtained, it was matched with original crystal structure of GDC10 from the database ICDD file number 01-075-0161.which is in red color. From the Figure II.1, it can be seen that all the peaks were exactly matching the database. There were no new peaks found, which confirms that the nano powders obtained were pure without any impurity. The broad peaks refer to the large surface area of the powders. The particle size was also calculated by Scherrer formula in equation 3.1 where D= diameter of particle in nm, λ is the wavelength in nm, βr is the peak width in radian, θ is the scattering angle in degree.

$$D=\frac{\lambda}{\beta r cos\theta} \qquad (3.1)$$

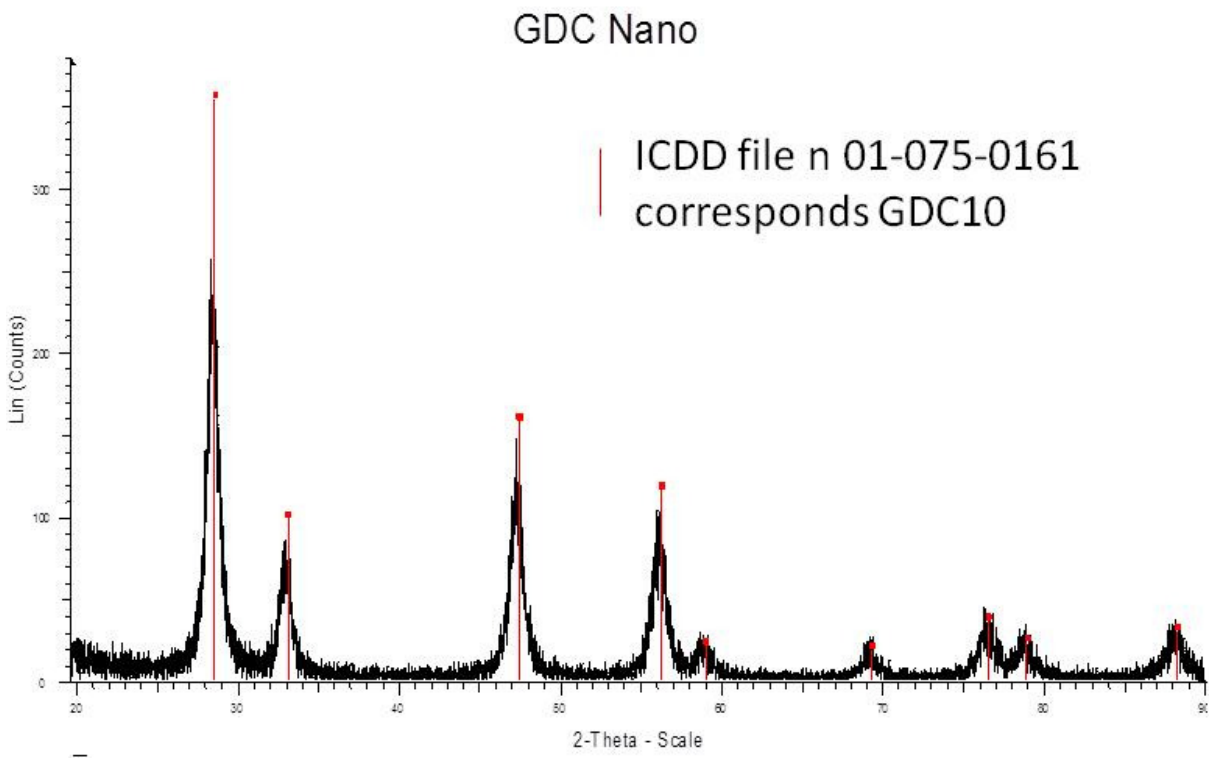

Figure II. 2 XRD of GDC10 powder synthesized by citrate process

The particle size calculated by Scherrer formula was 28 nm. These particles were also observed and measured by Scanning Electron Microscope (SEM) for its size.

I.2.2. GDC10 Characterization by SEM

The nanopowders obtained were seen in clusters, after synthesis. These SEM measurements were carried on JEOL 7600F device. The figure II.3a) and b) shows GDC10 nano particles as clusters obtained. These powders were crushed manually in a mortar. The figure II.3c) shows the single nano particles. The size of particles measured by inbuilt scale in SEM was around 40 nm. This confirms that products of synthesis were only nano particles

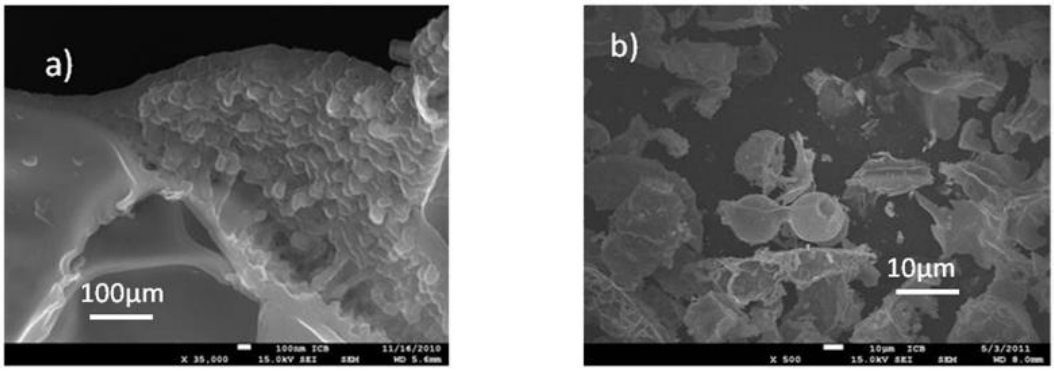

Figure II. 3a) 3b) GDC nano particles in clusters

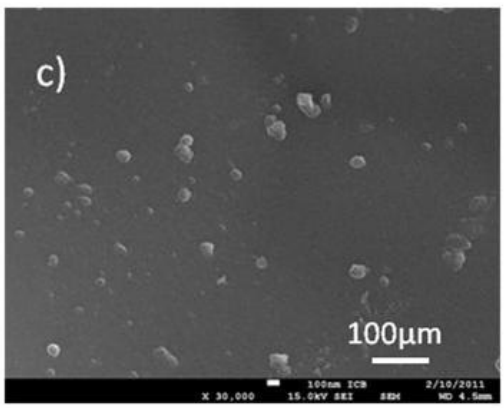

Figure II.3c) GDC10 single nano particles.

I.2.3.GDC10 characterization by BET

To measure the surface area of synthesized powders, BET method was used. The experiment was performed on micromeritics Tristar II 3020 device. Nitrogen was used as an adsorbative gas. This was kept in vacuum at 250°C for 2 hours. The sample mass of 0.3 g was used for experiment. When subjected to measurement, the powders possessed 28.8 $m^2.g^{-1}$ active surface area. The large surface area results explain that the particles were of very small in size. This implies powders were nano particles. The particle size were also found using the equation below where d is the diameter of particle in microns or nm, ρ is the density of GDC10 in $g.cm^{-3}$ S is the surface area in $m^2.g^{-1}$ found by BET.

$$d = \frac{6}{\rho S} \qquad (3.2)$$

The diameter of the particle estimated by equation (3.2) is 29 nm.

Thus by citrate process, pure nano particles were obtained. However by this synthesis procedure, nano powders yielded maximum of 2.5 grams per batch. The efficiency of this synthesis process is 94%. In order to fabricate cell by the new process, many trial cells have been made. For all these trial experiments, GDC10 was used in all layers of ASC, so the required amount was about approximately one and half kilogram. Due to lack of time and low yield of nano powders in lab, the process were continued with commercial GDC10 powders bought from Fuel cells Materials, supplied in France by Neyco.

GDC10-HP, high premium powders brought from Neyco with LOT n° 6A074, were also characterized by XRD for purity and BET for surface area. These powders were pure without any impurities. The powders had surface area of 12.1 $m^2.g^{-1}$.The diameter of particle estimated

by equation 3.2 was 70 nm. The Figure II.4 shows the XRD pattern of GDC10-HP powders. The base of peak in Figure II.4 was very narrow, compared to the Figure II.2 for nano particles.

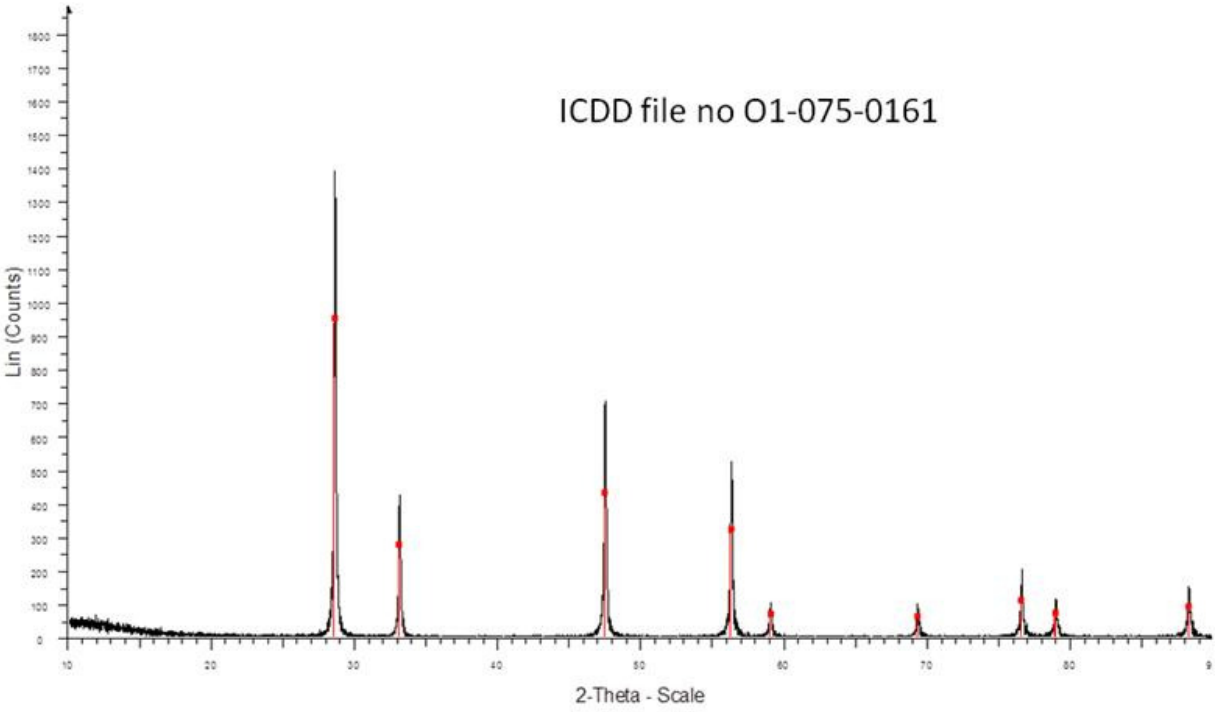

Figure II. 4 XRD of GDC10-HP powder

From now on, these GDC10-HP powders will be used for this work.

II. Cathode preparation its properties, and their characterization

II.1. LSCF48 preparation by solid state synthesis

Two preparation methods were investigated for cathode synthesis by E.Fatome Jacquelot in ICB lab. They were solid state synthesis and hydrothermal synthesis. The solid state process yielded micrometric particles, while hydrothermal synthesis resulted in nano metric powders. Since micrometric electrolyte powders were chosen for this work, solid state synthesis process was selected for cathode synthesis. By choosing these particles, there will be good cohesion

between electrolyte and cathode powders. This synthesis method was quite easy compared to hydrothermal synthesis process and larger quantities of powders can be achieved.

The synthesis of $La_{0.6}Sr_{0.4}Co_{0.2}Fe_{0.8}O_{3-\delta}$ (LSCF 48) was performed from precursors of strontium carbonate ($SrCO_3$), Lanthanum oxide (La_2O_3), Cobalt oxide (Co_2O_3) and iron oxide (Fe_2O_3). All these powders were brought from Sigma-Aldrich. The stoichiometric ratios of precursors were taken and milled by zirconium balls in ethanol for 15 hours. This was dried in furnace at 60°C for 24 hours at ambient temperature. Then the powders were calcined at 1100°C for 24 hours, with heating and cooling ramp of 100°C per hour.

II.2. LSCF48 characterization by XRD and its properties

The synthesized powders were subjected to XRD characterization, for checking their purity and structure. XRD was carried on D8 Bruker device, coupled with Kα radiation. The Figure II.5 shows the crystal structure of LSCF48. It exhibited rhombohedral structure. The lattice parameters were a=5.4919 Å, c= 13.364. Å. Its volume was 349.1 $Å^3$ [8]. La, Sr is shown in green, Co, Fe is represented in blue and Oxygen is depicted in red color. These LSCF48 powders were then characterized by SEM and BET.

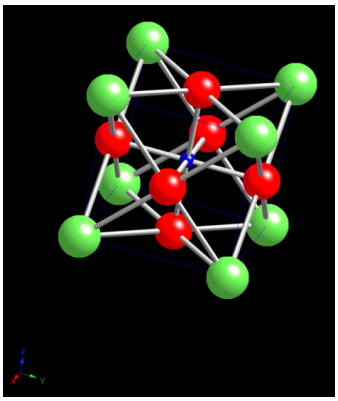

Figure II. 5 Crystal structure of LSCF48

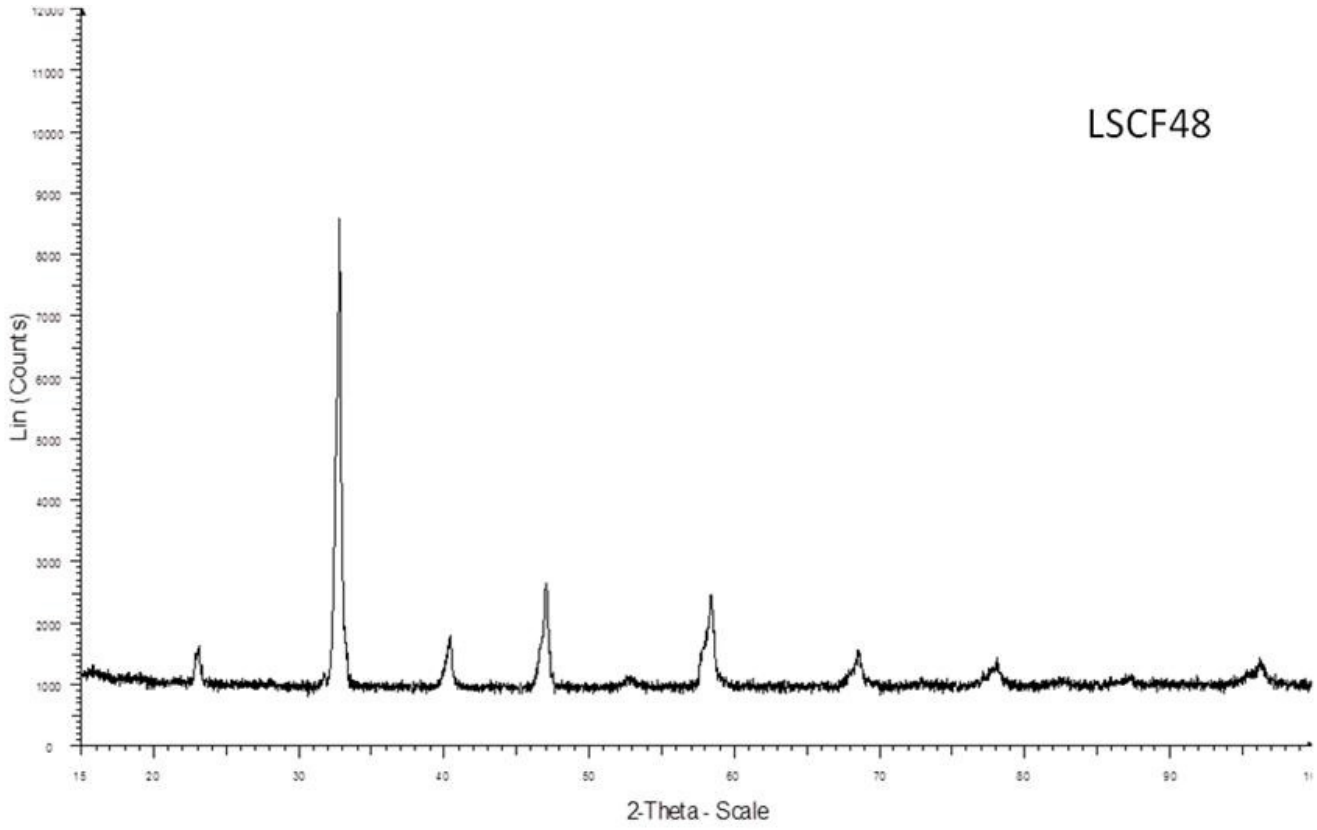

Figure II. 6 XRD pattern of LSCF48

The figure II.6 shows the XRD pattern of cathode synthesized. There is no ICDD file matching the composition of LSCF48. The lattice parameter was calculated by topaz software

and was similar to the values obtained from G.ch Kostogloudis et al [8]. From this, it was found that the obtained LSCF powders were pure and in single phase without any impurities.

II.3. LSCF48 characterization SEM and BET

The LSCF48 powders were characterized by SEM with the same conditions as an electrolyte powder measurement. These powders were also seen as agglomerates after synthesis. The morphology of powders by SEM studies shows that the grain was in microscopic size as seen in Figure II.7. Their surface area is calculated by BET under the same condition as for an electrolyte powder. Their surface area was found to be 0.7 $m^2.g^{-1}$. The diameter of particle estimated by equation 3.2 was 1.35 microns. From now on, this powder will be used in this process.

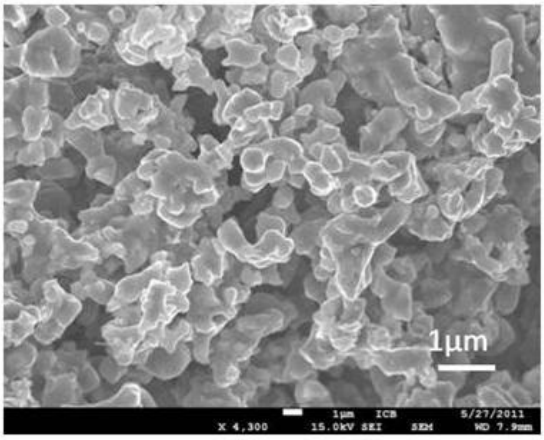

Figure II. 7 LSCF48 SEM picture

III. Anode properties and their characterization

Anode used in this study was NiO, this 99.99% pure powders brought from Sigma-Aldrich France. The Figure II.8 shows the NiO crystal structure. It was supposed to exhibit cubic

structure in Fm3m space group where a=4.178 Å. Ni is presented in white and O is in red. This powder were directly subjected to XRD characterization.

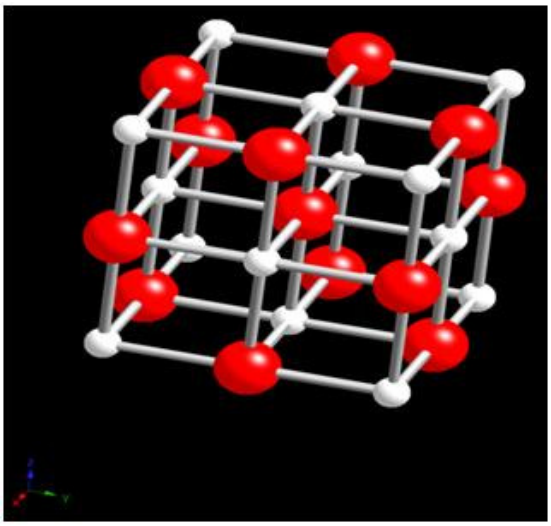

Figure II. 8 Crystal structure of NiO

The Figure II.9 shows the XRD pattern of NiO powders used. The peak in black shows the peaks of NiO powders, which was matched from NiO in database ICDD file number 01-071-1179, which was shown in red color. All the peaks were exactly matching with NiO structure from database. Since there were no new peaks, then it can be concluded that the powders were pure without any impurities

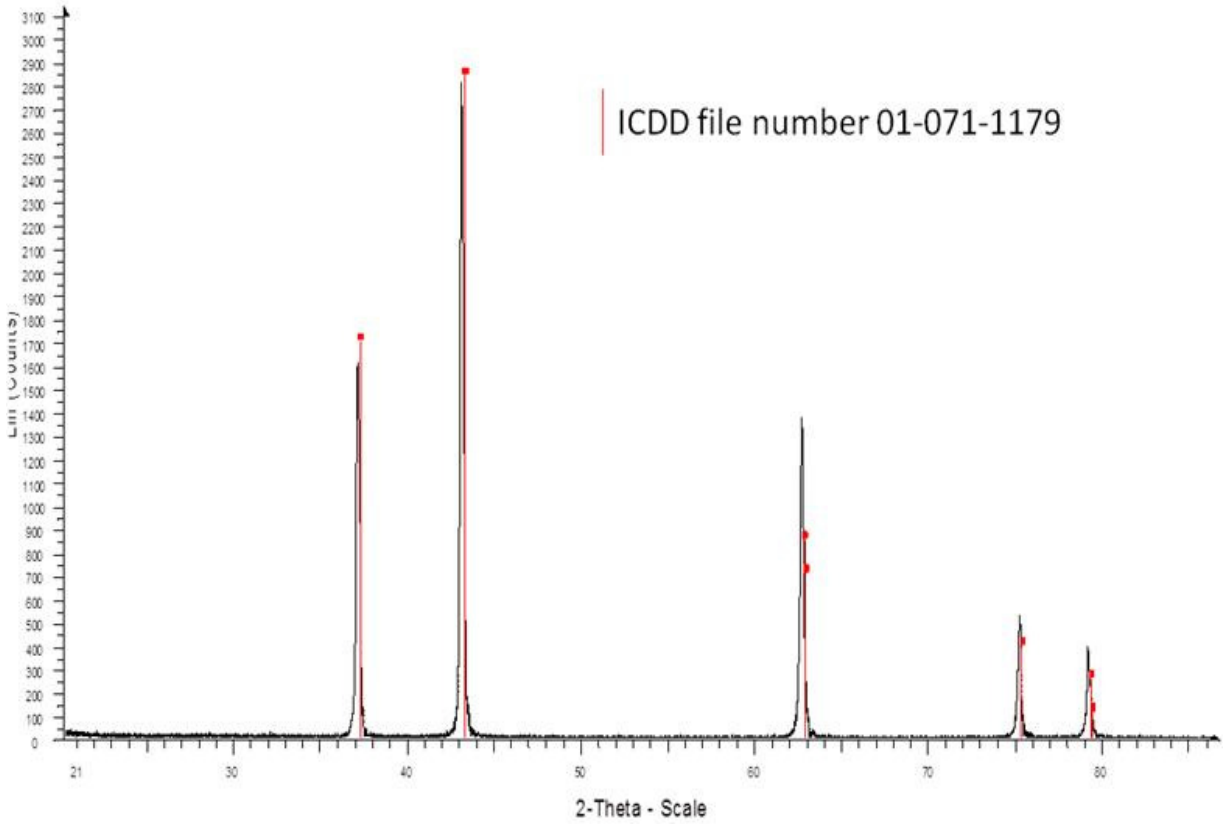

Figure II. 9 XRD of NiO

Further SEM and BET characterization were done on NiO. SEM characterisation was done in the same device as of GDC10, and LSCF48. The Figure II.10 shows the SEM observation of NiO. These were also seen as clusters. The morphology observed shows micrometric particles.

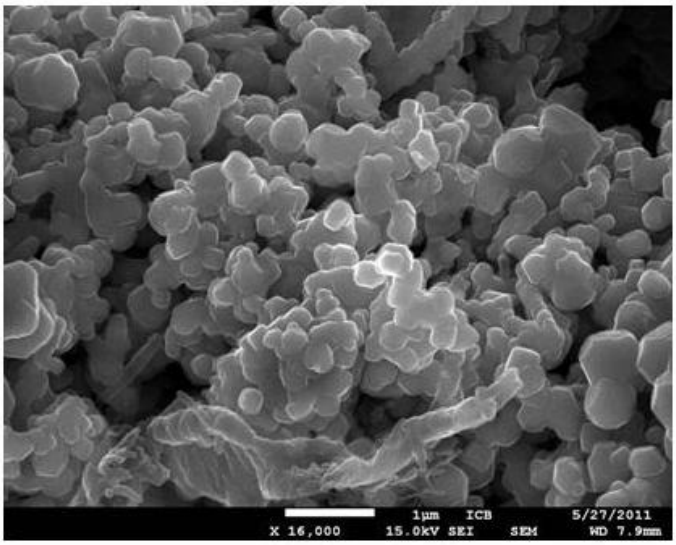

Figure II. 10 SEM picture of NiO

From this, we can also conclude that the NiO used was pure by XRD. BET measurements on the particles give the surface area of $3m^2.g^{-1}$. The diameter of particle estimated by equation 3.2 was 0.3 microns. So for this work, this NiO will be used from now on for all characterizations and formulations.

IV. Conclusion

Thus to conclude synthesis of nano powders would take long time and hence it was decided to switch over to commercial GDC10 from Neyco and use it for studying new process. NiO brought from Sigma Aldrich was used, and lab produced cathode particles were used for studying the full cell.

Patent Protected

Part II

II.1.Tape casting

Planar cell was the subject of study in this work. Since anode support planar cells were chosen to obtain the best possible performance, its fabrication is focused in detail in this thesis. When it comes to fabrication of planar cells, the key factor is to obtain a dense electrolyte. These fabrications of dense electrolyte are generally considered under two approaches namely particulate approach and deposition approach. The deposition approach requires either anode or cathode support formed by physical or chemical process, on which electrolyte will be deposited and sintered. The deposition methods are namely spin coating, physical vapor deposition, chemical vapor deposition, dip coating, sputtering, screen printing, plasma spraying, spray pyrolysis. All this process requires high initial investment and maintenance cost. This deposition approach to obtain dense electrolyte also require sequential and multi sintering steps to obtain a single cell. The particulate approach tends to usage of ceramic powders to form cell components by sintering at high temperature to form dense structure. There are two types of particulate process namely i) tape casting and ii) tape calendering. Tape casting is the process for making thin sheet of ceramic layers for SOFC. This involves formation of slurry and then casting it to thin films by using doctor blade on a glass plate support. These are then dried; green tapes are peeled, cut in required size and sintered.

In tape calendering, first the slurry containing ceramic powders and binders are made. This slurry is then cast to the required thickness and pressed between two rolls. This tape is sintered. Many layers of tape are made and can be laminated to form multilayer. Considering the fact of high initial investment, maintenance costs and ease of fabrication particulate approach is

preferred over deposition approach. In particulate approach, tape casting is chosen in this study since it does not require any laminating process, which further reduces the fabrication cost. They are generally the quickest process to obtain large area. So particulate approach by tape casting to form a full cell was carried out and discussed in detail.

II.1.1.General tape casting principle

In tape casting, firstly mixture of powders, organic solvents, dispersants, plasticizers and binders are made. These are called suspensions or slurry or slip. This slip must be stable to make a sheet which is later dried to form a tape. To obtain a tape, the slurry should be homogeneous which refers to even mixing of powders. It should not be of high viscosity, there should not be any settling of powders, as well as it should form a single monolithic structure after sintering. The various ingredients for the suspension are discussed below.

II.1.2.Stability

The ceramic particles in solid medium when mixed with liquid organic medium are subjected to various forces. First, it can possibly settle causing sedimentation. This settling or sedimentation is caused by weight and size of particles used, gravity forces of the particles causing sedimentation. Second the particles can be attracted by Vanderwaals force, which cause dipolar interactions. It can be avoided by constant stirring or agitation, the later being always preferred. The stability of the suspensions are improved and maintained by altering the composition. The sedimentation problem can be avoided by using small particles of the same

size. The Vanderwaals force can also be avoided by usage of dispersant. The different properties of materials used in suspension are mentioned below.

II.1.3 Solvent

There are generally two types of solvents that are used in the process of tape casting. They are namely aqueous and organic solvents. The aqueous solvents are always considered as the best in regards to economical and environmental conditions. Although aqueous solvents has the best qualities to suit the purpose, the fabrication process by using them is considered as difficult in respect to drying of tapes and it will be time consuming to study a new process. Since this work is focused on the development of new fabrication process which is already time consuming, choice of organic solvents was preferred. Usage of organic solvents paves way for adding mixture of different solvents in the same suspension. It also helps in dissolving all the other ingredients in the suspension.

By using organic solvents, viscosity and drying rate of suspension can be controlled. The viscosity is measure of shear stress to shear rate, this viscosity measurement was done by rheology studies. The suitable viscosity researched for tape casting was found to be 20 mPa.s at shear rate of $10s^{-1}$[9]. Drying is the next major parameter to be controlled in tape casting. Drying can be made in controlled atmosphere or in open air. Solvents are the material which is used to evaporate during drying. Drying performed in controlled atmosphere is always better and preferred, but in general case drying is performed in open air. Some solvents used in suspension can dry very quickly on opening the slurry to atmosphere which is not suitable for tape casting

ex Ethyl Methyl Ketone [MEK]. This gives necessity to use mixture of solvents. The other solvent which can be used is ethanol. Normally ethanol evaporates a bit slower compared to MEK. In suspension generally, azeotropic mixture of ethanol and MEK which has the same drying rate in liquid and gas phase are used. By using this mixture, drying rate can be controlled as per requirement. So in this work mixture of ethanol and MEK were used as solvent to have a controlled drying rate. This was brought from Sigma – Aldrich.

II.1.4. Dispersant

For the suspension, the solvents used should be enough to disperse the powders in the slurry. But this is not actually the case. So dispersant are added to suspension to ensure the stability. These dispersants helps to avoid agglomeration of particles and sedimentation. They are also called surfactants. They are polymer which adhere to the surface of the particle and keep them separate. Triethanol amine is the dispersant used in this work.

II.1.5 Binder

There are water soluble aqueous binders and non aqueous binders. Since an organic solvent was used in this study, non aqueous binders are chosen. The main prerequisite of usage of binders is to give mechanical strength to tape. These binders form a network of different constituents in the suspension. During drying when all solvents have evaporated, the binder's forms link between powder particles, forms a long chain that gives the tape after casting. There are two types of organic binders available: namely polyvinyl and poly acrylic binders. In this

work Polyvinyl Butyral (PVB) binder was chosen that can be soluble in selected solvent ethanol. This binder is brought from Sigma-Aldrich whose commercial name is Butvar B98. This is insoluble in MEK.

II.1.6. Plasticizer

Plasticizers are additives used, while making suspension for SOFC tape casting. They increase the fluidity of suspension and increase the plasticity of tape after it has dried. Once the tape is dried on glass plate, it will be peeled of from glass plate and kept in furnace for sintering. For removing a green tape, it has to have mechanical strength provided by binder and the plasticity provided by them. This plasticizer also helps to avoid the breakage or tearing or cracking of tape while peeling from glass plate. Benzyl Butyl phthalate (BBP) and Poly ethylene glycol (PEG) were selected to be used in this work, since it is compatible with chosen solvents. Both plasticizers were bought from Sigma-Aldrich.

II.1.7. Pore formers

Pore formers are additives used in the preparation of suspension for tape casting. Their main role is to form pores by burning themselves during the sintering of tape. Since an electrolyte needs to be as dense as possible, pore formers are not used in electrolyte suspension preparation. These are normally used in anode suspensions and cathodes if necessary. It makes electrodes porous which in turn will increase the performance of cell. The common pore formers are namely carbon black, potato starch, rice starch and graphite [10]. In this work both carbon

black and potato starch were tried among which carbon black was most preferred due to its advantages. Carbon black and potato starch are bought from Sigma-Aldrich.

II.2. Slurry or suspension preparation

Once all the ceramic powders, solvents, dispersants, binders, plasticizers, poreformers are selected; these are taken in grinding jar. The zirconia balls of diameter 10mm were used along with the ingredients to grind or mill them. Slurry preparation is generally done in two steps to ensure homogeneous suspension. Firstly ceramic powders, dispersants, solvents are added in and made to disperse well, pore formers are also added in the first step of the preparation of electrode slurry. This is made to mill well for 24 hours. In the second step binders, plasticizers are added and milled for another 24 hours. So now the suspension is ready to use. The viscosity of the suspensions is already custom made according to the amount of powders and solvents used.

II.2.1. Preparation of an anode support slurry

The chosen anode material was NiO. It was used with GDC10 electrolyte to make a composite cermet. This cermet structure will be employed to give high fuel conversion efficiency and create as large TPB as possible to enhance performance [11]. The chosen ceramic powders in suspensions was prepared with mass ratio of 65:35 for NiO to GDC10, while maintaining the ratio of solid content to liquid 60:40 [12.13]. This gives the best optimal performance and after reduction, the amount of 40% volume of Ni remains in the cermet [14]. The pore formers are not active materials as it burns out during sintering step. In first attempt, potato starch was used as

pore former. Different percentage of pore former was tried and results are discussed and then other pore former carbon black was also tested.

II.2.2. Preparation of an electrolyte slurry

For electrolyte preparation two different amounts of solid active materials to liquid content were tried. The ratio containing 45:55 of solid to liquid content was first used [15] which is later optimized to have best density at chosen temperature. The optimized ratio in this work was 55:45 for solid to liquid for selected temperature.

II.2.3. Preparation of cathode slurry

For preparation of cathode slurry LSCF48 is chosen as an active material, this is mixed with GDC10 to make composite slurry to improve cell performance by polarization of cathode [16, 17]. In this work mass ratio of 65:35 for LSCF48 to GDC10 was chosen, so that the composition remains the same for anode and cathode while maintaining the lowest polarization for cathode. However in literature different mass ratio of 70:30 [18] and 50:50 [19] were used to reduce polarization. It was concluded that, cathode polarization also depends on microstructure, sintering temperature and composition of cathode material used [20-21].

II.2.4.Preparation of an anode functional layer slurry

Anode functional layer (AFL) is used in an ASC, to increase its performance. Since an anode support is very thick and with lot of pores, there will be less TPB. The thickness of anode

support can lead sometimes to large polarization. So to avoid polarization, to maximize TPB and to increase the performance, AFL is used in the cell [22]. The thickness of the anode functional layer also plays a crucial parameter. Generally thin layer should be used in the cell. The optimal thickness of AFL should be between 10-20 µm [23-25]. There are many techniques used for deposition of this AFL on anode support layer. They are namely dip coating, spray coating, slip casting, and tape casting [26-30]. Since anode support was fabricated by tape casting in this work, it will be easy to deposit AFL by tape casting. The composition for an anode functional layer is the same as the anode support layer, but the pore formers were not used.

II.3. Casting of suspension

Once the suspensions are made, they are casted. Normally casting is done on a flat, clean surface. This is done usually on glass plate or on a mylar plastic sheet made of polyethylene terephthalate. This will help to peel the tape easily after drying. The thickness of layer to be casted will depend on the electrode or electrolyte suspension. Since anode support is the case of study in this work, the anode support layer will be made thicker. The thickness of casting layer was adjusted by the doctor blade, which helps to obtain uniform tape. The electrolyte suspension was casted to a thin layer on glass plate and anode support on it. The subsequent layers are casted only after the layer dried well in air. The casting was performed by automated machine in this study. The casting was always done at a constant speed of 4 $mm.s^{-1}$ for all the layers. The Figure II.11 shows an automated tape casting machine used in this study.

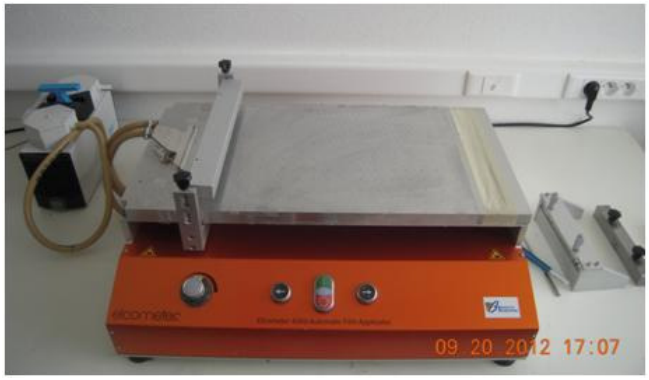

Figure II. 11 Automated tape casting machine

There is certain minimum thickness of blade to be maintained during casting for an anode support. This range is from 500 to 800 µm [31, 32]. The optimal thickness necessary for an electrolyte layer to give best performance after sintering is 5-20 µm [33]. First an electrolyte layer with blade thickness of 40 µm was casted on a clean glass plate. The Figure II.12 shows the electrolyte layer casted.

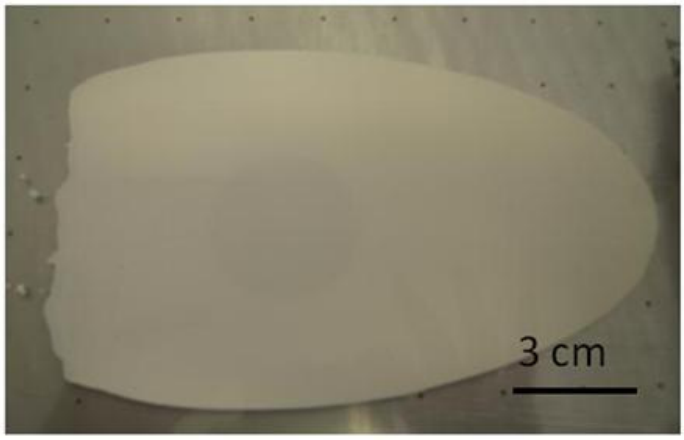

Figure II. 12 Electrolyte layer

Once the electrolyte layer is casted, it is followed by drying step. As discussed earlier the drying is preferred in controlled condition to avoid any difference in temperature change. In this

work drying step is carried out in constant room temperature in air. The drying step is crucial because, if the drying time is too long it can allow evaporation of dispersant along with solvents, which may lead to cracks in the dried tape. If dispersants are evaporated due to long time drying, it may also leave adhesion problem between different layers of tape. So drying time is always controlled to have an effective tape. Mostly the drying time is less for thin layers, but when it comes to anode support it may take bit more time due to large thickness. But in this study the drying times are optimized for all the layers after serious of experiments and are kept constant at 60 min before casting the subsequent layers to obtain a green tape.

Then AFL layer is casted on top of the electrolyte layer (Figure II.13). The blade thickness maintained during casting was 40 µm.

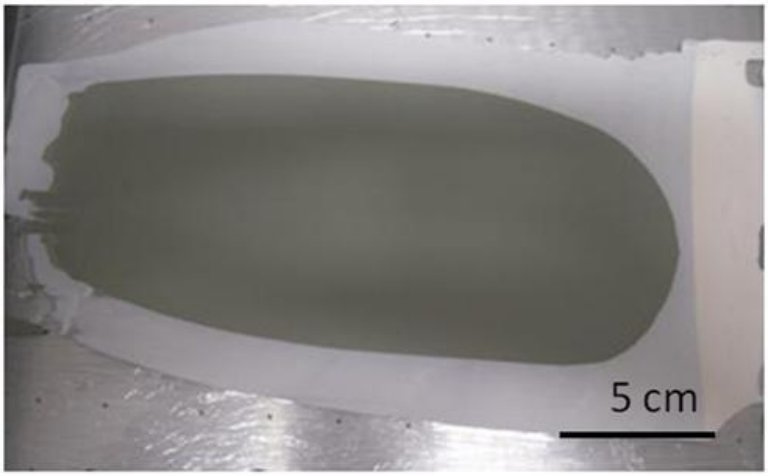

Figure II. 13 AFL on top of electrolyte layer

This layer was dried for 60 min before casting the next layer of anode support. With the blade thickness of 720 µm, anode support layer is cast above the AFL. This is shown in Figure II.14.

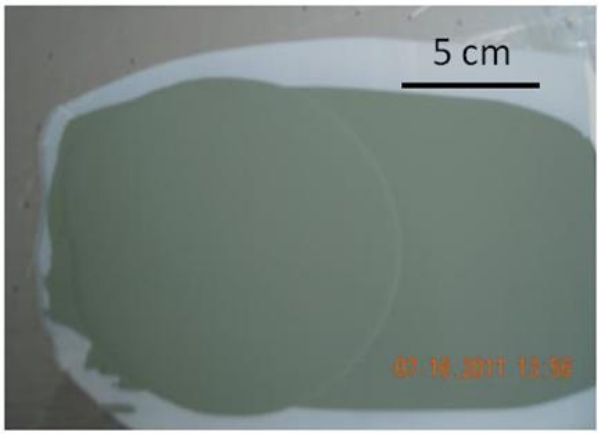

Figure II. 14 Anode support layer above AFL

This was also dried for an hour and then it is carefully removed and sintered. This structure consisting of anode support layer, AFL and electrolyte layer is called half cell.

Once the suspension is dried to form a green tape, it is removed and cut in required shape. In this work both coin cells of active area 2 cm^2 and large planar cells of active area from 10 cm^2 till 50 cm^2 were prepared. Cutting was done by normal knife blade for large area and by mold punches for button cells. This cutting of electrode seems to be crucial step, because if there are little deformed edges, it affects the consequent layers and leads to breakage of cell during sintering. The preparation of button cells was easy and quick compared to large area cells because, it leaves less deformed area during cutting. Cutting of large area electrode was always difficult and lot of time and efforts are taken to perform it to have least possible deformation and obtain a good cell.

II.4 Sintering

Sintering is the heating step done to a tape. Sintering is the normal process of heating of a ceramic material to a temperature below its melting point to obtain a required shape or structure. This is always facilitated at higher temperatures. During sintering the diffusion of atoms takes place at higher temperature and also it helps in grain growth. It also helps in getting a compact microstructure.

During sintering, all the solvents, binders, dispersants, plasticizers, poreformers are evaporated and burnt. The burning of binders and poreformers leave enough porosity in electrodes, while sintering at higher temperature helps in attaining dense electrolyte. This sintering of green tape was always peformed on sintering plates made of alumina silica plates which are non reactive to chosen electrode active materials. Sintering is one of most important step in obtaining a cell.

The choice of temperature is crucial to obtain porous electrodes while maintaining the best possible dense electrolyte. Generally for an anode support consisting of NiO/GDC10 and electrolyte layer of GDC10, the sintering temperature used in literature is 1350°C for 3 hours [15]. In this work, the cell was sintered at 1350°C for 3 hours to test. Rising of temperature during sintering is another factor to be chosen carefully. Rapid increase of temperaure can cause cracks in tape, which eventually leads to deformed cell structure. In this study rising of temperature was done at 1°C per minute to avoid any deformation in green tape. Gradual increase of temperature to sintering temperature leads to irregular burn out of pore formers. So increasing temperature was done at constant rate. For burnout of pore formers, different temperatures were tested and

optimized to 280°C isothermal for 1 hour and then it is raised to final temperature. Once after sintering the furnace is also cooled to room temperature at same rate as heating. Once sintering is done, a required structure will be obtained. This process of sintering many layers together is called as cosintering. All this sintering was done in air atmosphere. The Figure II.15 shows the sintering protocol used.

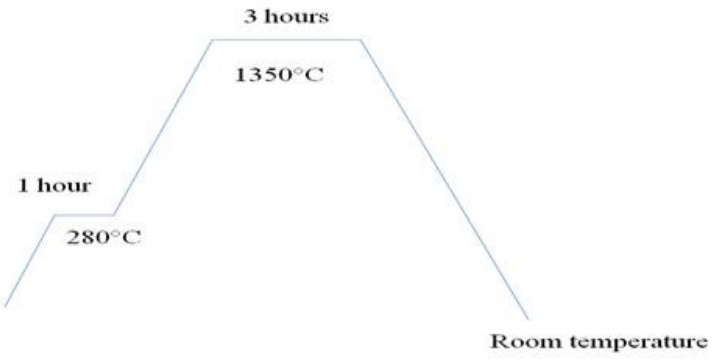

Figure II. 15 Sintering protocol for anode support half cell

Then the sintered half cell with an anode support layer, AFL, and electrolyte layer were taken out from the furnace. The Figure II.16 shows the sintered half cell: The half cell obtained is leached by the sintering plate during sintering; the electrolyte layer is on top.

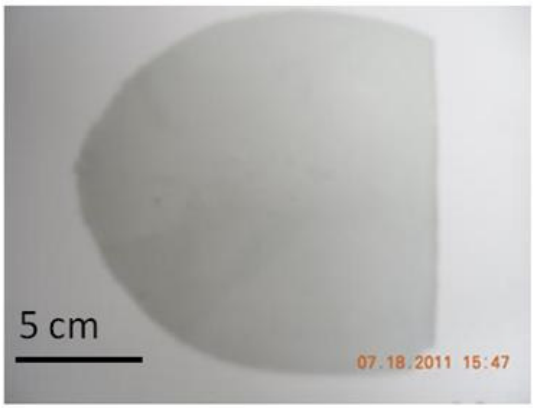

Figure II. 16 Sintered half cell

The obtained half cell was placed on the glass plate. The deposition of cathode layer was performed on the half cell. Care was taken to avoid breakage of half cell during deposition of cathode layer. The thickness of blade was adjusted to 60 µm. Figure II.17 shows the full cell obtained only by tape casting. The black layer is the cathode deposited by tape casting on top of an electrolyte layer of half cell. It was observed from the Figure II.17, that the cathode layer is non homogeneous in thickness. It was dried in air for 1 hour and then sintered at 1100°C for 1 hour with heating and cooling ramp of 1°C per minute. The Figure II.18 shows sintering protocol for cathode layer.

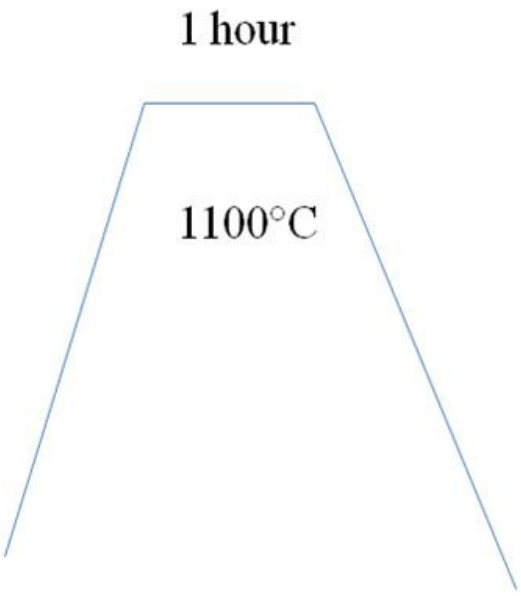

Figure II. 17 Full cell by only tape casting **Figure II. 18 Sintering protocol for cathode layer**

The obtained cell after sintering was seen without any deformation or crack. A part of cell is polished and then studied under SEM. This SEM studies were performed on SUI1510 device. The Figure II.19 shows the cross section of cell obtained after polishing by SEM. Many observations were done by SEM. First by the usage of potato starch as poreformer, the pores

seen after sintering were very large, and they were irregular in structure. In some places they were continuous from anode to cathode. The C refers to cathode layer on the left side of electrolyte in the SEM picture. E refers to electrolyte layer in the middle and A refers to anode support layer on the right side in the SEM picture.

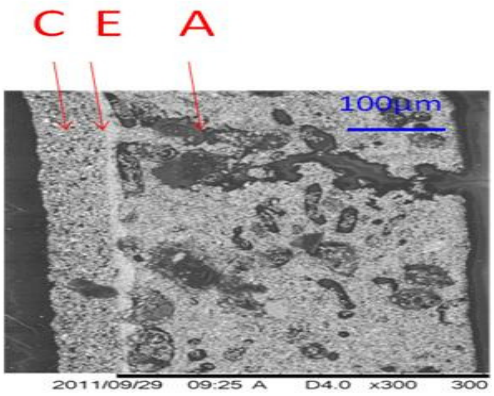

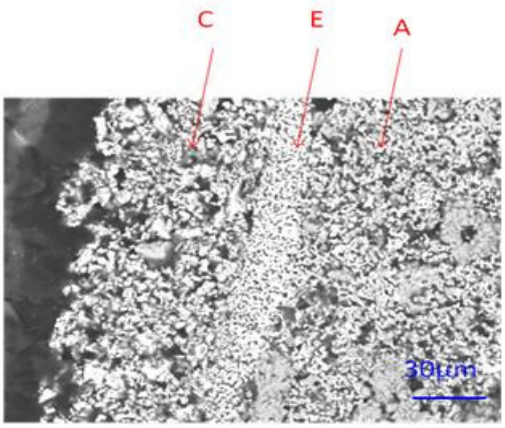

Figure II. 19 Cross section of cell by SEM **Figure II. 20 Focus on electrolyte layer with 45% of solids**

The thickness of full cell was also estimated by SEM. The Figure II.20 shows the focus on electrolyte layer of cell which is represented by E in the middle. The Anode layer is represented by A on the right side of the electrolyte in SEM picture and Cathode layer represented by C on the left side of the electrolyte. More effort was made to study an electrolyte layer. The thickness of electrolyte layer obtained after sintering was 8 µm. The cathode layer thickness estimated by SEM was 35 µm. The thickness of AFL and anode supported was 245 µm. The main observation was the GDC layer was porous after sintering.

EDX analysis was done on sample to check if there is any infiltration or interfacial reaction at electrode /electrolyte interface. The Figure II.21 shows the EDX analysis on back scattered SEM image. From Figure II.21, GDC10-HP can be seen in white colour. The black dark patches on the anode layer come from pore formers after sintering.

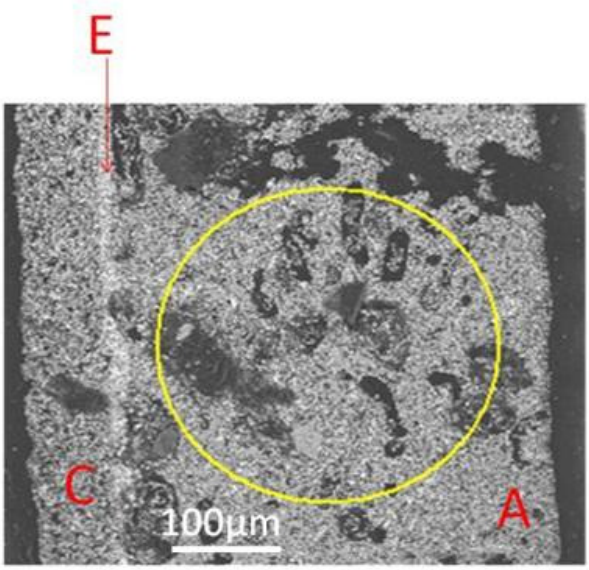

Figure II. 21 EDX analysis on an anode layer

The Figure II.22 shows the EDX spectra on an anode layer. It can be seen that there are not spectra seen from any of cathode material in the anode part: it can be concluded that there is no infiltration.

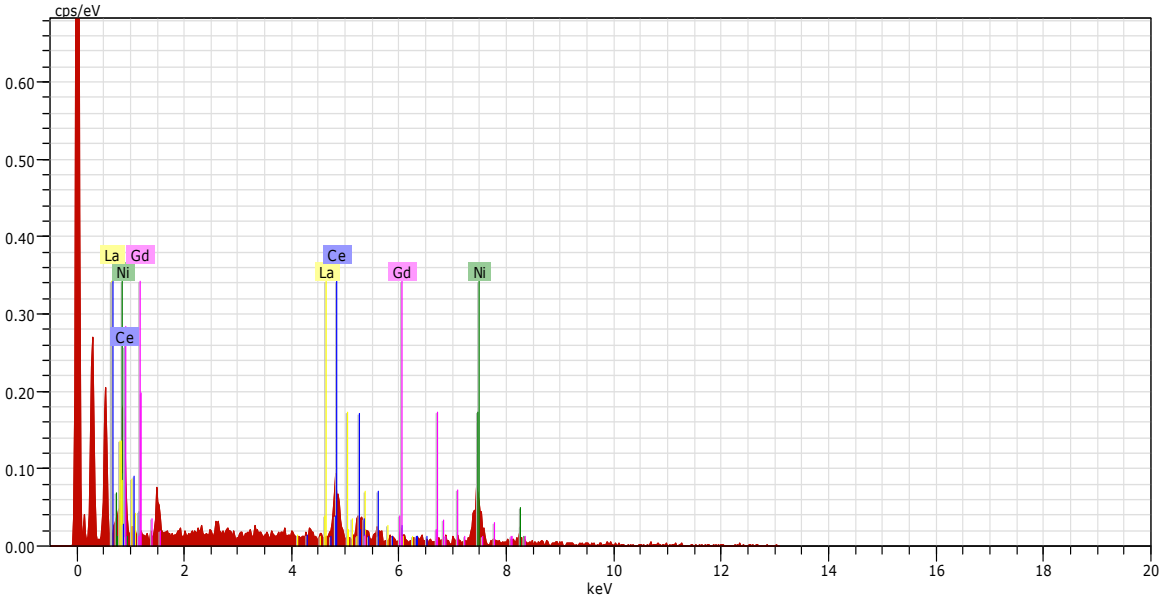

Figure II. 22 EDX spectra on an anode layer

From the EDX analysis, it can be seen that in the anode layer, there is no infiltration of cathode material because no La was found.

II.5 Conclusion

Firstly, from the initial trial it was observed that the two steps sintering process, by making an anode half cell first and then tape casting cathode layer on top of it, made difficult to obtain a homogeneous thickness of cathode layer. So the method of fabrication needed to be changed and adopted to obtain a flawless cell. Secondly, it was concluded that the percentage of solid content in electrolyte was not enough to make a dense layer. So the percentage of solid content should be increased. Thirdly, by using potato starch poreformer, large, irregular pores were seen. So, changing the percentage of starch was also suggested, including usage of grinded pore former to reduce the pore size. If the pores remain connected and irregular even after changing the percentage of potato starch, different pore former should be recommended.

Part III

III.1. Adaptation of new process for fabricating a cell

Since the fabrication of an anode half cell and the tape casting of the cathode layer on top of it to make a full working cell was futile, new simple fabrication process was conducted. This development method is simple, cost effective process, and it was patented [34, 37] because it was the initial attempt to make and report a fabrication process of full working cell only by i) tape casting, ii) involves only one step sintering, at low temperature to obtain a full cell, iii) no usage of sintering aids iv) no usage of lamination step. This new process is discussed below. First the composition of an electrolyte layer ratio was changed to 55:45 of solids to liquids. This enhanced the dense packing of solids in electrolyte layer after sintering. This was studied through SEM and EDX. The Figure II.23 shows the EDX and back scattered analysis on electrolyte layer containing 55% weight of solids in slurry. Nickel is represented in green, Cerium is represented in orange and Gadolinium in pink color. Comparing this Figure II.23 with Figure II.20, it can be clearly seen that the packing of solids in electrolyte layer is very close and dense after changing the solid content in electrolyte slurry. So from now on, electrolyte layer with 55% of weight of solid contents will be used and discussed.

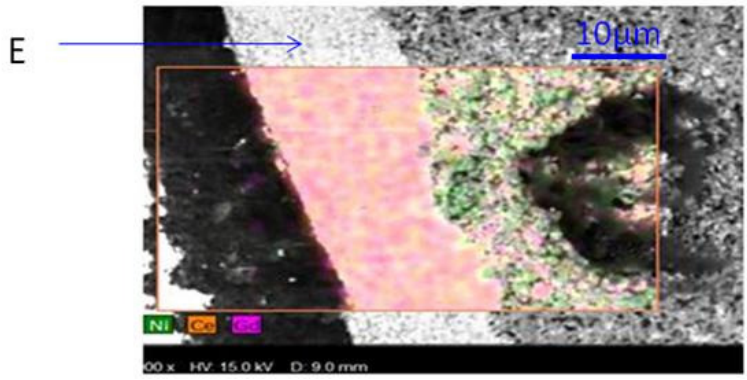

Figure II. 23 EDX on electrolyte with 55% weight of solids

The Figure II.24 shows the EDX anlaysis on the electrolyte and anode layer of half cell containing 55 weight percentages of solids. It was observed that there was no infiltration either by sintering plates or anode materials on the electrolyte layer; pure dense electrolyte layer only with GDC10 was obtained.

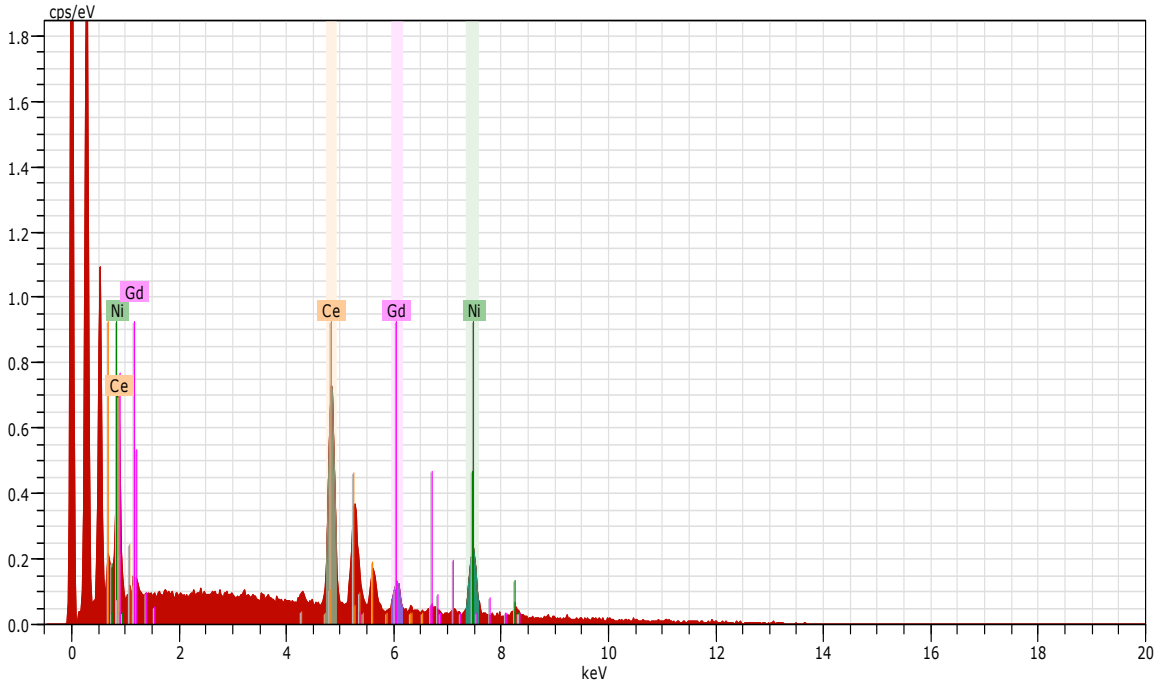

Figure II. 24 EDX analysis on half cell containing 55% weight of solids

III.2. Development of new fabrication process by tape casting approach

In order to obtain a homogeneous cathode layer thickness by tape casting on an anode support cell, new idea was drawn, and implemented in the fabrication process. By implementing the new idea, it was possible to obtain a complete full working cell. This idea also leads to many other advantages as discussed below.

III.2.1. Tape casting from cathode layer

The conventional process of fabricating a cell by tape casting includes only formation of a half cell which includes (electrolyte layer, anode functional layer and anode support layer) [15, 24, 38, 39]. Cathode layer deposition by tape casting on an anode half cell was never reported before since it was difficult to obtain. So other techniques like screen printing were employed to deposit a cathode layer. After deposition, the cell required to undergo another thermal heat treatment at high temperature sintering. So by using this conventional process, two sintering steps are used. (i.e) sintering of anode half cell and then sintering of cathode layer.

In the development of new process, the idea of casting cathode layer first was incorporated on a clean glass plate. By doing this homogeneous thin layer of cathode could be obtained. This was then dried for an hour and cut. The Figure II.25 shows the new process of casting sequential layers, which is later dried in air and cut to the required size for sintering and to suit electrochemical measurements device.

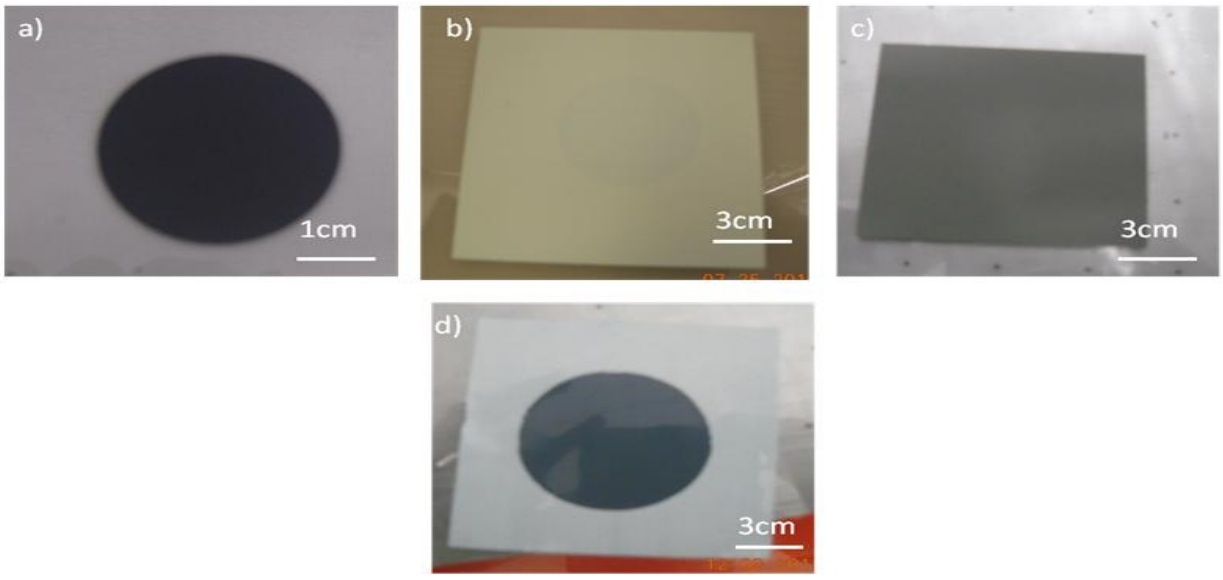

Figure II. 25a) Cathode layer b) electrolyte layer on cathode c) AFL and anode support layer on electrolyte, d) green cell before sintering

This green cell obtained was sintered at conventional sintering temperature of maximum 1400°C in first instance, and then it was reduced to 1300°C. The cathode cannot be sintered above 1300°C, considering the fact that higher sintering temperature of cathode leads to microstructure change, increases the grain size, lowers electrical conductivity and makes it dense. These high sintering temperatures of cathode reduces also the activation energy for oxygen permeation in cathode and in turn increase of oxygen permeation flux. [40]. After sintering, the cell was taken and observed to be broken as shown in Figure II.26. The reason for broken cell was unkown in initial stages. All the cells co-sintered by one step sintering at 1300°C were broken. After fabrication of several cells at the same sintering temperature it was concluded that the sintering temperature was the problem and a change of sintering temperature was adopted.

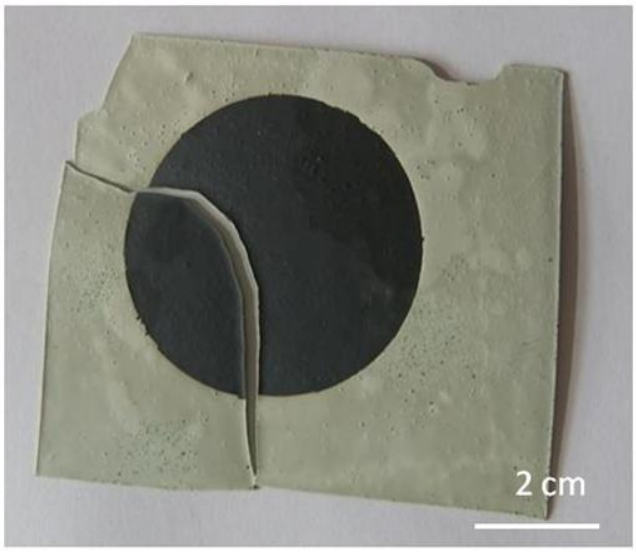

.

Figure II. 26 Full cell by tape casting sintered at 1300°C

The reduction of the sintering temperature may be good for cathode to be porous, but care should be taken because reducing the sintering temperature will lead to porous electrolyte. This

porous electrolyte will give low open circuit voltage and low power performance of the cell. So reducing the sintering temperature was optimized keeping in mind the density and porosity of electrolyte and cathode layers.

III.2.2. Optimizing of sintering temperature

Reducing of sintering temperature has direct impact on material characteristics such as particle size, surface area, etc. For example nano particles can be sintered at low temperature to obtain the similar density as high temperature sintering of micrometric particles. Different sintering temperature was tried and the results are discussed below.

First the cell was sintered at 1100°C, 1215°C, 1300°C, and 1400°C for 5 hours with one hour isothermal at 280°C with a ramp of 1°C per minute. The electrolyte sample density was calculated by pycnometer device named AccuPyc 1340 V1.05. Helium gas was used in the experiment. The literature density of GDC10 was 7.2 $g.cm^{-3}$.

Sintering temperature °C	Density after sintering ($g.cm^{-3}$)	Relative density (%)
1100	6.50	90.2
1215	6.83	94.86
1300	6.60	91.6
1400	6.74	93.6

Table II. 1 Density after different sintering temperature

From table II.1, it was observed that sintering temperature starting from 1100°C had density of 6.5 grams cm^{-3}. It was estimated that the maximum relative density was obtained at

1215°C. The normal phenomenon is increase of density with respect to temperature. However decrease in density after the threshold temperature of 1215°C was observed. The reason observed was that rather than forming a dense microstructure, the particles seems to coarsen. The maximum density which can be obtained for the particles produced by co precipitation process was 95% [41]. This is however evident from SEM pictures. The Figure II.27 a) shows the electrolyte sintered at 1100°C. At this temperature much pores in electrolyte layer were observed and it is directly ruled out to use this temperaurte further. The Figure II.27 a) shows the cross section of cell, where the left layer corresponds to cathode, the white layer in the middle is the electrolyte layer which is represented as (e). Figure II.27 b) shows electrolyte sintered at 1215°C. It was seen that the packing of solids in electrolyte layer was close and has less or no pores in comparison with Figure II27 a) which was sintered at 1100°C. This temperature can be used in the process as it exhibits highest density of electrolyte layer.

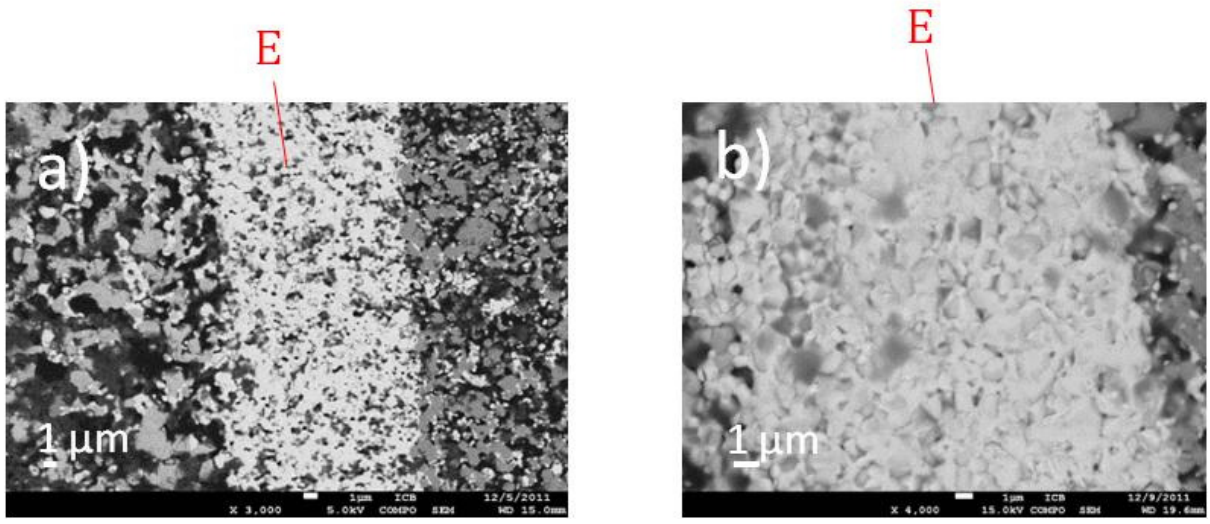

Figure II. 27a) Electrolyte sintered 1100°C b) Electrolyte sintered 1215°C

The figure II.28 a) shows the electrolyte sintered at 1300°C and Figure II.28 b) shows an electrolyte sintered at 1400°C.

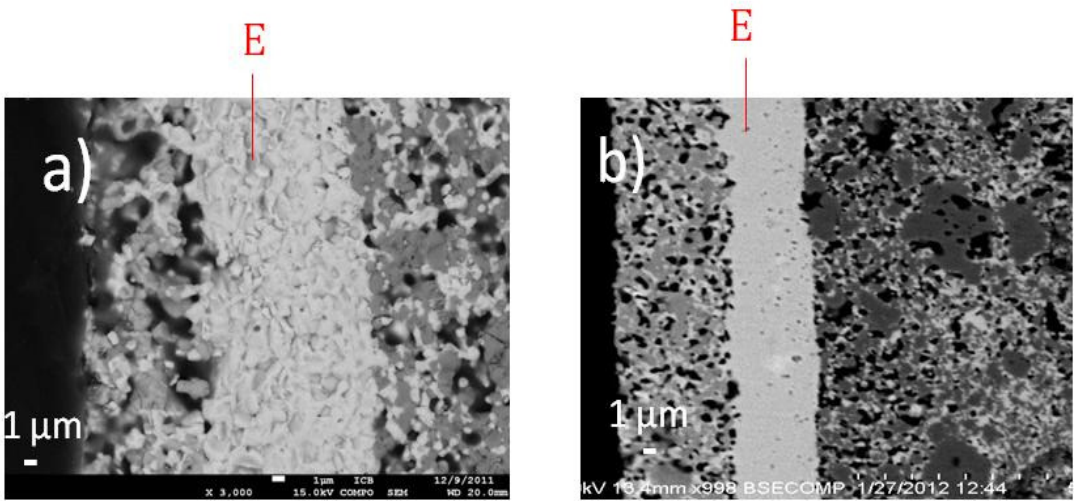

Figure II. 28 a) Electrolyte sintered at 1300 °C 28b) Electrolyte sintered at 1400°C

At high sintering temperature of 1300°C and 1400°C, the SEM pictures in the Figure II.28 show that the electrolyte particles are coarsened. The density measurement exhibits a decrease in relative density of the electrolyte layer. There are also other problems at high sintering temperature such as breakage of whole cell structure as shown in Figure II.29. There seems to have a problem in co-sintering at a temperature above 1300°C.

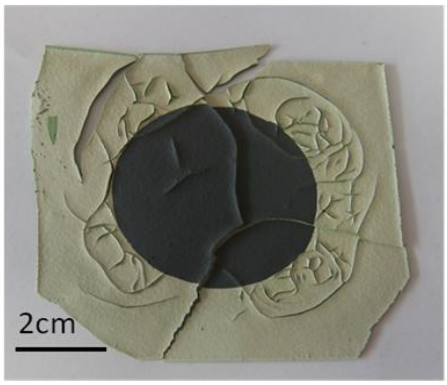

Figure II. 29 Cells sintered at high temperature above 1300°C

XRD characterization was performed on the anode sample, to check for any change in the lattice parameter. The Figure II.30 shows the XRD pattern of NiO-GDC obtained after different sintering temperatures starting from 1215°C in red, 1255°C in blue, 1300°C in green, and 1400°C in pink. The black color peaks represents the raw NiO-GDC before sintering. It was observed that there is no change in material structure at sintering temperature till 1400°C. Further no new peaks were also seen. It shows that there is no interdiffusion between NiO-GDC10.

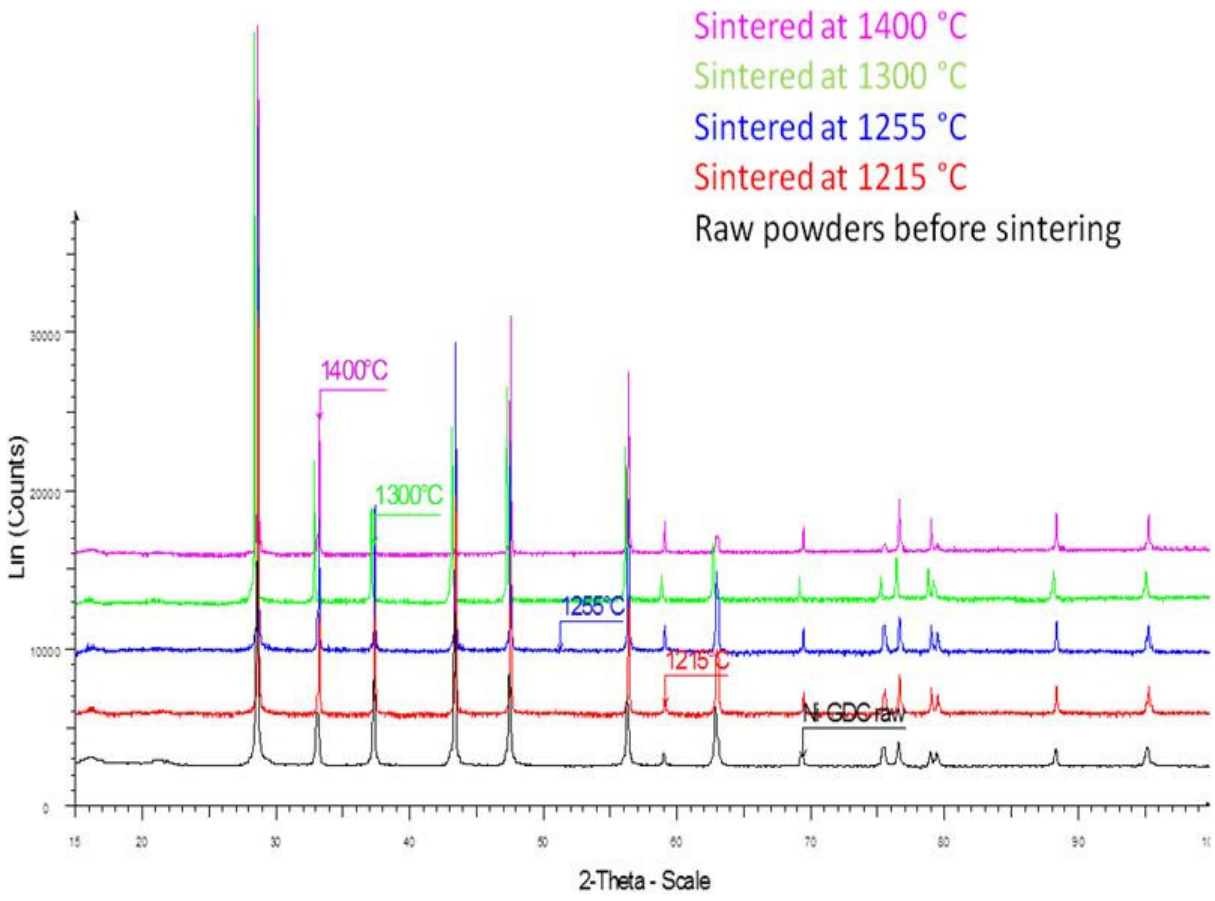

Figure II. 30 XRD pattern of anode at different sintering temperature

The characterization was also performed on the cathode side, where some change was expected at higher temperature. Figure II.31 shows the XRD pattern of cathode side which was sintered at different temperature starting from 1215°C in red, 1300°C in blue, and 1400°C in green. The peak in black color represents raw cathode composite (LSCF48+GDC10). To surprise there was no change obtained even at 1400°C, and further no mutual diffusion were seen between LSCF48 and GDC10. EDX analysis also showed no diffusion.

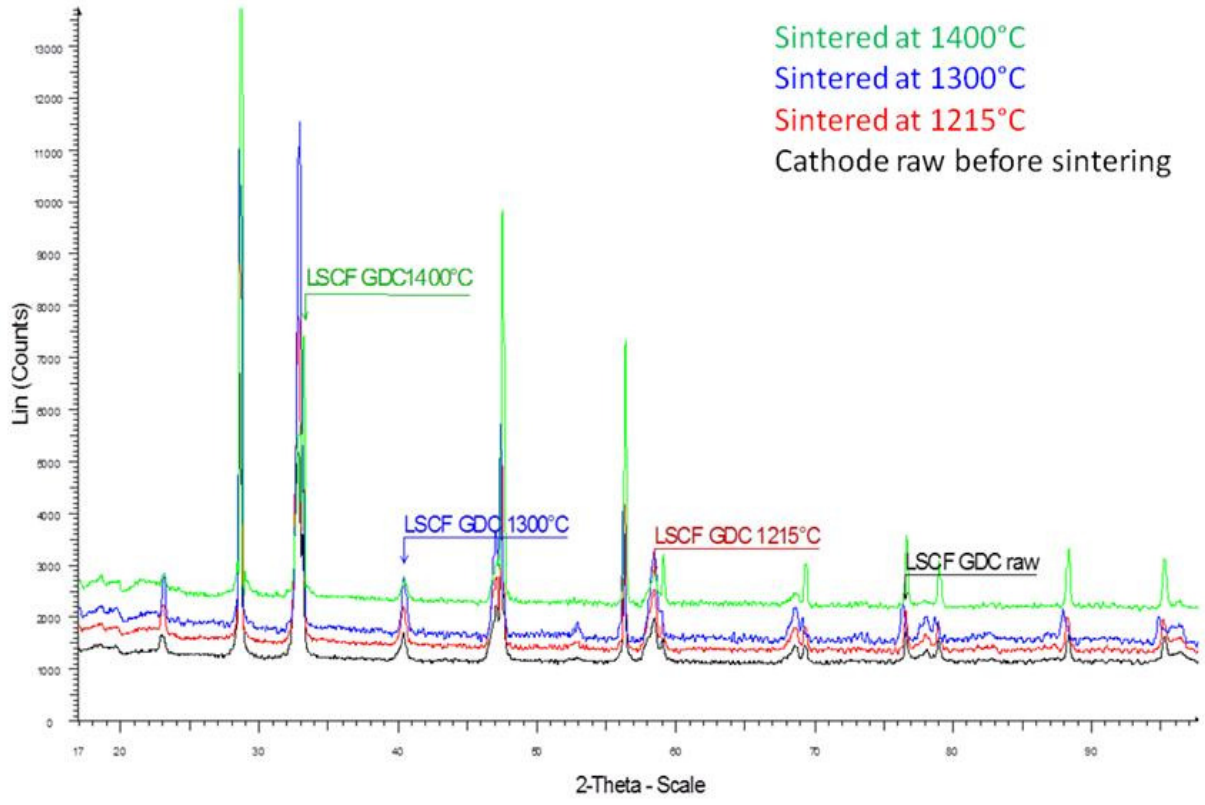

Figure II. 31 XRD pattern of cathode at different sintering temperature

So from all the sintering temperature experiments done, the suitable temperature for co sintering of full cell was found to be 1215°C, which has the highest relative density of 94.8.

Moreover at this temperature the cell obtained was very good without any flaw as shown in the Figure II.32. This full working flaw less cell was prepared by only tape casting, without using any sintering additives at high temperature; the cell was sintered at low temperature compared to conventional sintering temperature of 1500°C. It must also be noted that there was no lamination step used in the process. So by using only tape casting approach and sintering at low temperature, a full working cell was obtained. This work was patented by V.Sivasankaran et al. [34,37]. This process enjoys the advantage of cheap fabrication process, using no sintering aids, no lamination process, and single step sintering to obtain a full working cell, compared to conventional 2 steps sintering process, which adds to fabrication costs.

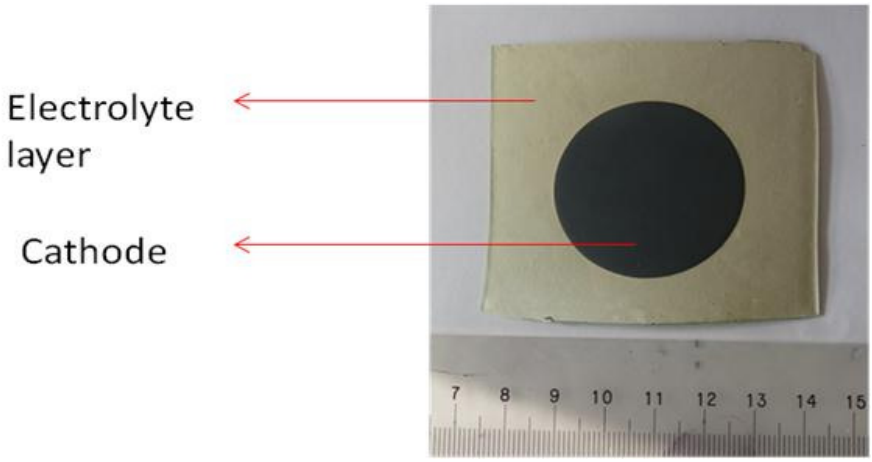

Figure II. 32 Flaw less cell obtained by only tape casting after sintering

III.2. Pore former selection.

Cells of different architecture were prepared by this method. Different pore former percentages were studied employing different pore formers. Cells including large area up to 50 cm^2 cathode areas were prepared. This method can be easily extrapolated to large area of more

than 100 cm^2 active area, provided there is an availability of furnace to sinter. The obtained cells were studied by SEM to optimize poreformer parameter. The Figure II.33 shows R-Cell (Rectangle cell) obtained by tape casting process.

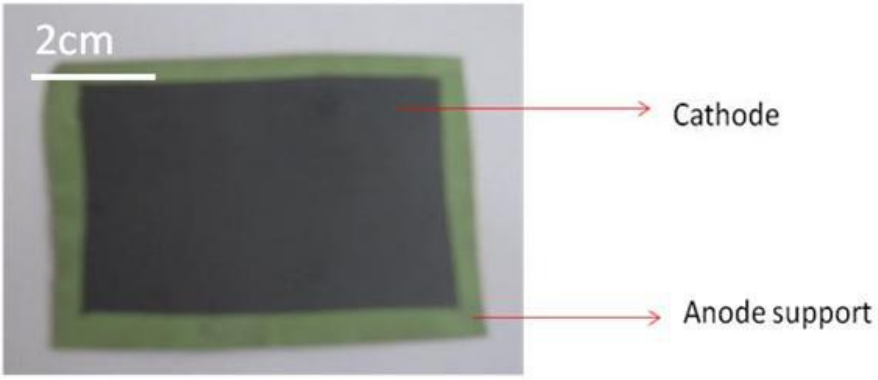

Figure II. 33 R-Cell of 24 cm^2 active area

This Figure II.33 is a proof to show that any architecture can be prepared by this new process. The black part shows an active cathode area of 24 cm^2, the green part represents an anode support and anode functional layer embedded together. Once after optimizing the main parameter of sintering temperature, the next parameter focussed was pore former and its percentage to be used.

The first trial was done by using potato starch as pore former. The Figure II.34 shows the cross section of cell using starch as pore former. It is very evident from this picture that by using potato starch poreformer, the pores obtained after sintering were very big in size and non homogeneous along the anode support. The 10 weight percentage of starch was used in the formulation.

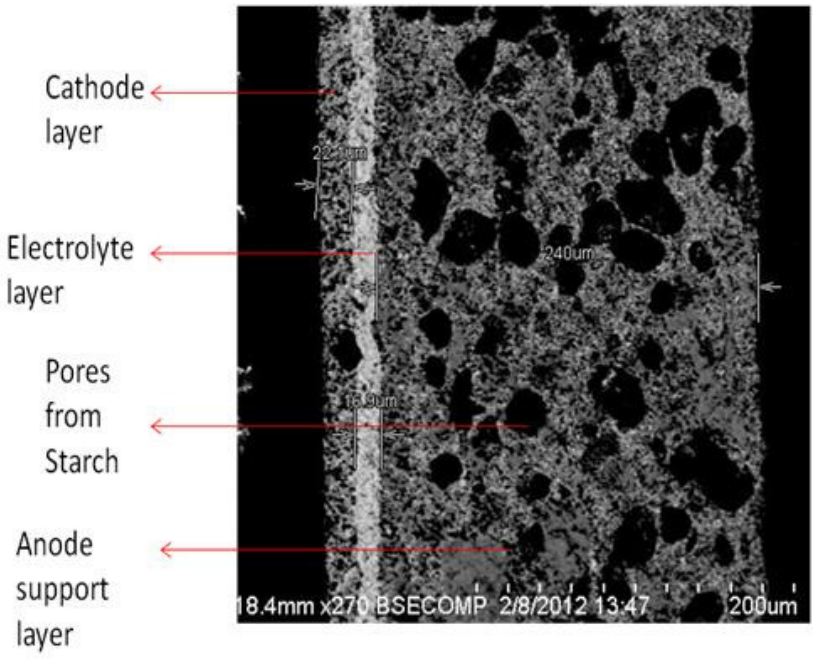

Figure II. 34 Cross section of cell with starch poreformer

This non homogeneous pore structure will have an impact in the performance of cell with regards to high polarization in anode. So this was optimized. Using high percentage of pore former in anode support leads sometimes to breakage of cell during sintering. So a change in pore former percentage formulation was done to reduce the pore size and breakage. The Figure II.35 a) shows the cross section of cell with 8% of starch and Figure II.35 b) shows the cross section of cell with 5% in weight of starch in anode. It was observed that when using lower percentage of starch in an anode support layer the pores were reduced in size and seems to be more homogeneous across the anode. However, cell with 5% in weight will be subjected to electrochemical characterization later. The layer on the left side represents cathode and the white intermediate layer is electrolyte, the layer next to electrolyte is the anode functional layer with no pores, the layer with pores is an anode support layer.

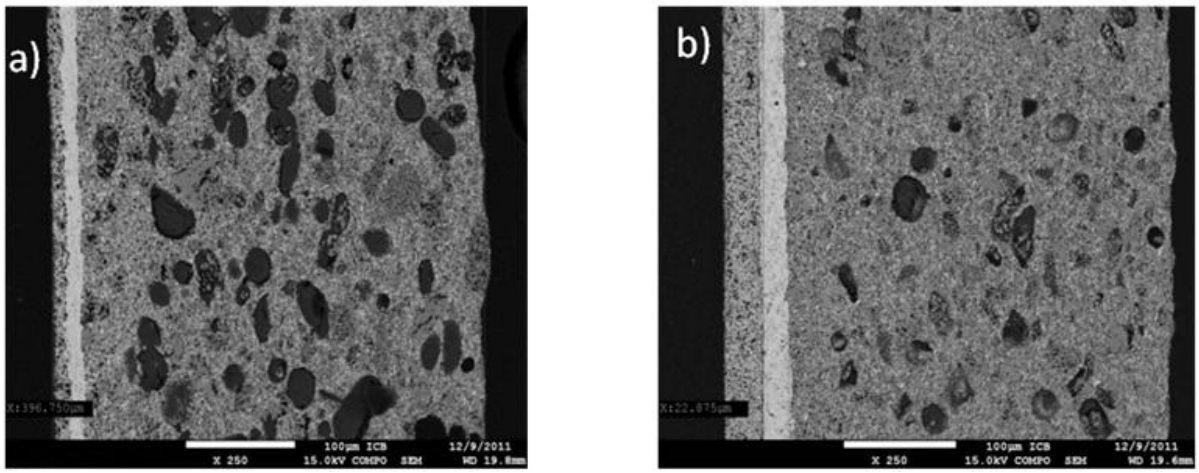

Figure II. 35 a) Cross section of cell with 8% of starch in anode b) 5% of starch in anode

Another pore former named carbon black was also employed in preparation process. It can be seen from the Figure II.36 showing the cross section of cell using carbon black as poreformer that the pores obtained were very small and homogeneous. There was no difficulty or breakage during sintering. The dispersion of carbon black in the initial step of slurry was a very important factor to be noted. After adding the carbon pore former, the jar should be manually agitated for some few minutes to make the carbon disperse well. On direct milling of carbon, settling of carbon was observed, which leads to unhomogeneous slurry not suitable for casting. The layer on left side represents the cathode and the white layer is the electrolyte, the anode functional layer is clearly seen when using carbon pore former and the large layer on right is the anode support layer. So after electrochemical characterization, carbon black was chosen as the best pore former, (ranging from 2-5%) and all optimizations from now will be based on carbon poreformer. All the results are discussed in detail.

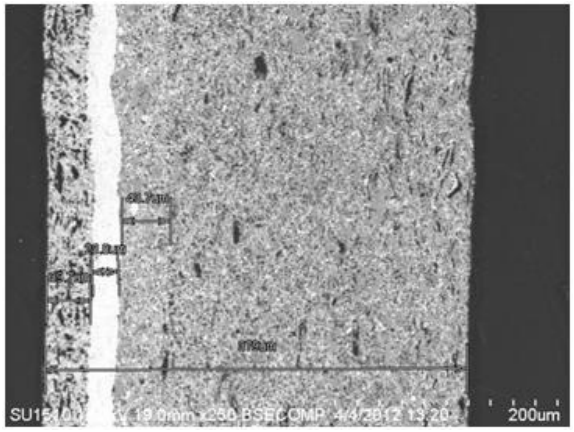

Figure II. 36 Cross section of cell with carbon black pore former

III.3. Shrinkage measurement.

During sintering due to compaction of particles in different layers, the size of the green body before sintering differs from the sintered cell. This difference is denoted as shrinkage. Shrinkage is an imporant parameter in controlling the active area of cell and anode support structure. Generally the shrinkage and relative density were measured to check the sinterability of cell structure.

Shrinkage is calculated by the formula

S shrinkage (%) = [(L0-L1)/L0]*100% where Lo is the size of the green body and L1 is the size of the sintered body.

In this work, maximum of 50 cm^2 of cathode active area was fabricated. For stacking purpose a planar cell is fabricated with minimum of 1mm gap between the cathode area and the anode support structure. This 1mm should be dense so this area should also be covered by electrolyte layer. The cell should be fabricated considering this 1mm gap after sintering. So the shrinkage estimated in this work, at 1215°C was 12.5%.

III.4. Optimization of warpage.

Warpage is a phenomenon seen during cosintering of SOFC. The cells in this work are fabricated by new patented process was flawless that can be used for electrochemical measurements. Since all these cells are fabricated by cosintering process they are naturally prone to warpage. The fabrication of button cells with 1.6 cm^2 active area was easy. It had shown no or little warpage that can fit to measurement equipment without breakage during application of load. The Figure II.37 shows the button cells. The top cell shows the ASC with black cathode layer on it, the cell in the bottom shows the anode side of ASC. On careful examination it can be seen that the cell is not so flat and it has a little warpage other than the cathode part. These cells were fit in to the measurement device and characterized. There was no breakage of cell observed during application of load to seal the cell. However this might be a problem when it comes to fabrication of large active area and stacking large cells. So care was taken to reduce warpage as much as possible, as it is impossible to completely avoid warpage in cosintering process of cell.

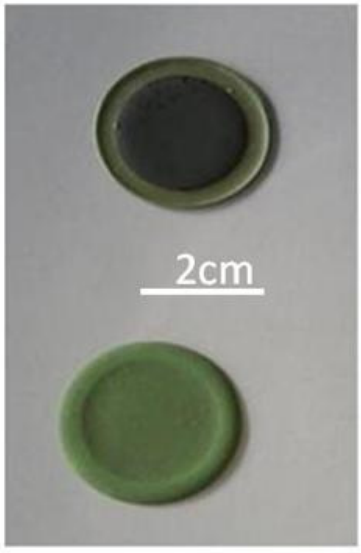

Figure II. 37 Button cells

The optimization of warpage is the next parameter considered for the study. This warpage normally occurs due to compaction of solid particles during cosintering. This compaction leads to dense structure. The main layer which is subjected to undergo compaction and become dense at sintering temperature is electrolyte part of cell. Since this process deals with cosintering of multilayers, care was taken to study from where and which temperature warpage tends to occur. It was observed that an electrolyte leads to more warpage at high sintering temperature.

In multilayers, cathode layer will also warp concave at lower temperature. This warpage of multilayers can be reduced by changing the viscosity properties of GDC layers [42]. The other possible solution is gradual loading during sintering [43]. It was also shown that loading the green body was a failure. To the contrary, the warpage was successfully drastically reduced in smaller area of less than 1.6 cm^2 button cells by loading the initial green body during sintering. After series of trials with different load, it was found that the optimal threshold load weight required for 1.6 cm^2 was 115 g equally distributed along the sintering plates. Even, by placing 5 grams more could break the cell as in the same way, 5 grams less could lead to distortion in cell structure. By using this way maximum of 4 cells can be sintered at once. This weight is the load exclusive of the sintering plates that used to cover the green cell structure. Hence by this way introducing the load initially before sintering, we were successful in reducing the warpage for cell, by optimizing the load required for it. The Figure II.38 shows the button cell with reduced warpage after loading the green body during sintering. The load required for reduction of warpage is different for different architecture.

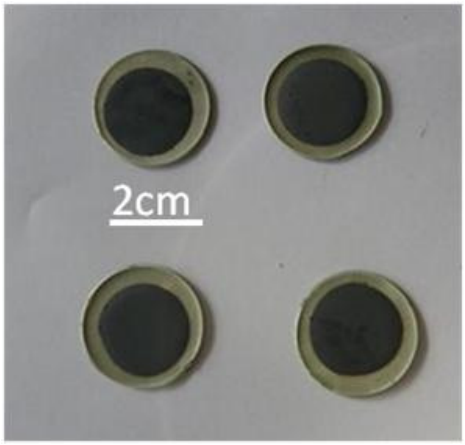

Figure II. 38 Button cells after sintering with load

For large cathode area of 10 cm^2 it was observed that warpage was more concave, due to cathode. And hence, more weight was needed to reduce it. The optimal load was estimated to be 268 g for 10 cm^2 cathode area on 8 cm*8 cm anode support.

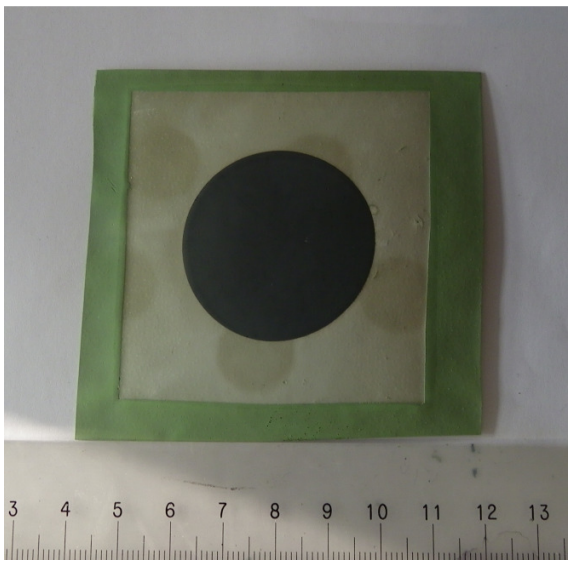

Figure II. 39 cell with 10 cm^2 active area

To prepare a square or rectangle architecture for stacking, with cathode active area above 25 cm^2, there should be 1 cm area on all sides for sealing. Reducing warpage in this type of cells was a huge task as to optimize the load needed. It was optimized to 310 g rectangular load equally distributed all along the sintering plates. The Figure II.40 shows the schema of cell prepared for stacking with cathode active area of around 36 cm^2. By this way flawless cell with large active area of 36 cm^2 fabricated by only tape casting and single step sintering at low temperature was obtained.

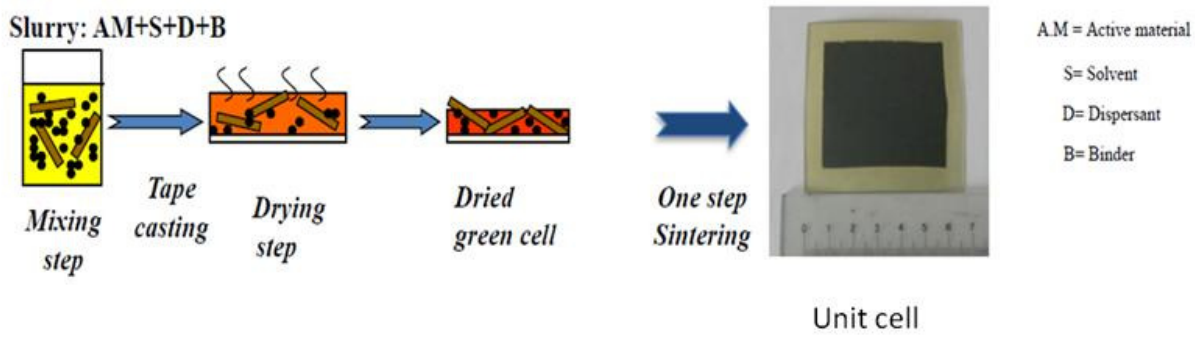

Figure II. 40 Schema of cells preparation for stacking with 36 cm^2 cathode active area

The Figure II.41 shows the cross section of cell after optimizing, all parameters including electrolyte slurry solid percentage, pore former, and sintering temperature.

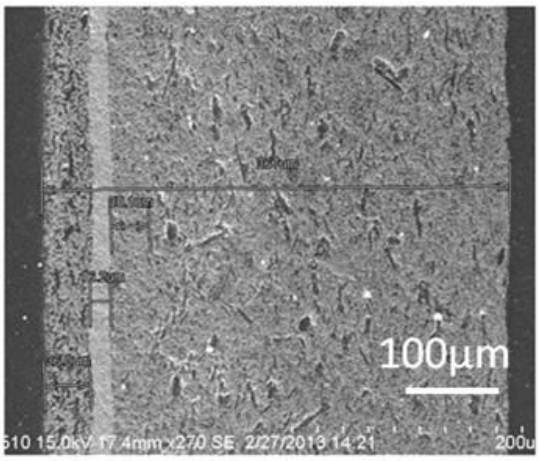

Figure II. 41 Optimized cross section of cell

III.5. Conclusion

So, in this part the solid content of electrolyte slurry was optimized. New approach of fabricating a full cell only by tape casting was presented considering the optimization of sintering temperature, selection of different pore former and its percentage to be used and reduction of warpage. By this new process, it is possible to obtain different architecture of cell right from small area that can be extrapolated to large active area as explained in detail.

Part. IV. Electrochemical results obtained by 10 cm^2 active area cells fabricated by new single step sintering process

This part will detail the electrochemical results obtained from the cells fabricated only by tape casting process. All the electrochemical experimental results presented here are obtained at Fiaxell Sarl in EPFL scientific park in Switzerland, Lausanne in Raphael Ihringer lab. The Figure II.42 shows the Fiaxell set up used for the electrochemical measurements. This is an open flange setup where all experiments were done without sealing for cells. This set up was inbuilt on ceramic insulation plates to avoid loss of temperature, which is shown in the Figure II.42 as (p). This has 4 spring load steel tubes, through which spring load rod is placed which is shown as (c) steel tube is mentioned as (m) in the figure. Through these tubes it is possible to put enough load on the system, by using spring from outside the device. The fuel feeding tube is represented by (o) through which fuel gas is fed to anode part of cell during experiment. This tube is made of inconel. The flat bottom flange is made of inconel which is represented as (i). This is the place where the cell will be placed during experiment. In the bottom, flange alumina felt will be placed to reduce the gas leakage. This is represented as (f) on top of the bottom plate. There are two other bores in ceramic insulation where there is provision for current and voltage collection. Provision for voltage measurement is denoted by (i), cathode current collection is represented by (j). For an anode current collection nickel anode meshes are used which is represented as (k). For cathode current collection, gold meshes are used which is shown as (g). To measure the temperature of cell during experiment, a thromocouple type K is used. There is special provision for thermocouple port which is shown in the figure as (b). Once the cell is placed on alumina felt with nickel meshes at bottom of cell and gold meshes at top of the cathode another alumina felt is used to cover the cell to reduce leakage of gases. Now this part is covered by inconel upper

flange which is represented as (e). This upper flange is connected with air feeding tube through which an oxidant gases are fed to the cell during experiment. This is represented as (a).

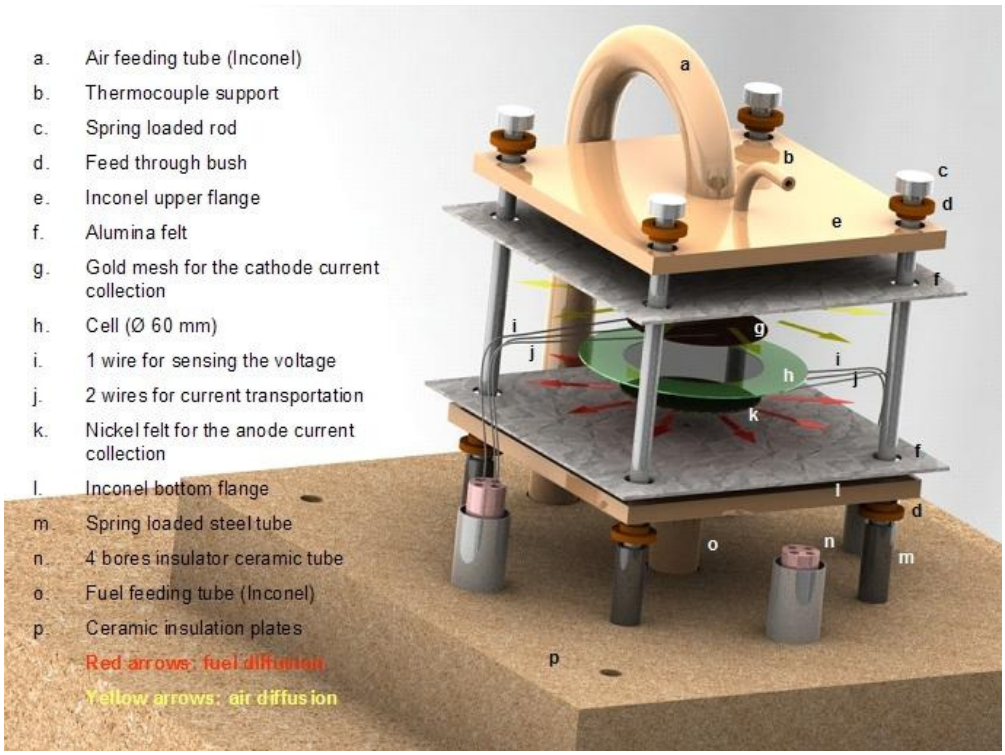

Figure II. 42 Fiaxell Set up

Once the cell is placed on the device, it is screwed well to tighten so that there is no movement of cell during experiment. Care should be taken in order not to break the cell while mounting. Then flange set up are placed on the furnace where temperature rises up and readings will be measured. All the cells were measured in the same device, using hydrogen as fuel gas with 3% of H_2O and air as the oxidant gas. After placing the device on the furnace, automatic fixed controller program will rise the temperature of the furnace. The furnace is manually programmed for rising the temperature.

The rise up of temperature is always accompanied by feeding air gas at both sides of cell. This is done to avoid any damage of cell during rise up. Once the furnace has reached the operating temperature, the air gas on the anode side of furnace is slowly replaced by mixture of N_2 and H_2 in the ratio 90:10. This gas mixture was used in the initial step of reducing the cell. This mixture will avoid the sudden reduction of anode and avoids breakage of cell. This gas was used for first 10 min of reduction step and then it is slowly replaced by supplying pure hydrogen. Care should be taken during this step of reduction when this mixture is fully replaced by pure humidified hydrogen gas. Reduction of an anode was done for 2 hours at 750°C before measurements. Now the voltmeter, ammeter, and electronic load are connected to the system for taking electrochemical measurements. This rise up of temperature and reduction of the cell takes approximately 7 hours. All the gas flow was kept at constant rate all the experiments. The results obtained on different cells are detailed taking in consideration the different configuration of the cells with active area of 10 cm^2.

IV.1. Cell with starch pore former

The first cell used starch as a pore former, the electrochemical results obtained are shown in Figure II.43. The Figure II.43 shows the graph of V vs I and P vs I at different temperature. This cell was characterized at 610°C and 640°C and exhibited OCV of 0.924 V and 0.879 V respectively. The maximum power density obtained 610°C and 640°C were 120 $mW.cm^{-2}$ and 123 $mW.cm^{-2}$ respectively. It was observed that in first test of cell, when using starch as a poreformer there was not much difference in power density at temperature higher than 610°C, even though there is little difference in the polarization at such a temperature. The reason for

lower power density was known only after studying the cross section of cell by SEM. Cathode thickness was 10 µm and Electrolyte were 20 µm.

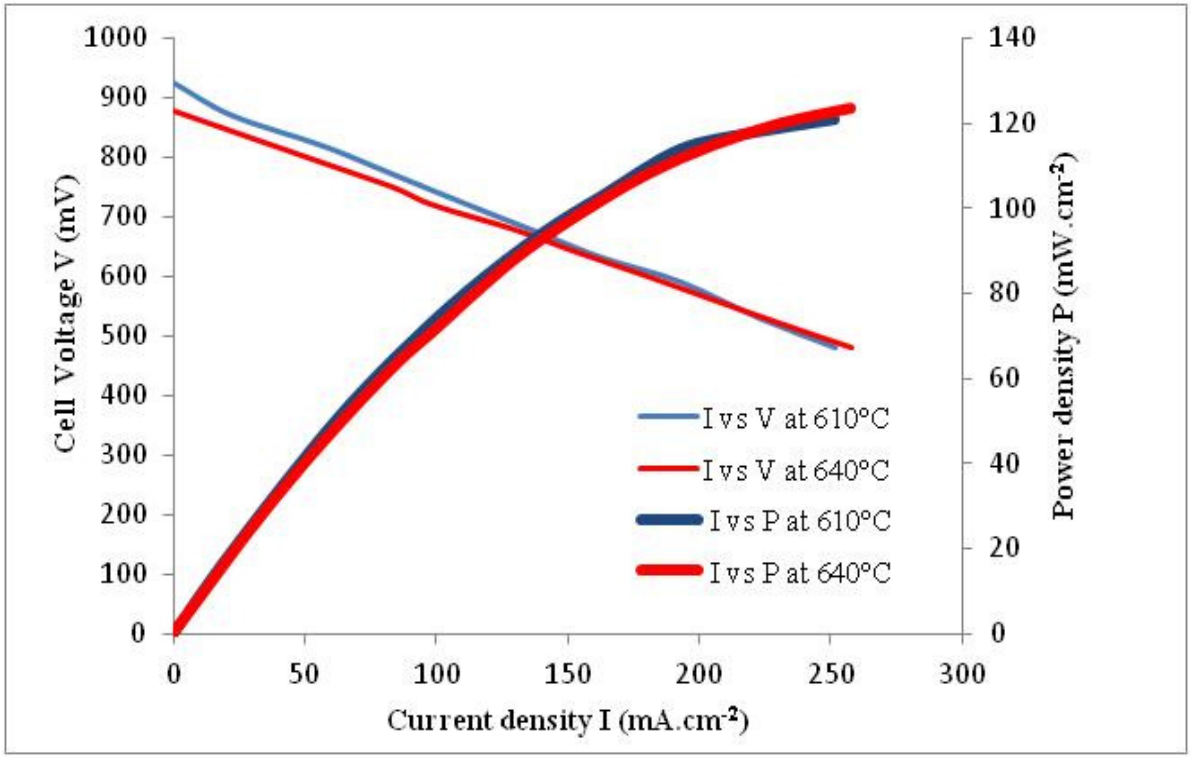

Figure II. 43 V vs I and P vs I curves of cell with starch pore former [44]

The cell was observed for morphology by SEM. The Figure II.44 shows the cross section of the cell. It shows the cathode on the left side, followed by the electrolyte layer in white, then by AFL and finally by the anode support, which is seen with large pores obtained from burning of starch pore former. These were irregular in shape and inhomogenous along the anode support, leading to lower TPB. These inhomogeneous and large pores also create large polarization and poor power density. Thus it was concluded to stop using starch pore former and proceed only by using carbon as pore former. From now on, all the cells will be using only carbon pore former.

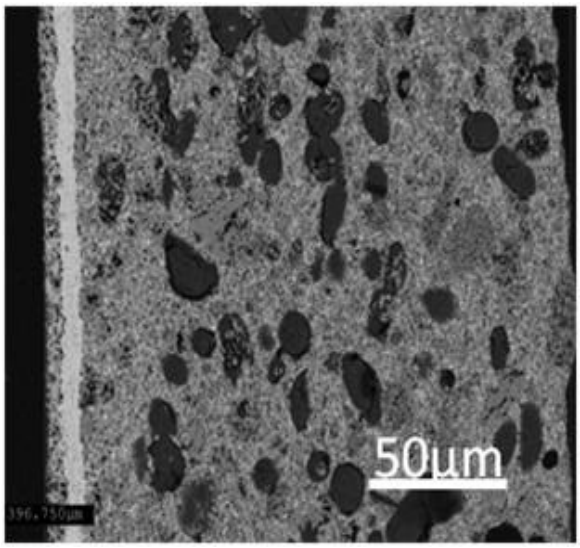

Figure II. 44 Cross section of cell

IV.2. Cell with carbon pore former

Cells were prepared by using carbon as pore former. As explained earlier the cells were little warped and in the optimization process, one trial was done by reducing the thickness of the cathode layer. The Figure II.45 shows the electrochemical results obtained from the cell with cathode layer of approximately 10 µm. The Figure II.45 shows the I vs V and I vs P at temperature starting from 500°C till 650°C at interval of every 50°C. The OCV values obtained are 0.920 V, 0.862 V, 0.785 V, 0.667 V at 500°C, 550°C, 600°C and 650°C respectively. The maximum power density of 46 $mW.cm^{-2}$ was obtained at 600°C. When using carbon as pore former, there was clear difference in OCV and power density above 550°C. The cell was observed by SEM for morphology and cross section. Several interesting results were obtained.

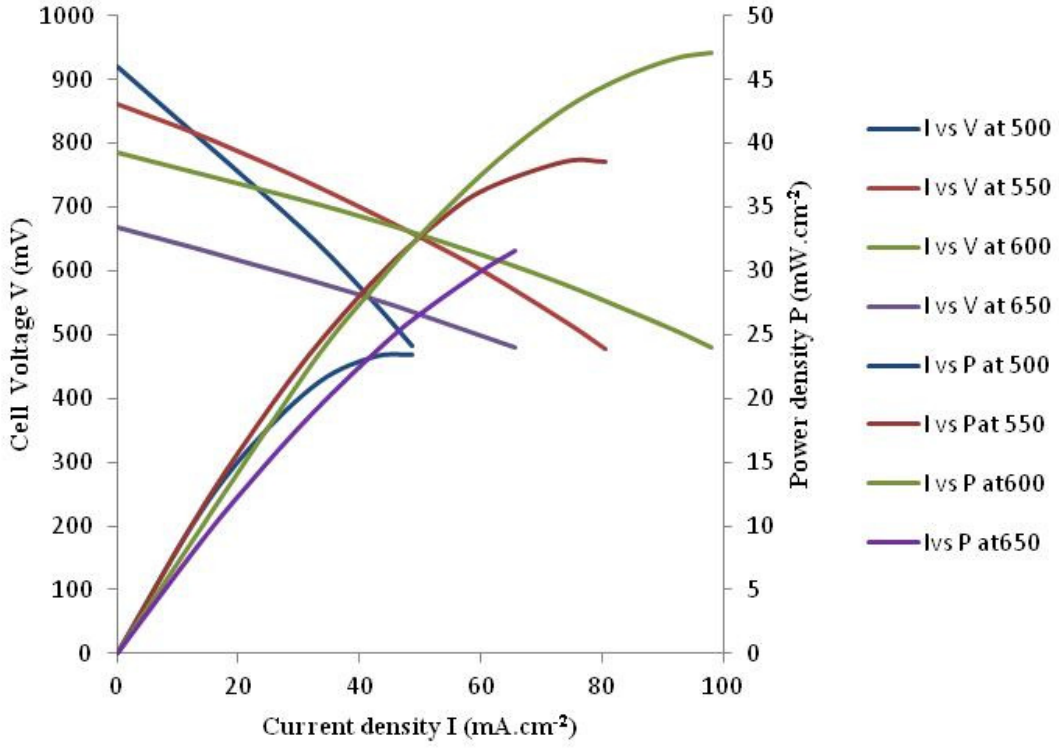

Figure II. 45 Electrochemical results of cell with carbon poreformer

The Figure II.46 a) shows the cathode surface area. It clearly shows the presence of large bubbles on the surface. The FigureII.46 b) shows the cross section of cell whose cathode thickness was found to be 10 µm. approximately. The reason for lower power density was found to be the bubbles and perceived as during the electrochemical reaction, water from anode side passed through the electrolyte and water was logged on the bubbles surface, this leads to higher polarization at operating temperature. Due to higher polarization by bubbles, there was also a degradation of the cathode surface at temperature above 650°C. They were the reason for lower power density while obtaining good OCV values. From this cell it was concluded that the

thickness of cathode will play a big role in performance of cell and from now on using carbon pore former, the thickness of the cathode layer will also be increased.

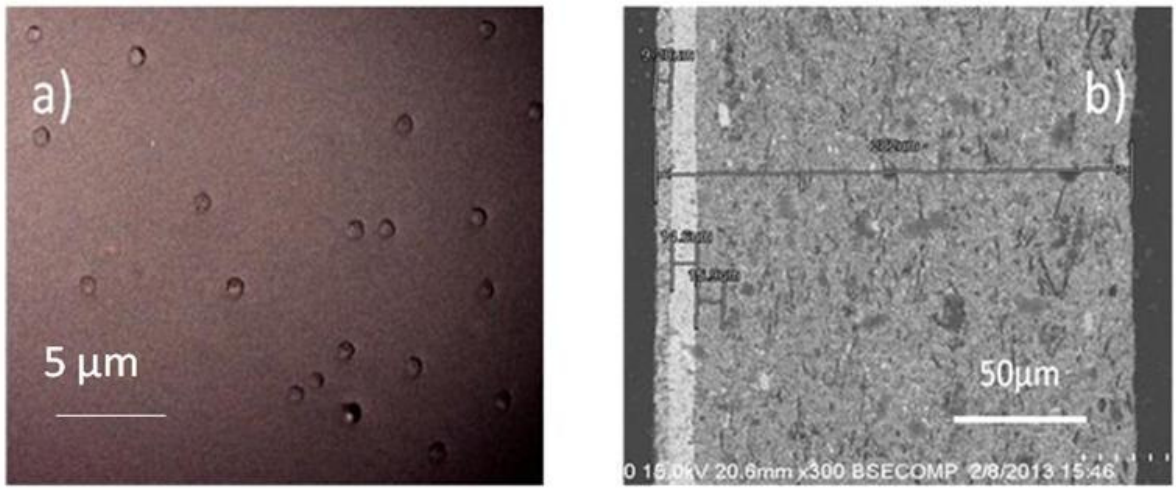

Figure II. 46 Surface and cross section of cell with carbon pore former

IV.3. Effect of cathode layer thickness and carbon pore former

So by impoving the thickness of the cathode layer, a cell was prepared with little warpage and it was characterized. The Figure II.47 shows the electrochemical results obtained from the cell. The thickness of cathode layer was around 50 µm. The values of I and V were measured from 500°C till 650°C in the interval of 50°C. The observed OCV values are 0.943 V, 0.920 V, 0.874 V, 0.798 V at 500°C, 550°C, 600°C and 650°C respectively. The maximum power density measured at 500°C, 550°C, 600°C and 650°C were 85 $mW.cm^{-2}$, 124 $mW.cm^{-2}$, 177 $mW.cm^{-2}$ and 225 $mW.cm^{-2}$ respectively. It was observed that the increase of power density were linear with respect to increase of temperature. This shows that the obtained cell was very good and obeys the theory.

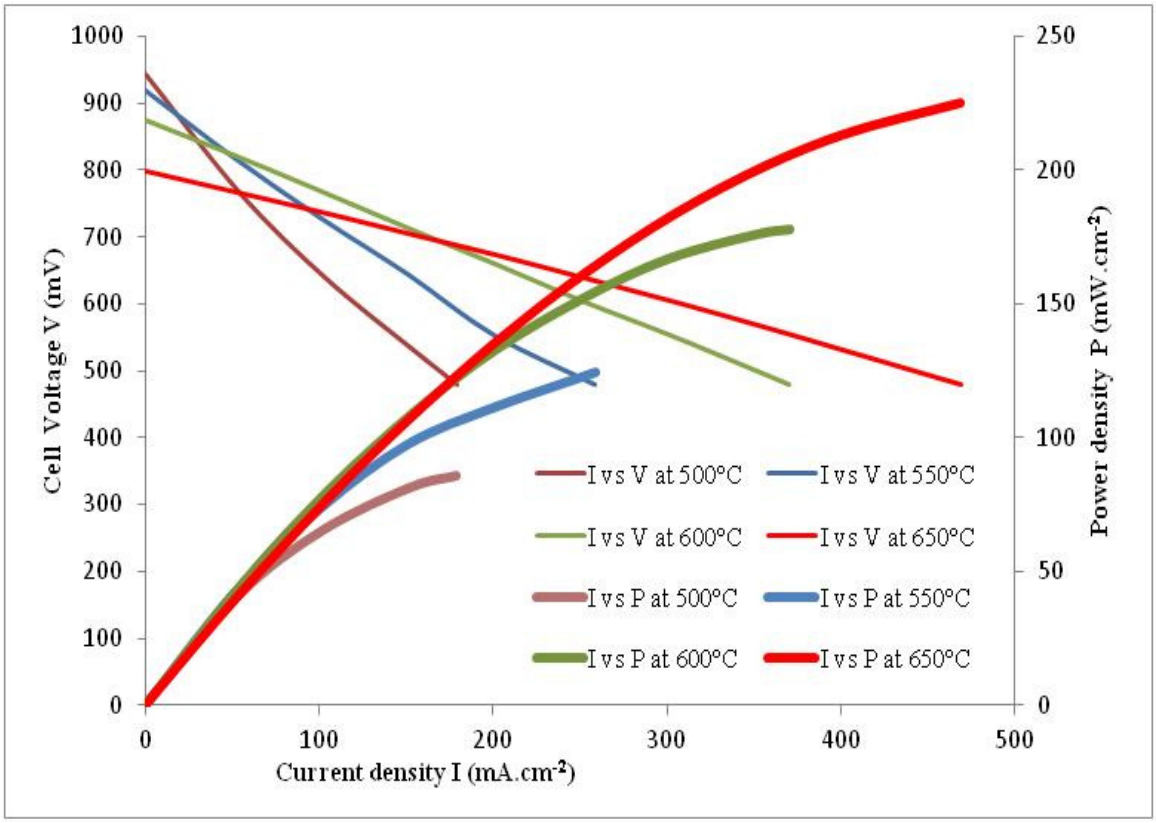

Figure II. 47 Electrochemical results of cell with thick cathode layer[44]

The Figure II.48 shows the cross section of cell with thick cathode layer which is on the left side. The cathode layer thickness measured was approximately 50 µm. The cathode layer was followed by an electrolyte layer of 21 µm, AFL and anode support layers consecutively. It was also observed that the pores in anode support were very homogeneous. Unlike the starch pore former, there were no large pores observed. By using this carbon pore former, it was also noted that the measured power densities were higher than compared to cells which used starch as pore former. Thus even pores helps in increased TPB and hence increases the performance of the cell. So it was found that by using carbon pore former and 50 µm cathode layer the performance

was improved drastically twice. This was considered as one of the best improvement on this patented process. Next studies were carried on by changing the thickness of electrolyte used.

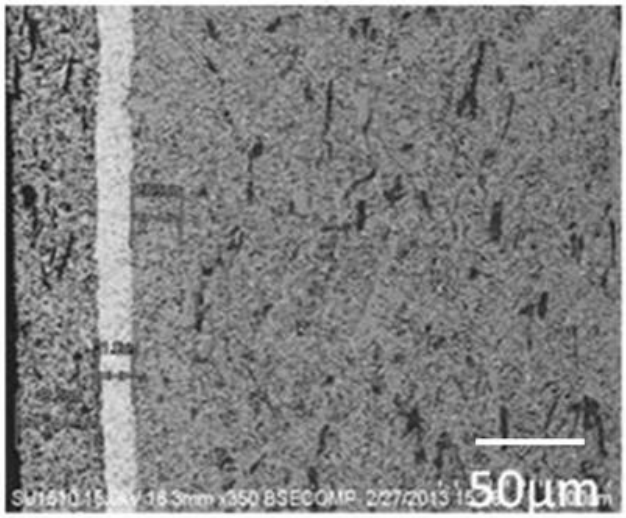

Figure II. 48 cross section of cell with thick cathode layer

IV.4. Effect of electrolyte thickness in the cell

So from the results obtained so far, it can be concluded that by using carbon pore former a cathode layer of 50 µm and a 21 µm electrolyte, the power density was increased by twice when using carbon pore former. Further studies were done by changing thickness of the electrolyte layer by keeping all the other parameters constant. The thickness of the electrolyte was doubled approximately. The Figure II.49 shows the electrochemical results obtained from the cell. The obtained OCV values were 0.879 V, 0.825 V, 0.732 V, 0.632 V at 500°C, 550°C, 600°C and 650°C respectively. The measured maximum power densities at 500°C, 550°C, 600°C and 650°C were 149 $mW.cm^{-2}$, 190 $mW.cm^{-2}$, 175 $mW.cm^{-2}$ and 110 $mW.cm^{-2}$ respectively. Several interesting results were obtained. It was noted that by increasing the thickness of an electrolyte layer, the OCV obtained was lower starting from 500°C. The thickness of an

electrolyte layer plays crucial role in performance of cell. By increasing the thickness of the electrolyte layer, the path for transfer of oxygen ion increases and much of the energy is lost in the thickness. Ohmic losses were also high with thick electrolyte. This leads to low OCV and in turn low power density. It was also discovered that the maximum power density was obtained at 550°C and at higher temperature than 550°C, the power density seems to be reduced.

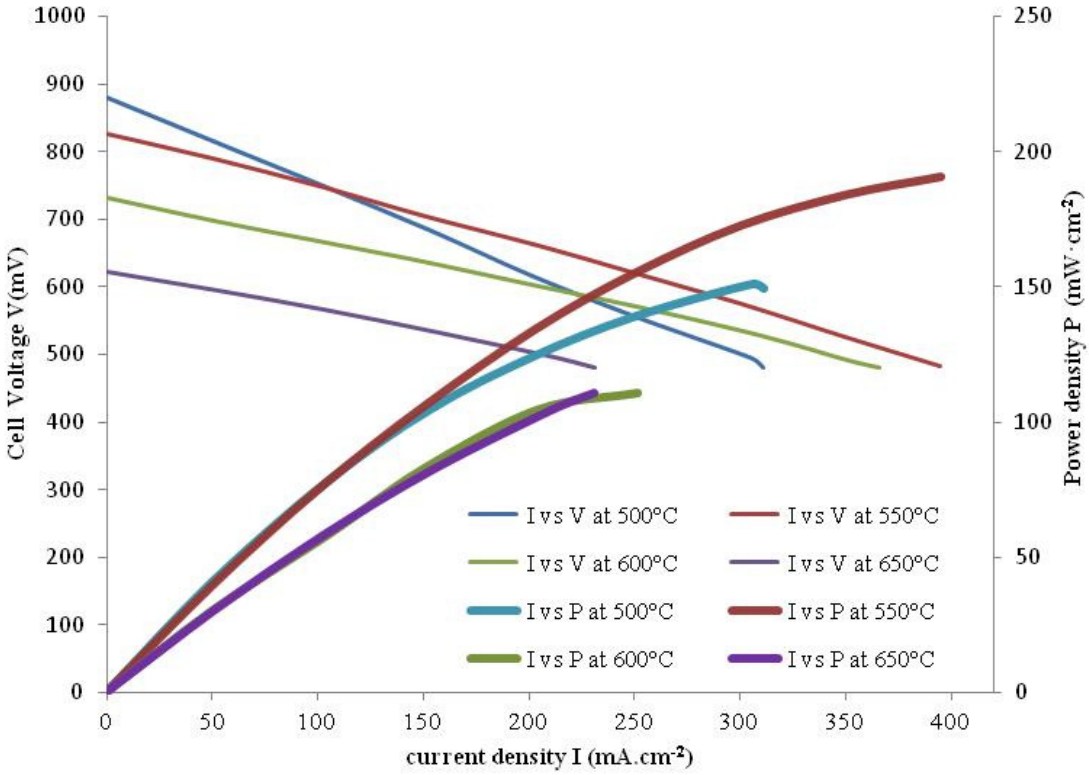

Figure II. 49 Electrochemical results of thick electrolyte cell [44]

The Figure II.50 shows the cross section of cell. It was measured that the thickness of cathode layer was 37 µm approximately. The cathode layer is on the left side followed by electrolyte, AFL and anode support layers. By increasing the thickness of electrolyte layer, the

incorporation of oxygen ion takes place and GDC10 is thus reduced at electrochemical reaction and power generation. This leads to lower OCV and power density. Thus to conclude by changing the thickness of an electrolyte layer there was no major improvement in performance rather, it reduces the OCV and power performance of cell. Thus other possible optimization was further studied on different aspects.

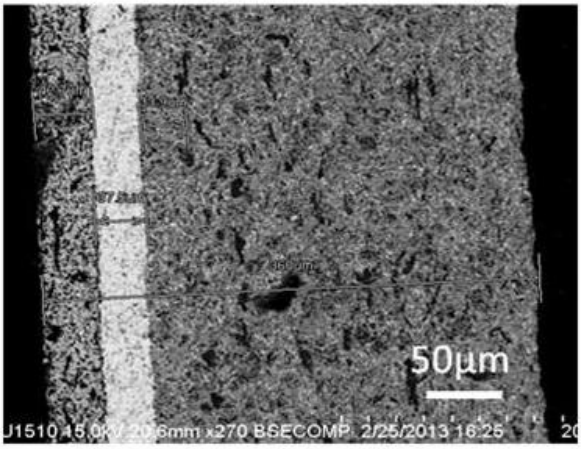

Figure II. 50 Cross section showing thick electrolyte

IV.5. Effect of using carbon pore former in cathode layer.

The next optimization was performed by changing the microstructure of the cathode layer. The Figure II.51 shows the electrochemical results of cell with different microstructure of cathode. The carbon pore former was introduced into the cathode slurry. The obtained OCV were 0.943 V, 0.911 V, 0.863 V, 0.808 V at 500°C, 550°C, 600°C and 650°C. The maximum power densities calculated were 138 $mW.cm^{-2}$, 227 $mW.cm^{-2}$, 305 $mW.cm^{-2}$, and 363 $mW.cm^{-2}$ at 500°C, 550°C, 600°C and 650°C respectively. The results are interesting: incorporating carbon pore formers in cathode layers induced some pores in cathode layer after sintering. These pores were homogeneous and it increased the TPB on cathode side thus favouring the performance of

cell. The power densities increased gradually starting from lower temperature. The power density of 363mW.cm^{-2} was seen as another important improvement in the optimization.

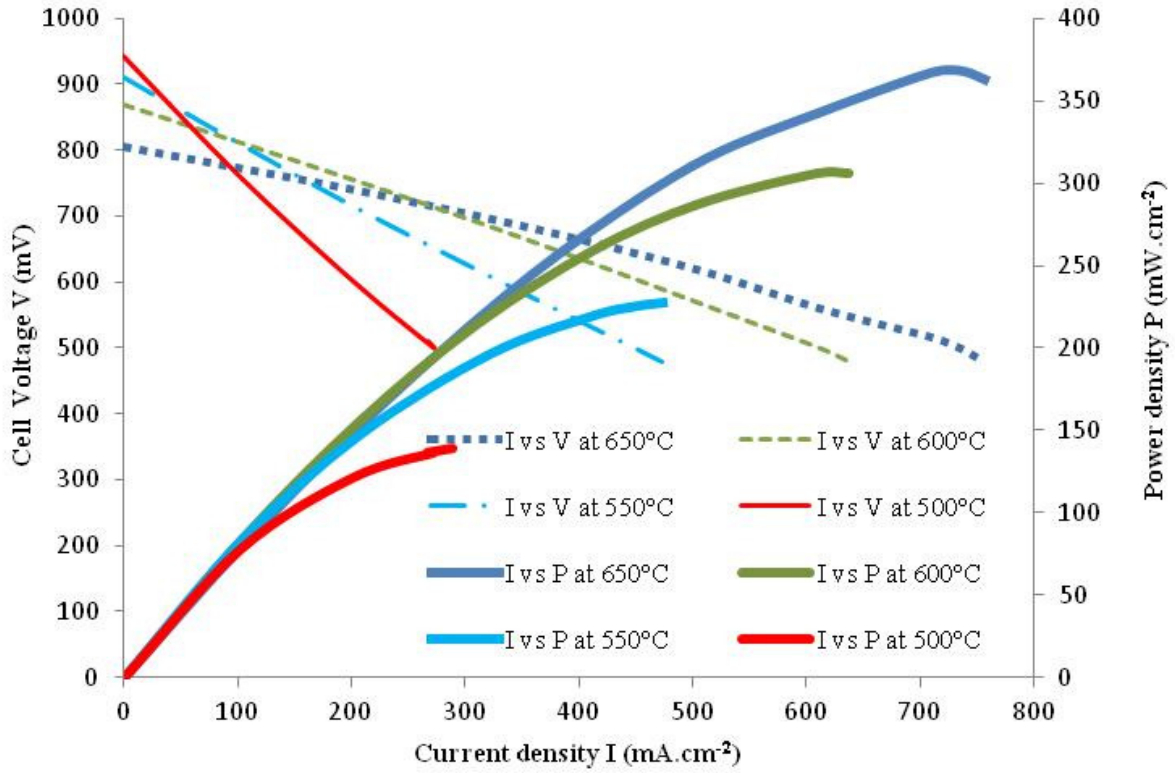

Figure II. 51 Electrochemical result of cell with carbon in cathode layer [44]

The Figure II.52 shows the cross section of cell with carbon incorporated cathode layer. Thus the cathode is represented as C and the electrolyte is represented as E and the anode is represented as A. From Figure II.52 it can be clearly seen that there is an even distribution of pores in the cathode layer which gradually increased the power density by 140 mW.cm^{-2} at 650°C.

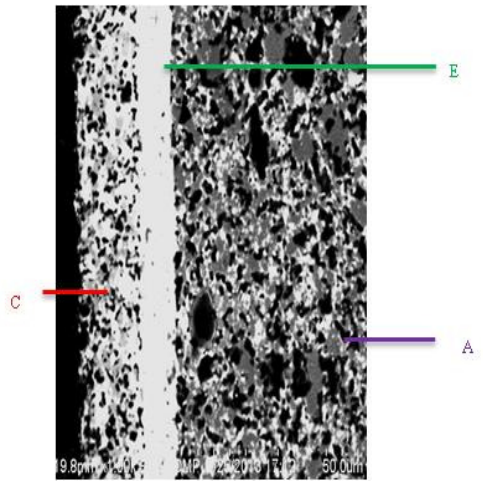

Figure II. 52 Cross section of cell showing pores in cathode layer.

IV.6. Final optimization performed.

So by using the knowledge obtained, further optimization was considered by keeping pore former in cathode, maintaining electrolyte thickness of around 20 µm. The next optimization was considered by reducing to optimal thickness of cathode layer while avoiding bubbles that may degrade the cell quickly, but by providing good performance of the cell. The thickness of cathode and electrolyte layer was reduced by almost half. The thickness of the whole cell was around 325 µm, the cathode layer was approximately 19 µm the electrolye was 10 µm and the AFL and anode support layer measuring the remaining thickness of cell. The Figure II.53 a) shows the cross section of full cell. II.53 b) shows magnified cathode, electrolyte and anode functional layer.

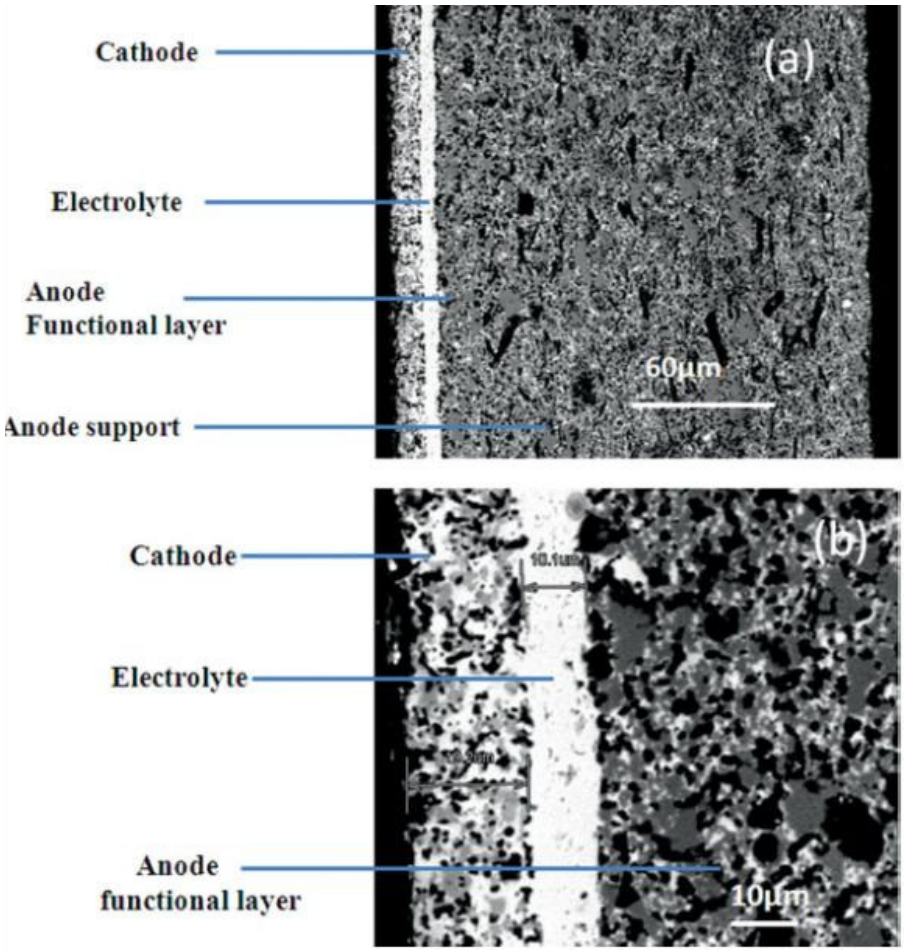

Figure II. 53 Cross section of cell

The Figure II.54 shows electrochemical results obtained from the cell. The measurements were done at 500°C, 600°C and 648°C. OCV values obtained are given as 1.002 V, 0.920 V, 0.863 V. respectively. The maximum power densities calculated were 124 $mW.cm^{-2}$, 364 $mW.cm^{-2}$ and 466 $mW.cm^{-2}$ at 500°C, 600°C and 648°C respectively. Thus by reducing the thickness of cathode layer by half and an electrolyte layer by half power density was increased by 110 $mW.cm^{-2}$ at 648 °C. Practical value above 1 V was obtained at 500°C.

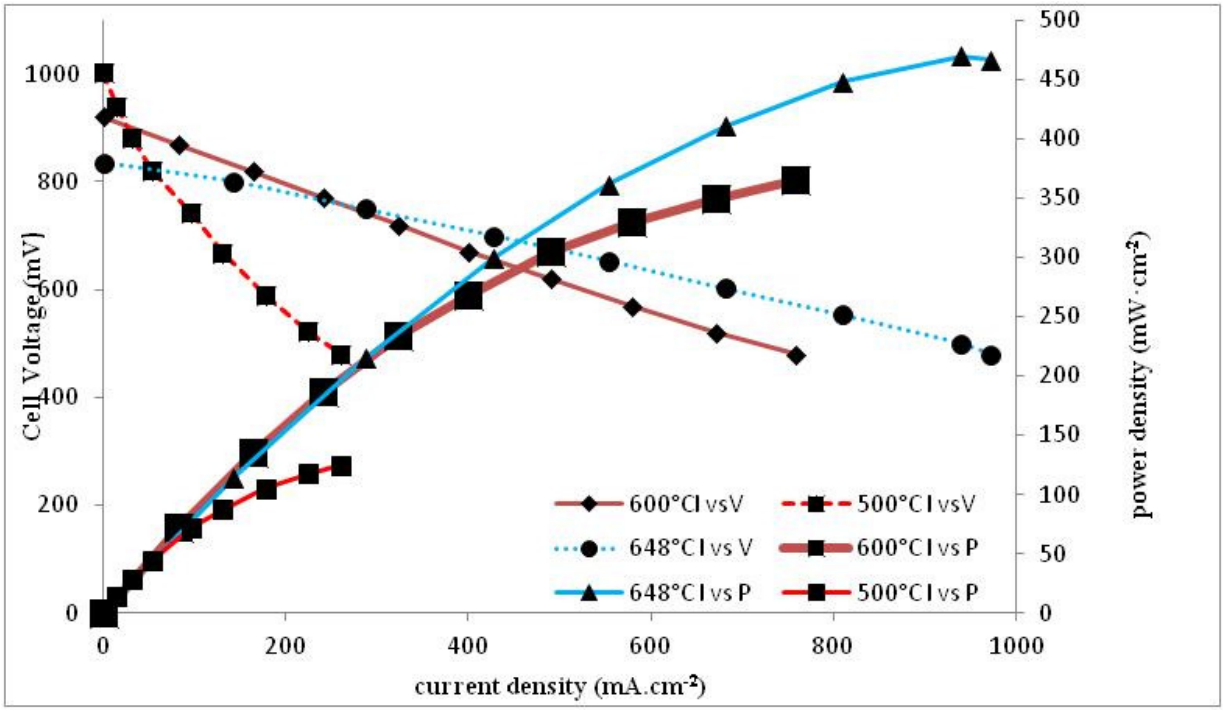

Figure II. 54 Final optimized electrochemical results [35]

These values are compared to the theoretical values, and to similar cells from literature. The linear voltage drop of a cell with respect to increasing current density proves that the cell was not broken under load conditions and exhibits good cell behavior. The results showed that, achieved OCV values at 500°C and 600°C is 1.002 V and 0.920 V (with 10 µm electrolyte sintered at 1215°C) and it is 42 mV and 10 mV higher at respective temperatures with 4 µm electrolyte sintered at 1300°C reported by C.Ding et al [45]. Conventional sintering temperature for nano particles of GDC is 1300°C and micro sized particles are 1500°C. However cell voltage reported in this study at 500°C and 600°C, (using GDC10-HP particles sintered at 1215°C) is 38 mV and 56 mV lower at respective temperatures when compared to C.Ding et al [46] using nano particles of GDC with high surface area and high sintering temperature of 1300°C. However, it is possible to achieve a large number of TPB, using nano particles with higher surface areas, which

in turn will give higher OCV. The OCV values from this study were also compared and found to be higher than Q.L.Liu et al [47] using higher sintering temperature of 1500°C and two steps of sintering to achieve a single cell. This explains that GDC layer obtained by this process is dense, crack free with no open pores at low sintering temperature of 1215°C compared to conventional sintering temperature of 1500°C which is used for micro metric particles.

The maximum power density obtained at 500°C, 600°C, and 648°C are 124 $mW.cm^{-2}$, 364 $mW.cm^{-2}$, and 466 $mW.cm^{-2}$ respectively. The reported power outputs were lower compared to [45-47]. The difference in power density can be linked to first the fact of using higher sintering temperature of cathode. In this one step sintering process a temperature of 1215°C is used which is 315°C higher compared to [45-47]. Higher sintering temperature of cathode plays a major role in microstructure and high densification of cathode. These results in low porosity and in turn very few numbers triple phase boundaries for reaction to occur in cathode. The second reason can probably be the use of low surface area of cathode and electrolyte powders in this process. Even with such low surface area powders, it was still possible to achieve higher OCV values when compared to J.Ding et al [48]. The maximum power density obtained were also higher at lower temperature of 500°C and 550°C, though they have used BSCF as cathode in [48] which is expected to provide higher performance than LSCF used in this study. The other reason for lower power density can also be due to high internal resistance due to co-sintering of many layers as explained by H.Ohrui et al [49].

So the preliminary results obtained prove that our process of fabrication of unit planar cell by tape casting and single step sintering at low temperature was successful and can be

extrapolated to large area cells of any architecture and dimension. The large area cells obtained by this process are about to be stacked and studied for long term performance.

IV.7. Conclusion.

Thus in this chapter the process of obtaining large area cells by using only tape casting and single step sintering was explained. The major factors included the selection of material, slurry preparation process, casting the multilayers, drying time of green body, optimization of sintering temperature and pore former, playing with thickness of different layers of cell. Thus to conclude the cell was fabricated by using only tape casting process, by sintering at low temperature without using any sintering aids, lamination process and multistep sintering process and costly techniques. The optimized cell possessed 20 µm thick cathode layer with carbon pore formers incorporated in the cathode slurry, the thickness of electrolyte layer was 10 µm and the thickness of whole cell was 325 µm. OCV obtained at 500°C was 1.002 V and maximum power density obtained at 648°C were 466 $mW.cm^{-2}$. The main factor to be noted is that all the results were obtained from cells of 10 cm^2 active area, and all measurements were done in open flange set up without using any costly sealing materials. There is further larger room for optimization with regards to many parameters in cell. Considering the goal of 400 $mW.cm^{-2}$ was reached and with little time left for preparation of cells above 25 cm^2 and stacking, preparation of large area rectangular planar cell was focussed. The other goal of long term ageing was also performed and results are presented in the next chapter.

References

1. C. Xia, M. Liu, *Solid State Ionics* 144, 249, 2001.
2. C. Xia, M. Liu, *J. Am. Ceram. Soc*. 84, 1903, 2001.
3. S. Dikmen, P. Shuk, M. Greenblatt , H. Gocmez *solid state sciences 4*, 585, 2002.
4. K. Higashi, K. Sonoda, H. Ono, S. Sameshima, Y. Hirata, *J. Mater.Res.* 14, 957, 1999.
5. J. Van herle, T. Horita, T. Kawada, N. Sakai, H. Yokokawa, M.Dokiya, J. Am. Ceram. Soc. 80,933, 1997.
6. Rodolfo O.Fuentes Richard Baker, *J.Hydrogen Energy* 33, 3480, 2008.
7. Rodolfo O.Fuentes Richard Bake, *J.Power Sources* 186, 268, 2009.
8. G.Ch. Kostogloudis , Ch. Ftikos *Solid State Ionics* 126,143, 1999.
9. V.Sivasankaran Master Thesis Engineering of intermetallic based negative electrodes 2010.
10. A. Sanson, P. Pinasco, E. Roncari *J of European Ceramic Society* 28, 1221, 2008.
11. Yoshio Matsuzaki, Yoshitaka babu, Teruhiro Skurai *Solid state Ionics* 172, 81, 2004.
12. C.J.Fu, Q.L.Liu, S.H.Chan, X.M.Ge, G.Pasciak *Int*. *J.Hydrogen Energy* 35, 11200, 2010.
13. T.L.Wen, D.Wamg , H.Y.Tu, M.Chen, Z.Lu, Z.Zhang,H.Nie,W.Huang *Solid state ionics* 152-153, 399-404, 2002.
14. Tahereh Talebi, Mohsen Haji, Babak Riasi, Amir Maghsoudipour *Int. J. Hydrogen Energy* 35, 9455, 2010.
15. Jung-Hoon Song, Sun-Il Park, Jong-Ho Lee, Ho-Sung Kim *Journal of materials processing technology* 198, 414, 2008.
16. Murray EP, Barnett SA. *Solid State Ionics* 143, 265, *2001*.
17. Leng YJ, Chan SH, Khor KA, Jiang SP. *J Solid State Electrochem* 10:339, 47, 2006.

18. Dusastre V, Kilner JA *Solid State Ionics* 126, 163, 1999.

19. Murray EP, Sever MJ, Barnett SA. *Solid State Ionics*; 148, 27, 2002.

20. Liu QL, Khor KA, Chan SH. Proceeding of the third international conference on Materials Processing for Properties and Performance (MP3). East Asia: Institute of Materials, 657, 2004.

21. Qiang F, Sun KN, Zhang NQ, Zhu XD, Le SR, Zhou DR. *J Power Sources* 168, 338, 2007.

22. W.Z. Zhu, S.C. Deevi, *Mater. Sci. Eng*. A 362, 228, 2003.

23. Zhenrong Wang, Jiqin Qian, Jiadi Cao, Shaorong Wang Tinglian Wen, *J. Alloys and Compounds* 437, 264, 2007.

24. Hwan Moona, Sun Dong Kima, Sang Hoon Hyuna, Ho Sung Kimb *Int.J. Hydrogen Energy* 33, 1758, 2008.

25. Young Min Park, Hoo Jung Lee, Hong Yeol Bae, Jin Su Ahn, Haekyoung Kim Kimb *Int.J. Hydrogen Energy, 37, 494, 2012.*

26. Kim, S.H. Hyun, J. Moon, J.-H. Kim, R.H. Song, *J. Power Sources* 139, 67, 2005.

27. T.L. Reitz, H.M. Xiao, *J. Power Sources* 161, 437, 2006.

28. R.Q. Yan, D. Ding, B. Lin, M.F. Liu, G.Y.Meng, X.Q. Liu, *J. Power Sources* 164 567, 2007.

29. R.N. Basu, G. Blass, H.P. Buchkremer, D. Stover, F. Tietz, E. Wessel, I.C. Vinke, *J. Eur. Ceram. Soc*. 25, 463, 2005.

30. Hae-Gu Park, Hwan Moon Sung-Chul Park, Jong-Jin Lee, Daeil Yoon, Sang-Hoon Hyun, Do-Heyoung Kim. *J.power sources*. 195, 2463, 2010.

31. G.M Christie, J.P.P.Huijsmans, U.Stimming, S.C.Singhal, H.Tagava , W.Lenhert(Eds), Proc. 5th international symp Solid Oxide Fuel Cells , *The Electrochemical Society*, Pennington NJ,.718,1997.
32. G.M Christie, J.P.Ouweltjes, R.C.Huiberts, E.J.Siewers, F.P.FVan Berkel, J.P.P.Huijsmans, 3rd international fuel cell conf.Nagoya, Japan, 361, 1999.
33. F.Tietz, H-P.Buch Kremer, D.Stover *Solid state ionics* 152-153, 373, 2002.
34. V.Sivasankaran, L.Combemale, G.Caboche. FR12/59643 *French Patent*, 2012.
35. V.Sivasankaran, L.Combemale, M.C.Pera, G.Caboche. Doi: 10.1002/fuce.201300159.
36. V.Sivasankaran, L.Combemale, M.C.Pera, G.Caboche ECS transactions, volume, 53, 30, 159-162, Doi:10.1149/05330.0159 ecst.
37. V.Sivasankaran, L.Combemale, G.Caboche PCT/FR2013/0542408, *World patent,* 2013.
38. Hwan Moon, Sun Dong Kim, Eon Woo Park, Sang Hoon Hyun, Ho Sung Kimb *Int. J. Hydrogen Energy* 33, 2826, 2008.
39. Zhenrong Wang, Jiqin Qian, Jiadi Cao, Shaorong Wang and Tinglian Wen *Fuel cell bulletin* 2007, 12, 2007.
40. Pingying Zeng, Ran Rana, Zhihao Chen, Hongxia Gua, Zongping Shao, J.C. Diniz da Costa, Shaomin Liu *Journal of Membrane Science* 302,171, 2007.
41. J.Cheng, S.Zha, X.Fang, X.Liu, G.Meng, *Material research bulletin* 37, 2437, 2002.
42. Jaemyung Changa, Olivier Guillonb, Jurgen Rodelb, Suk-Joong L. Kanga, *J.Power Sources* 185,759, 2008.
43. Sang-Ho Lee, Gary L. Messing, Masanobu Awano, *J. Am. Ceram. Soc*., 91, 2 421,2008.
44. V.Sivasankaran, L.Combemale, M.C.Pera, G.Caboche Manuscript to be submitted to advanced energy.

45. C. Ding, H. Lin, K. Sato, T. Hashida, *J. Membr. Sci, 350*, 1, 2010.

46. C. Ding, H. Lin, K. Sato, T. Hashida, *Scr. Mater. 60*, 254, 2009.

47. Q. L. Liu, S. H. Chan, C. J. Fu, G. Pasciak, *Electrochem.Com. 11*, 871, 2009.

48. J. Ding, J. Liu, G. Yin, *J. Membr. Sci.*, *371*, 219. 2011.

49. H. Ohrui, T. Matsushima, T. Hirai, *J. Power. Sources*, *71*, 185, 1998.

NDA Protected with DLR

Chapter 3: Long term ageing results, development of test bench and stack

Chapter 3: Long term ageing results, development of test bench and stack

I. Introduction

The last part of this thesis is dedicated to the path towards an IT-SOFC stack. Three contributions are described: the ageing results on large cells, the stacking process of the newly developed planar cells and the development of a stack test bench. The results of the ageing perfomance of 10 cm^2 cells performed in Fiaxell device, and their post mortem analysis are reported. Then the step and products involved in stack building are briefly described. The stack foot print was provided by the DLR, German Aerospace Center. Finally, a test bench dedicated to the study of the stacks is presented. A test bench was already available in Belfort [1], at FCLAB, a CNRS Research Federation on fuel cell systems, but it needed a complete updating to comply with the test of the developed cell. The developments were made in collaboration with DLR.

II. Ageing results of cells

In order to achieve an operational stack, a mile stone is the measurement of the ageing performance of large cells. A Fiaxell open flange device, similar to the one described in Chapter 2, at EPFL, has been set up in ICB, Dijon. A single cell of 10 cm^2 active area cells was tested for long term ageing performance in Dijon. The cells are comprised of Ni/GDC//GDC//LSCF/GDC with best known configuration. This set up includes a Kittec Furnace squadro11, a humidifier for

hydrogen, connecting wires, mass flow meters, a voltmeter, an ammeter, a power load and a hydrogen detecting valve.

Once after all the gas pipes, voltmeter, ammeter, and power load are connected, the furnace was started to increase the temperature. During start up, air was supplied in both sides while increasing in temperature. During reduction, firstly a mixture of hydrogen and nitrogen was supplied to the cell, then it was slowly replaced with hydrogen. The reduction of NiO to Ni took place under pure hydrogen at 750°C for 2 hrs. The hydrogen and air flows were kept constant during measurements. The humidified hydrogen passing through the tube of water was supplied at flow rate of 100 $ml.min^{-1}$ and air was supplied at 600 $ml.min^{-1}$. The Figure III.1 shows the Current density Vs Cell voltage and Power density of the cell. The voltage measurements were started at 500°C in intervals of 50°C till 650°C. The OCV obtained at 500°C, 550°C 600°C, and 650°C were, 0.917 V, 0.874 V, 0.772V, 0.644 V respectively. The reasons for the lower values was perceived as all the current collectors and device were new, there was some initial resistance due to the oxidation of the anode current collector mesh. Second thickness of nickel meshes were different. Third flow rates of gas were different from ICB lab and Fiaxell lab. Still the experiment was performed on the new set up in Dijon to study long term ageing performance. In practical situation, the OCV obtained will be always lesser than the theoretical value. The reason for lower OCV in the practical condition than the theoretical OCV is due to leakage of electrons through the electrolyte. The OCV values decreases with increasing temperature, it implies that the cell is working and in good condition. In OCV conditions, the GDC is more reduced at higher temperature than at lower temperature, this result in higher

conductivity of electrons and in turn leads to higher leakage of electrons. The maximum power density obtained at different temperatures are given in Table III.1

Temperature in °C	Voltage in V	Current (I) in A	Power density in $mW.cm^{-2}$
500	0.917	0.695	44
550	0.874	0.695	52
600	0.772	0.695	43
650	0.664	0.695	28

Table III. 1 Results obtained from cell

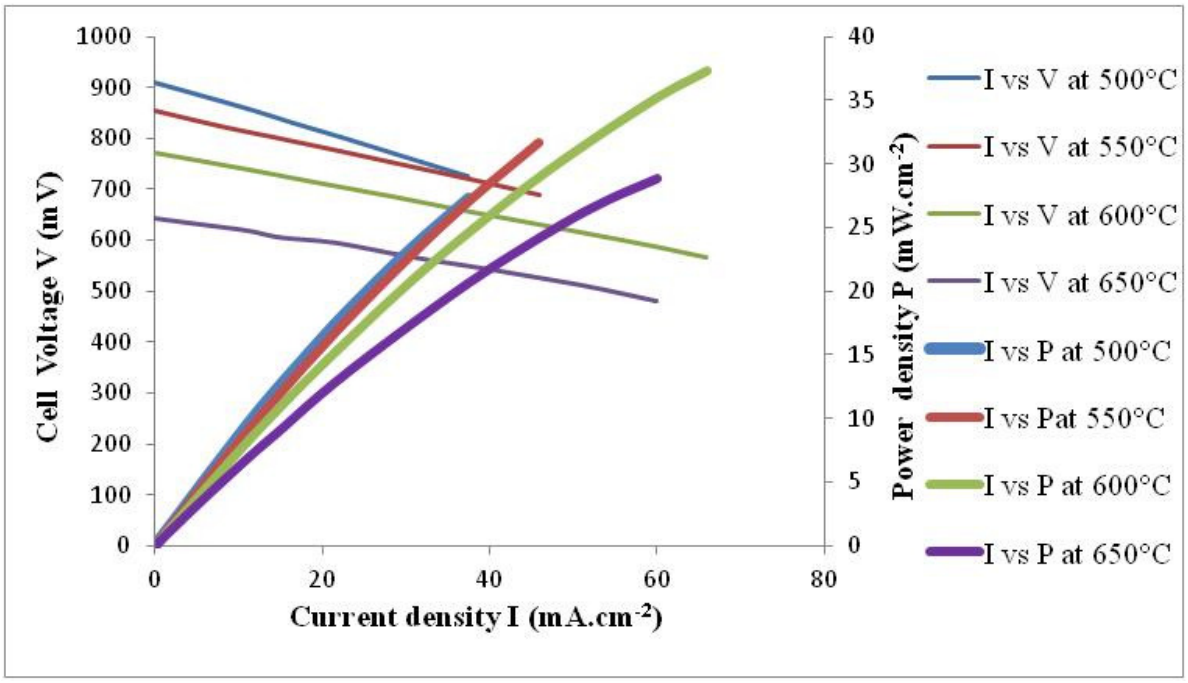

Figure III. 1 Cell Voltage and Power density Vs Current density [5]

The Figure III.1 shows the cell voltage and power density vs current density. During electrochemical reaction at temperature of above 600°C, the application of current increases the

temperature of the cell and in turn results in higher electronic conduction through the cell. The results obtained in long term ageing tests shows high power density of 52 $mW.cm^{-2}$ at 550°C. During electrochemical reaction and power generation, the oxygen is incorporated and GDC10 is reduced, then it results in a decrease of the conductivity of electrons. The lower OCV with leakage of electrons was responsible for lower power density at higher temperatures. For long term ageing test with thin GDC10 electrolyte, the characterization is always preferred at temperature lower than 600°C irrespective of the shape of the cell. The results obtained in this work from planar cells were in correlation to results obtained with tubular cells presented at 31st international ceramics and composite symposium [2,3].

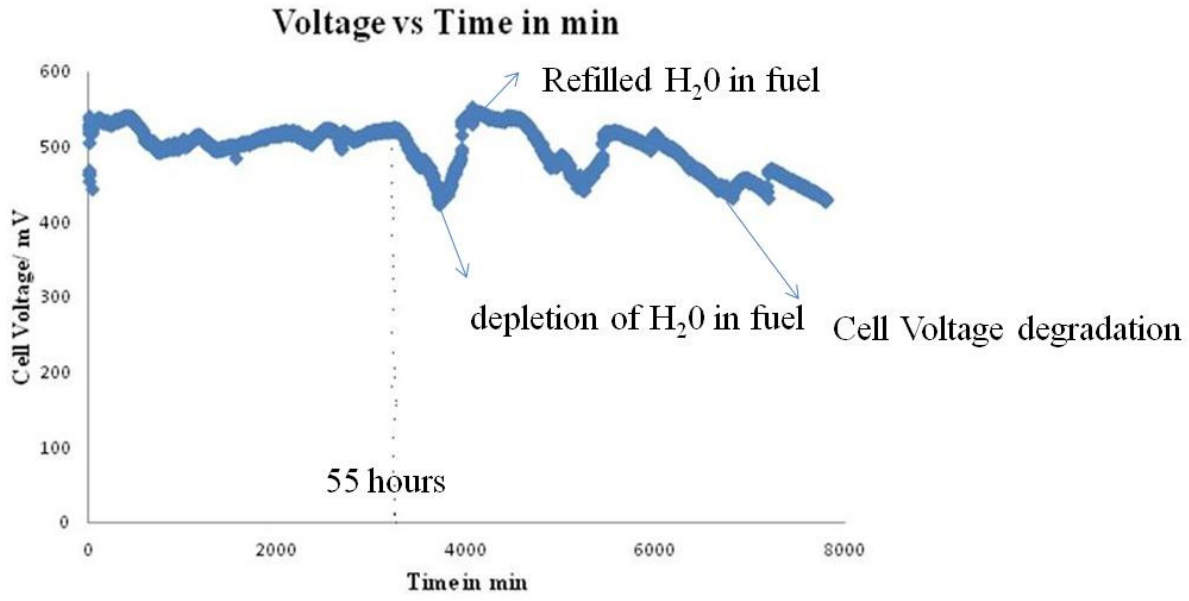

Figure III. 2 Long term results showing Cell Voltage Vs Time at 505°C with 69.5 $mA.cm^{-2}$

Figure III.2 shows the long term ageing results of cell voltage vs time. The measurement was carried under constant hydrogen and air supply. The temperature was maintained at 505°C.

The initial voltage was 0.529 V and current supplied for 10 cm^2 were maintained at 0.695 A that is a current density of 69.5 $mA.cm^{-2}$. The cell was monitored at regular intervals for temperature and gas flow readings. The cell exhibited around 0.529 V for the first 3300 min with little fluctuations of current which in turn lead to fluctuation of voltage. Then after this time, there is a gradual drop of cell voltage. This was due to the humidication of hydrogen gas: during the experimentation, the level of water in the tube containing the humidification water became too low to ensure a sufficient level of humidity for the gas. Since, hydrogen gas passed through the tube containing water for humidication, the level of water starts to reduce in the tube. This leads to low humidification percentage of hydrogen supplied to the cell. The cell voltage worsened, when there was no water in the tube and dry hydrogen was directly passed to cell. Then the tube was refilled with water and measurements were continued.

Once the hydrogen gas pass through water, the cell voltage increased to the original value of 0.529 V. After the first 100 hours, the cell started to degrade continuously showing reduction in voltage as shown in Figure III.2. Once the cell was completely dead, it was dismantled from the device and post mortem studies were done by SEM and XRD.

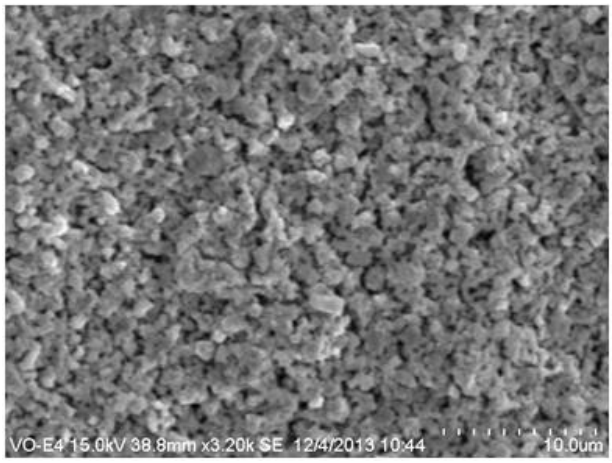

Figure III. 3 Anode microstructure after reduction

The Figure III.3 shows the surface of anode microstructure after 100 hours ageing. No changes were observed in microstructure, but on the surface, as shown in the Figure III.4.lots of micro fissures and large cracks are seen. This was also seen during dismantling the cell. The Figure III.4 explains that, during long term ageing, the Ni in the cell formed from the reduction of NiO, started to reoxidize. Only a part of Ni starts to reoxidize which was seen later from XRD measurements. Due to the reoxidation, there was volume expansion in the lattice structure and caused the fissures or cracks as seen in Figure III.4. The strain developed on this anode side extends to the whole cell, causing the cell to break.

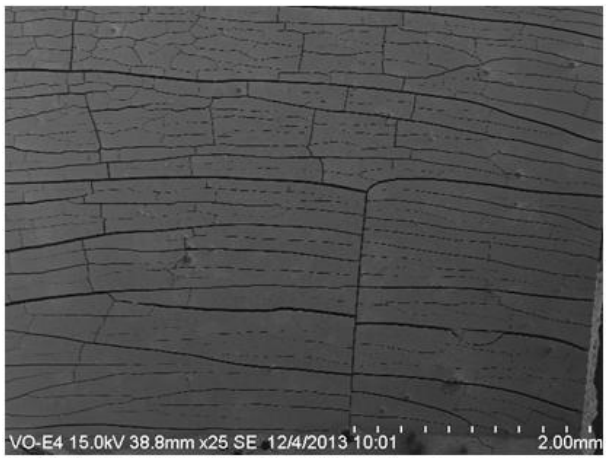

Figure III. 4 Anode surface after 100 Hours

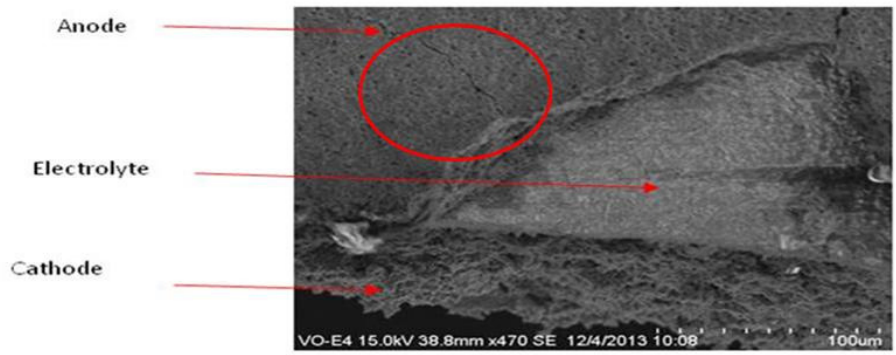

Figure III. 5 Image of cell with different layers

The Figure III.5 shows evidently that the cracks developed only on anode side and were due to reoxidation. There was no deformation seen in electrode or cathode layer in particular.

XRD studies were performed on anode and cathode sides, before long term ageing test and after ageing for 100 hours. This also confirms the changes occured only on anode side during long term ageing.

The Figure III.6 shows XRD pattern of anode before and after ageing. The graph represents peak intensity versus 2 theta. The peaks in red color show the NiO/GDC before the test. The peaks in black color show the Ni/GDC after 100 hours ageing. During the electrochemical reaction NiO which was reduced to Ni. While ageing test was conducted some of the particles of Ni were again oxidized to NiO. The structural change is clearly seen by reduction in intensity of peaks of NiO, as well as strong peak of Ni was observed at 44, 52, 79, and 94 on 2 theta scale.

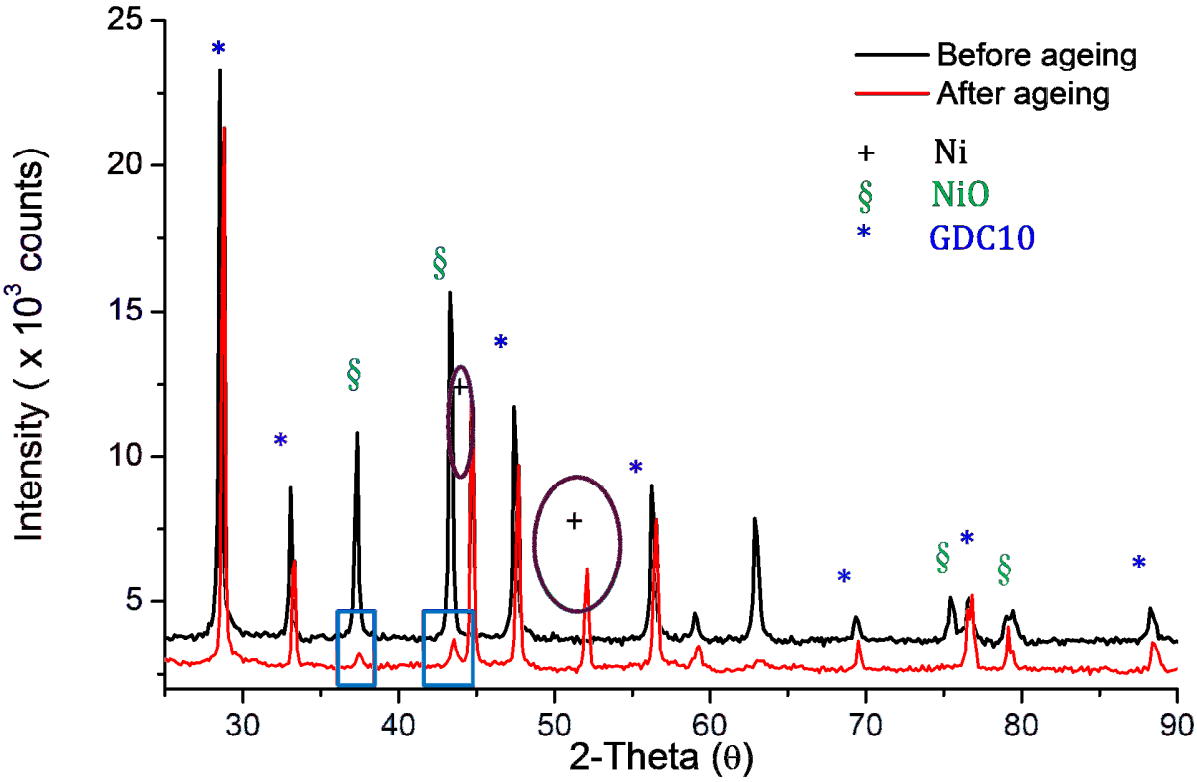

Figure III. 6 XRD pattern before and after ageing

The figure III.6 clearly shows the presence of nickel along with NiO after ageing for 100 hours.

The Figure III.7 shows XRD pattern observed on the cathode side before and after ageing. The peaks in red color represent the cathode before ageing and the peaks in black color show the cathode after 100 hours of ageing. No change occurs on the cathode side, either with regards to GDC10 or LSCF48. This observation confirms that this is the volume expansion on the anode side which caused the fissures and extends to cathode resulting in degradation of the cell.

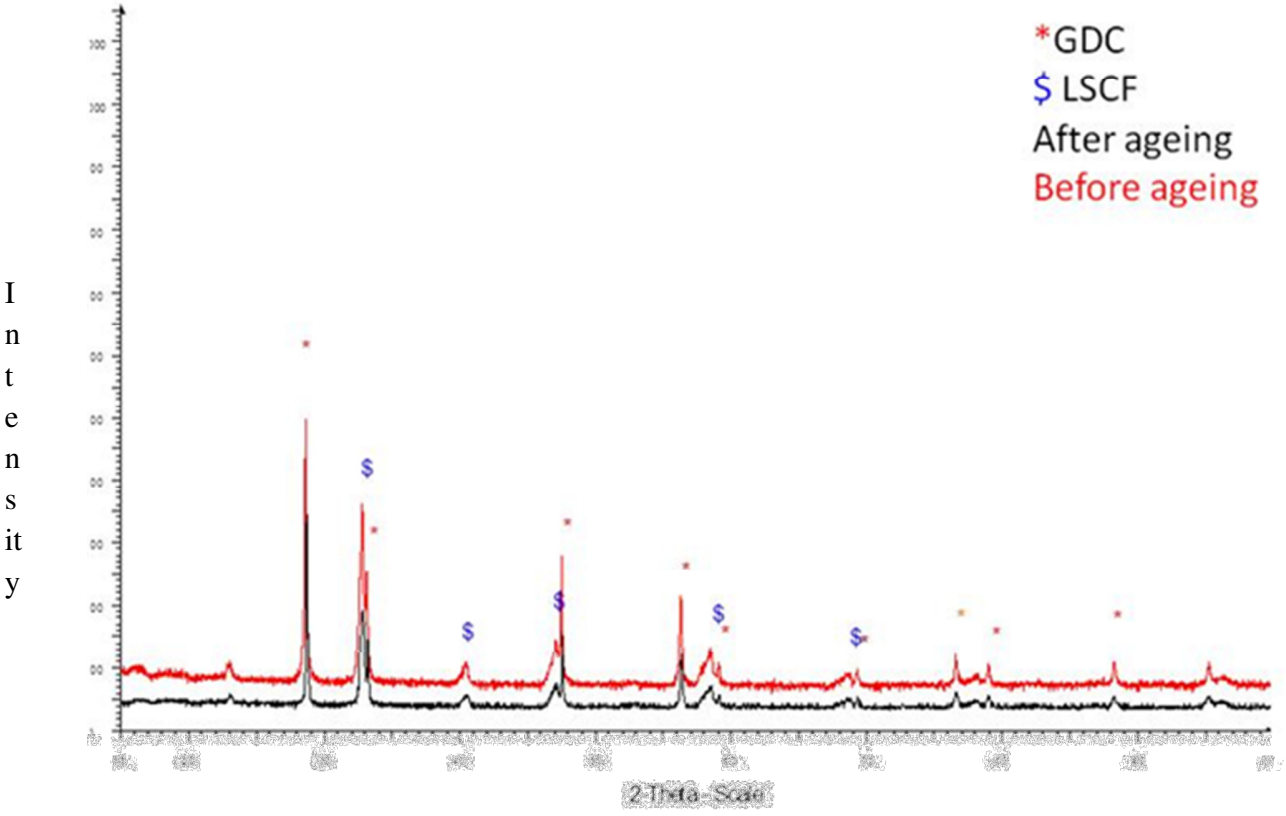

Figure III.7 XRD pattern of cathode before and after ageing.

The changes during the long term ageing were discussed. The operation of the cell was performed in an open flange set up which probably favored the reoxidation of Ni to NiO at the anode. The structural changes on the anode caused the strain on the cell which extended to electrolyte and cathode, leading to complete degradation of cell. This scenario was confirmed by the post mortem analysis by SEM and XRD. The future work on long term experiment will be focussed to study possible interfacial changes by TEM or other necessary experiments.

Considering the fact that the cell was prepared by the new patented tape casting process, the results obtained shows promising results for long term ageing. As the ageing test was done on open flange set up, without sealing, the results are expected to improve after sealing. This

process with little improvements on the formulation of cell could be extended to large scale mass production process for commercialization.

III. Products needed for stacking

The products which are mandatory for stacking process are explained.

III.1 Interconnectors

The main usage of interconnectors in SOFC stack relates to two functions. The first role is to provide gas separation in the stack; the second role is to provide electrical connection between the cells. Like other components of stack, main requirements for interconnectors are mentioned in chapter 1. Metal alloys of inconel type has TEC mismatch between other components. For this work, interconnectors made of crofer were chosen [4]. The interconnectors can be used for other tests after sand blasting.

III.2. Current collectors meshes in stack between cells

In a stack, the cell is sandwiched between current collector meshes. The stack in this work will be built with an anode supported cells (ASC). In general for testing single button cells of small area of around 2 cm^2, platinum current collectors are used. For ASC stack of an active area of 25 cm^2, anode current collectors generally nickel meshes nickel meshes are used. The cathode current collectors used in testing of single cells of small area are platinum and/or gold meshes. These have the least possible contact resistance, so that it can provide enough catalytic activity and as well help in current collection from cathode. However, for stacks of cells with large active area and many cells, usage of platinum gradually increase the building price and making it expensive. So in the stack of multiple cells, generally the cathode paste itself acts as

the current collector [4]. Since in this work the stack will comprise only one cell of above 25 cm^2, in order to avoid contact resistance between interconnectors, gold meshes are used and stack will measured with seal. The thickness of gold meshes was 100 microns. The advantage of using gold meshes in a short stack under development is that, after testing, it can be recovered and re-used for another set of experiments. The Figure III.8 shows nickel meshes used in stack placed on bipolar plates. These nickel meshes are generally replaced after every tests.

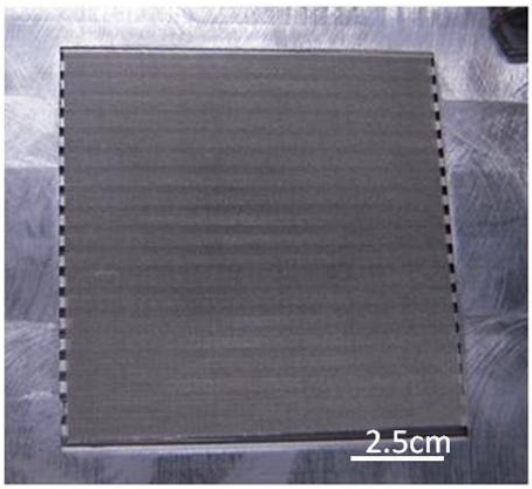

Figure III. 8 Nickel meshes placed on bipolar plates

III.3.Sealants

As explained in chapter 1 under sealant section, compressive seals will be used in this work. The glass paste will be supplied by Fraunhofer IKTS named AF 45. This is also called as Areva glass seal. They have TEC close to $13*10^{-6}K^{-1}$ at working temperature. This paste does not have any solid state reactions with the chosen crofer material at working temperature. These glass seals are applied in the interconnectors before the startup of the test bench. They can be scrapped off by sandblasting device after the experiment. Thus it allows reusing the interconnectors for future experiments.

III.4. Steel plates

Ferritic steel alloys will be employed during operation of the furnace. This steel weight of 40 Kilograms is needed to ensure tight sealing between the stack to avoid leakage of gas. During start up of stack measurement the temperature will be rised to 950°C, during this time sealants will expand due to high temperature. These steel plates placed on the top of the stack will give enough pressure on the the stack system and suppress the expansion of sealant and ensure leak tight stack sytem. Steel alloys types of 1.4742 or 1.4509 or 1.4307 can possibly be employed during operation of stack. These alloys can be reused for many times after possible polishing with salt paper to scrub off oxides formed due to high temperature. In our work steel alloys of type 1.4307 from KDI France are chosen. They have density of 8.03 $g.cm^{-3}$. These steel plates were cut in to size of 30cm*30cm to fit into the furnace.

III.5. Gas manifolds and gas flow directions

Gas manifolds are an important part of the stack. These manifolds will allow the gas to enter each cell and also collect the unused gases and products obtained after reaction at the other end. There are generally two types of manifold namely internal and external. In this work, internal manifold are connected to interconnectors of stack. There are different gas flow configurations available like cross flow, co flow and counter flow for fuel and oxidant gases. Each has its effect on various parameters such as temperature. The fuel gas and oxidant gas flow patterns can be varied such as Z flow, serpentine flow, radial flow and spiral flow. For Planar stack generally, Z flow or serpentine flow are used based on design. In this work serpentine flow model is used for both oxidant and fuel gas. The flow patterns generally designed with the

interconectors. The Figure III.9 shows the interconnector with serpentine flow pattern in the cathode side bipolar plate.

Figure III. 9 Interconnector with serpentine flow pattern

IV. Balance of plant components involved in building of test bench

The development of the test bench was made with the help of, FC-LAB engineers, Mr.Serge VIVES, Mr.Laurent GIRARDOT, and Mr.Fabien HAREL, Dr.Samir JEMEI was also involved in fruitful discussion regarding electronic load and other necessary components. The BOP was selected in accordance to suit intermediate working temperature range of 500-750°C. Previously available data acquisition system from the lab was used to collect and record datas of new test bench which will comprise of the stack.

IV.1. Furnace selection and requirements

The furnace needed to be replaced as the previous one was too small. In general the furnace should have enough accessible area where temperature will be maintained constant

during operation. The heating coil should be placed all around the furnace to have equal distribution of heat.

In order to fit a planar stack of 2 cells containing the active area of 50 cm^2 the accessible area should be minimum of 22 cm in breadth and 33 cm in width. The height of the working part of furnace is very crucial, where the stack and the load need to keep seal in contact will approximately occupy 80%. During operation of the stack, due to high temperatures, there will be oxide formation on steel weights, which will cause some volume expansion. This occurs, due to long exposure of the load to atmosphere. So a minimum height of 40 cm high will be preferred.

The bottom part of the furnace becomes important as most of the connections like gas feeding and exhaust pipes, current collectors are located here, so the bottom part must be easily removable and accessed. To have removable bottom part, there should not be any heating coils in it. Finally Kittec Furnace 150S as presented in the Figure III.10, which has all the requirements was bought for the new test bench.

Figure III. 10 Furnace with heating coils in sides and removed bottom plate

IV.2. Gas module

Gas module is a unit on which the stack will be built. This enables easy, flexible stack setup and it also serves as an interface. This gas module must be raised to a minimum of 5 cm from the base plate of furnace to facilitate the start up and to avoid the uneven temperature distribution if there is any. The gas module is equipped with 4 gas tubes of diameter 10mm and length of 400 mm. This will also comprise of 4 thermocouple ports with standard compression fitting for sheated thermocouple. There are also two holes at corners of opposite end of gas module to accomodate ceramic tube. This will help in alignment of stack position. This gas module was supplied by DLR as a part of collaboration. The provision of ceramic tubes was of diameter 7.2 mm.

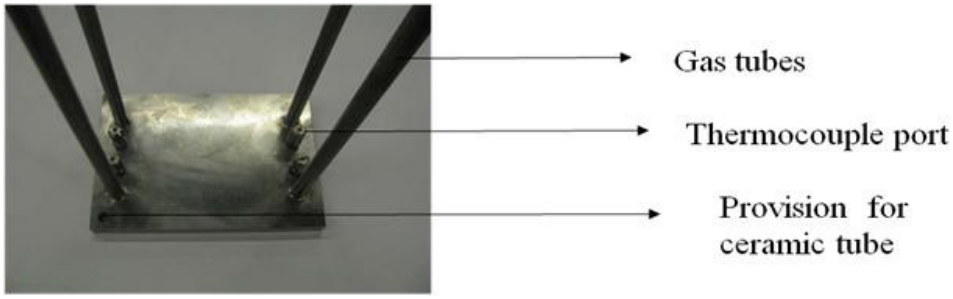

Figure III. 11 Photo of gas module

The Figure III.11 shows the gas module with thermocouple port, gas tubes and provision for ceramic tubes. This gas module was fixed on the furnace.

IV.3. Ceramic bricks

Ceramic bricks will be used to separate the bottom plate of furnace and gas module. The ceramic brick should be dense; it should also have high compressive strength, to carry the weight of stack and the steel weight. The ceramic brick from Silica ref 180-150B was choosen and its density is 1.5 $kg.m^{-3}$. It can handle maximum temperature of 1850°C and posses compressive strength of 10 Mpa. The dimensions of the brick used was 230*114*76 mm.

Figure III. 12 Gas module separated by brick from base plate

The Figure III.12 shows gas module mounted on bottom plate and it is separated by ceramic bricks from the bottom.

IV.4. Ceramic tubes

Ceramic tubes for alignment should be dense. The maximum external diameter can be of 7 mm to fit to gas module. This tube was bought from Umicore. The ceramic tube had density higher than 3.7 $g.cm^{-3}$. This ceramic tube can handle maximum of 1950°C.

Figure III. 13 Gas module alligned with ceramic tubes

The Figure III.13 shows gas module alligned with ceramic tubes in position.

IV.5. Current connectors

Inconel rods are used as current connector rods from the stack to connect to outside of the furnace. These inconel rods should be dense. Kanthal wires are used as current collection wires from the stack. These wires are welded to the inconel rods from the eyelet of bipolar plates. When using many cells, a bunch of wires is welded to eyelet and current rods at the other end. In single cell stack system as in this work, it is welded to lemo female plug that is directly clamped

to D40 flanges outside the furnace. This is then connected with M5 screws and nuts. To enhance the contact on the screws silver paste is used. This is then connected to the data acquistion system. The Figure III.14 shows bottom of furnace with fixed current connector clamped to D40 flanges.

Figure III. 14 Bottom plates with D40 flanges

IV. 6. Thermocouples

Thermocouples are chosen according to the working temperature of the stack. Since it is an IT-SOFC stack, the maximum of 650°C temperature will be maintained during measurement of data. During the start up of the stack and to set the sealing glass paste, the temperature of the furnace will be raised to maximum of 950°C. Thermocouple of type K was chosen. This K type can measure temperature range of -40°C to 1000°C. The diameter of this thermocouple will be of around 1 mm. Minimum of 4 thermocouples will be needed, each for fuel gas inlet, outlet and oxidant gas inlet and outlet. One more thermocouple can also be used to measure the temperature of around the stack, but normally, the average temperature of inlet and outlet gas temperature is considered as the temperature of stack. K type thermocouples used in the test bench were brought from Thermocoax. These are seen in the provision, drilled from base plate and will be

connected to the data acquring software externally. The Figure III.15 shows thermocouples fixed to test bench.

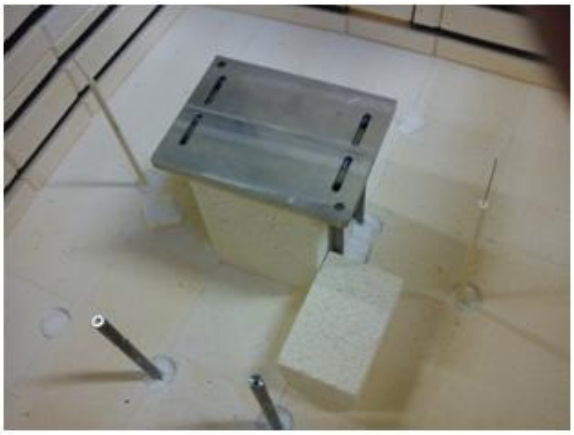

Figure III. 15 current connectors and thermocouples fixed in bottom plate

IV.7. Lab View software for data input and acquisition.

The test bench will be controlled by automated manner, using inbuilt software in FC-LAB, developed from Labview by Fabien Harel. This software helps the operator of test bench to provide and get data of stack either manually or in an automatic way. This inbuilt software will accept user instructions for operation of test bench and record the data. The other necessary auxillary sytems such as mass flow controller, pressure gauge, current wires, thermoucouple from test bench, solenoid valve voltage wires, and sensors are connected to the software by a frame grabber. The electronic load needed for operation is directly connected and controlled by the software. This software allows us to view all the parameters of stack during operation. The Figure III.16 shows the global view of the test bench with furnace mounted and connected with lab view software. The Figure III.17 shows lab view software parameter screen for verification during experiment.

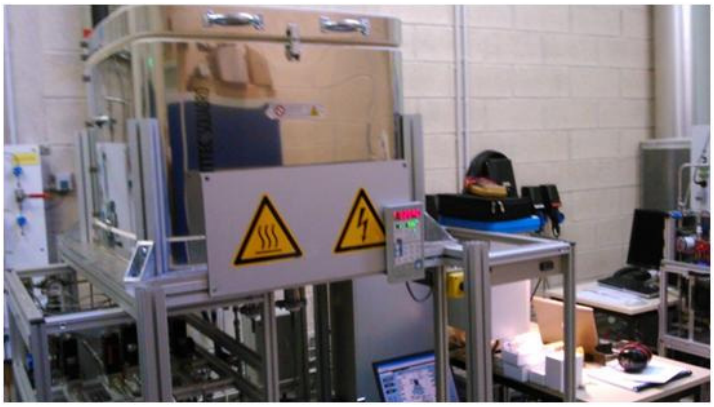

Figure III. 16 Global view of furnace and software

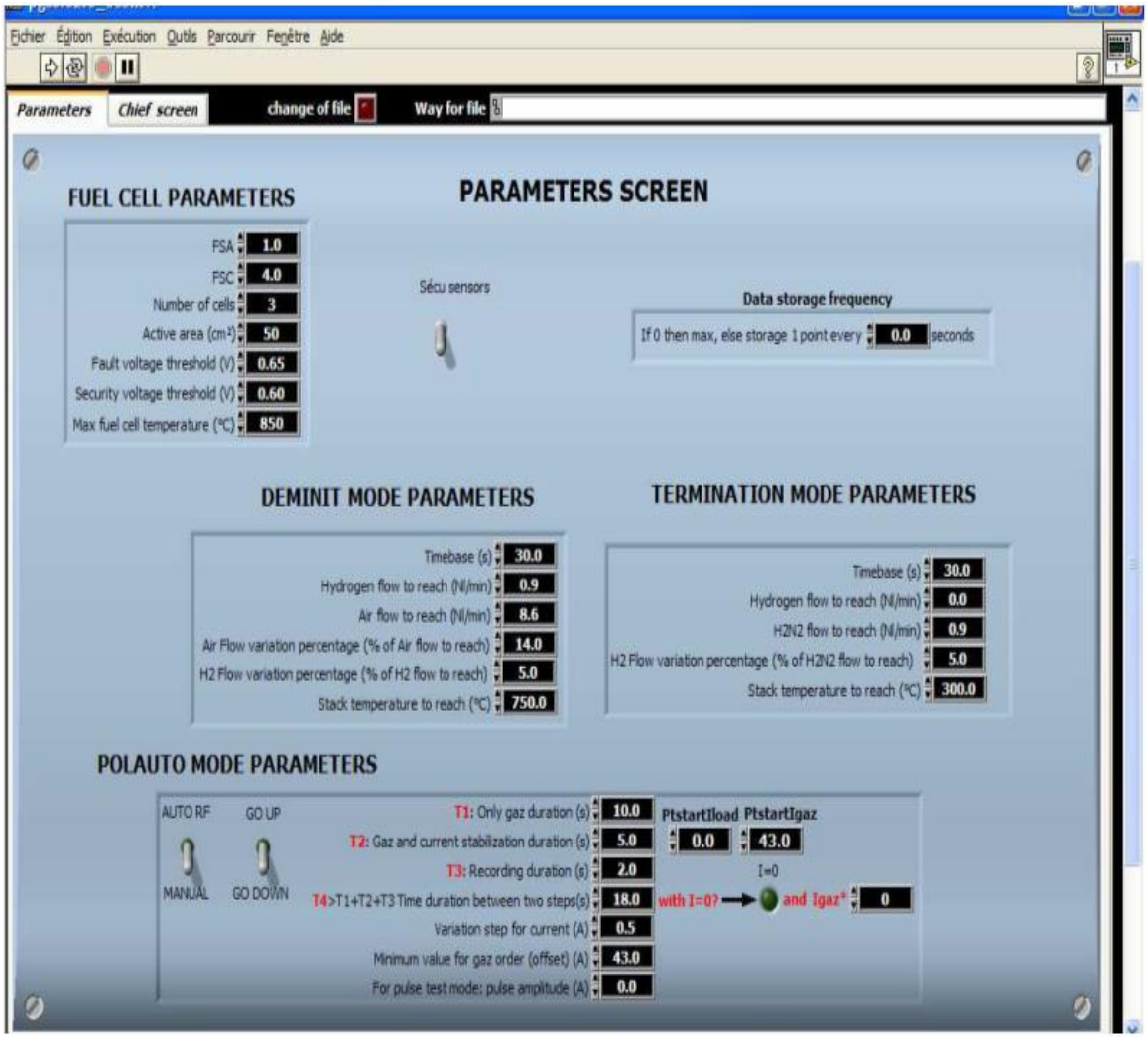

Figure III. 17 Lab view parameters screen

IV.8. Flow diagram of test bench

The Figure III.18 shows the flow diagram of test bench. It gives clear insights of fuel gas and an oxidant gas which flows to test bench from gas supply bottle. In this work, hydrogen will be used as fuel gas and air will be used as an oxidant gas for operation. However for startup, N_2 is mixed with hydrogen and used in the ratio of (95% N_2+ 5% H_2). This is used during start up, when the cell starts to reduce. When pure hydrogen is supplied, there is a possibility to damage the cells. So in order to avoid this, nitrogen and hydrogen mixture is supplied and then slowly replaced by humidified hydrogen for experiments. In this test bench generally 3 lines in parallel for fuel gases are used, one pure hydrogen, one mixture of (nitrogen + hydrogen) and third for reformate gases. Similarly air line and air mixed with nitrogen are installed, but for experiments in this work only air will be used.

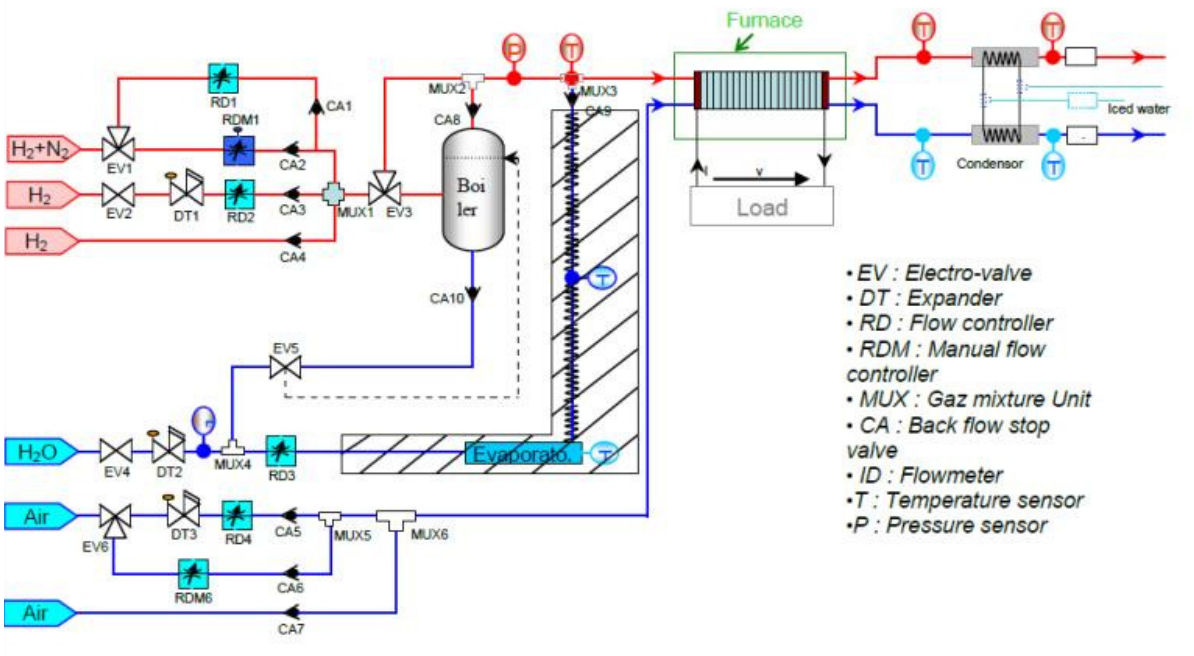

Figure III. 18 Flow diagram of test bench [1]

The boiler can be heated by a resistor which can increase the temperature of the steam supplied to fuel gas. The sensor inserted in the humidifier regulates the steam gas which is mixed and supplied to cell. There are also pressure and temperature sensor installed for gas measurements. In case of problem in the automatic gas supplying, there are also provisions for manual adjustments in the set up. The current supplied to stack is available from electronic load system installed which can be operated either manually or by software. The temperature, the voltage, the current wires and sensors are externally connected to software for accessing data. Trial of first stacking process with other necessary part was made and could not be disclosed due to NDA with DLR. The first stack of single cell with sealing will be made in near future and will be tested in this newly built test bench.

V.Conclusion

Thus in this chapter long term ageing performance obtained from 10 cm^2 cells are discussed. The products needed for stacking of cells were explained. The test bench preparation and the required products for making it are presented. As of now the new test bench is ready, temperature profile of furnace will be done before measuring the stack. Single cell will be stacked with sealing and the electrochemical performance will be performed on the newly built test bench.

References

1. M.Chnani "Modelisation macroscopic de piles PEFC et SOFC pour l'etude de leur couplage" These FC-LAB, France 2008.
2. T.Otake Misuzu Yokoyama, Kohki Nagai, Kenji Ukai, Yasunobu Mizutani 10th International Symposium on Solid Oxide Fuel Cells (SOFC-X), Japan, 2007.
3. T.Otake Misuzu Yokoyama, Kohki Nagai, Kenji Ukai, Yasunobu Mizutani 31st International Cocoa beach Conference & Exhibition on advanced ceramic and composites, USA, 2007.
4. M.Yokoo, Y.Tabata, Y.Yoshida, K.Hyashi, Y.Nozaki, K.Nozawa, H.Arai, *J. Power Sources* 178, 1, 59, 2008.
5. V.Sivasankaran L.Combemale, M.C-Pera, G.Caboche manuscript to be submitted to electrochemistry communications.

Conclusions and Perspectives

General Conclusion

In this thesis titled “Manufacturing and characterization of single cell Intermdeiate temperature Solid oxide fuel cells for APU in transportation application”, the fuel cells and its working principles were discussed. IT-SOFC and selection of materials to be used are briefed along with selection of planar design. The work presented here gives knowledge of the phenomena, obtained during development of new simplified fabrication process of planar IT-SOFC with large active area. The development, optimization of the new simplified process to achieve a large area planar cell, their limiting factors and difficulties in obtaining the cells are discussed. The goal of to i) prepare large planar cells of active area 25 cm^2 in first instance was achieved ii) Build a new test bench for adapting this geometry was done iii) testing electrochemical performance of single cells of 10 cm^2 was performed.

This fabrication of flawless planar cells by newly developed process was patented later The new fabrication process, its optimization partly with respect to factors such as i) pore formers, ii) thickness of layers.iii) Optimization of sintering temperature were detailed. iv) changing microstructure were performed and discussed.

The long term ageing performances in real time working conditions were studied and its results are presented. The products required and process involved in developing the new test bench, are explained in detail. The stacking process of cells is also briefed.

The fundamental objectives such as i) Fabrication of large active area planar cell of for stacking ; by simple and cost effective process; ii) Obtaining 400 $mW.cm^{-2}$ for large area cells;

iii) To study long term ageing performance of single cell under real working conditions, iv) Building a new test bench to fit the stack geometry, were done.

Perspectives

This process was carried out with organic solvents, next this process will be performed with aqueous solvents and using required binders and dispersants. The electrochemical performance on button cells will be done to study impedence performance on cell in probostat. The large cells will be stacked and tested in the new test bench prepared in Belfort for long term ageing performance, which includes impedence spectroscopy measurements.

The fabrications of large area IT-SOFC planar cell by new simple and cost effective process were explained.

The optimization of the new process with respect to pore formers, thickness of layers, sintering temperature were performed.

The electrochemical results of $10cm^2$ performed in Fiaxell open flange set up were detailed with respect to different configuration.

Long term ageing performance tests of single cells were conducted in Fiaxell device and results are discussed.

Preparation of new test bench and stacking process performed till now were briefed.

La fabrication de cellules de piles à combustible IT-SOFC de large dimension par un nouveau procédé simple et peu coûteux est présentée dans ce manuscrit.

L'optimisation de ce nouveau procédé en regard de l'utilisation d'agents de porosité, d'épaisseur de couches et de température de frittage a été réalisée.

Les résultats des tests électrochimiques sur des cellules de surface active 10 cm^2 réalisés dans le dispositif Fiaxell semi-ouvert ont été détaillés pour différentes cellules.

Des tests de performance de longue durée ont également été menés sur le dispositif Fiaxell, présentés et discutés.

La préparation et la réalisation d'un nouveau banc de test de stack a également été mené et présenté dans ces travaux.

Key words: IT-SOFC, tape casting, single step cell preparation, cosintering, Anode Functional Layer, long term ageing performance, stack, test bench.